Journal of Nanomaterials

Functional Carbon Nanomaterials

Guest Editors: Myoung-Woon Moon, Ho-Young Kim, Aiying Wang, and Ashkan Vaziri

Functional Carbon Nanomaterials

Journal of Nanomaterials

Functional Carbon Nanomaterials

Guest Editors: Myoung-Woon Moon, Ho-Young Kim, Aiying Wang, and Ashkan Vaziri

Copyright © 2014 Hindawi Publishing Corporation. All rights reserved.

This is a special issue published in "Journal of Nanomaterials." All articles are open access articles distributed under the Creative Commons Attribution License, which permits unrestricted use, distribution, and reproduction in any medium, provided the original work is properly cited.

Editorial Board

Katerina E. Aifantis, Greece
Nageh K. Allam, USA
Margarida Amaral, Portugal
Xuedong Bai, China
Lavinia Balan, France
Enrico Bergamaschi, Italy
Theodorian Borca-Tasciuc, USA
C. Jeffrey Brinker, USA
Christian Brosseau, France
Xuebo Cao, China
Shafiul Chowdhury, USA
Kwang-Leong Choy, UK
Cui ChunXiang, China
Miguel A. Correa-Duarte, Spain
Shadi A. Dayeh, USA
Claude Estourns, France
Alan Fuchs, USA
Lian Gao, China
Russell E. Gorga, USA
Hongchen Chen Gu, China
Mustafa O. Guler, Turkey
John Zhanhu Guo, USA
Smrati Gupta, Germany
Michael Harris, USA
Zhongkui Hong, China
Michael Z. Hu, USA
David Hui, USA
Y.-K. Jeong, Republic of Korea
Sheng-Rui Jian, Taiwan
Wanqin Jin, China
Rakesh K. Joshi, UK
Zhenhui Kang, China
Fathallah Karimzadeh, Iran
Alireza Khataee, Iran
Do Kyung Kim, Republic of Korea
Alan K. T. Lau, Hong Kong
Burtrand Lee, USA
Jun Li, Singapore
Benxia Li, China
Xing-Jie Liang, China
Shijun Liao, China
Gong Ru Lin, Taiwan
J.-Y. Liu, USA
Tianxi Liu, China
Jue Lu, USA
Songwei Lu, USA
Daniel Lu, China
Ed Ma, USA
Gaurav Mago, USA
Santanu K. Maiti, India
Sanjay R. Mathur, Germany
Vikas Mittal, UAE
Weihai Ni, Germany
Sherine Obare, USA
Atsuto Okamoto, Japan
Abdelwahab Omri, Canada
Edward Andrew Payzant, USA
Kui-Qing Peng, China
Anukorn Phuruangrat, Thailand
Suprakas Sinha Ray, South Africa
Ugur Serincan, Turkey
Huaiyu Shao, Japan
Donglu Shi, USA
Vladimir Sivakov, Germany
Marinella Striccoli, Italy
Bohua Sun, South Africa
Saikat Talapatra, USA
Nairong Tao, China
Titipun Thongtem, Thailand
Somchai Thongtem, Thailand
Alexander Tolmachev, Ukraine
Valeri P. Tolstoy, Russia
Tsung-Yen Tsai, Taiwan
Takuya Tsuzuki, Australia
Raquel Verdejo, Spain
Mat U. Wahit, Malaysia
Zhenbo Wang, China
Ruibing Wang, Canada
Shiren Wang, USA
Cheng Wang, China
Yong Wang, USA
Jinquan Wei, China
Ching-Ping Wong, Hong Kong
Xingcai Wu, China
Guodong Xia, Hong Kong
Zhi Li Xiao, USA
Ping Xiao, UK
Yangchuan Xing, USA
Shuangxi Xing, China
N. Xu, China
Doron Yadlovker, Israel
Yingkui Yang,
Khaled Youssef, USA
Kui Yu, Canada
William W. Yu, USA
Haibo Zeng, China
Tianyou Zhai, Japan
Renyun Zhang, Sweden
Bin Zhang, China
Yanbao Zhao, China
Lianxi Zheng, Singapore
Chunyi Zhi, Hong Kong

Contents

Functional Carbon Nanomaterials, Myoung-Woon Moon, Ho-Young Kim, Aiying Wang, and Ashkan Vaziri
Volume 2014, Article ID 202143, 2 pages

Decontamination of Surfaces Exposed to Carbon-Based Nanotubes and Nanomaterials, Paul Su, Babak Haghpanah, William W. Doerr, Zahra Karimi, Syed Hassan, Louis Gritzo, Ahmed A. Busnaina, and Ashkan Vaziri
Volume 2014, Article ID 249603, 9 pages

The Activity of [60]Fullerene Derivatives Bearing Amine and Carboxylic Solubilizing Groups against *Escherichia coli*: A Comparative Study, Dmitry G. Deryabin, Olga K. Davydova, Zulfiya ZH. Yankina, Alexey S. Vasilchenko, Sergei A. Miroshnikov, Alexey B. Kornev, Anastasiya V. Ivanchikhina, and Pavel A. Troshin
Volume 2014, Article ID 907435, 9 pages

Incorporated W Roles on Microstructure and Properties of W-C:H Films by a Hybrid Linear Ion Beam Systems, Peng Guo, Peiling Ke, and Aiying Wang
Volume 2013, Article ID 530959, 8 pages

Field Emission Properties of Carbon Nanotubes with Boron Doping and H_2O Adsorption, Yijun Wang, Liuding Wang, and Cheng Yan
Volume 2013, Article ID 404923, 6 pages

Nitrogen-Doped Carbon Nanotubes Synthesised by Pyrolysis of (4-[(pyridine-4-yl)methylidene]aminophenyl)ferrocene, Godfrey Keru, Patrick G. Ndungu, and Vincent O. Nyamori
Volume 2013, Article ID 750318, 7 pages

Adsorption of Eu(III) on oMWCNTs: Effects of pH, Ionic Strength, Solid-Liquid Ratio and Water-Soluble Fullerene, P. Liu, J. Wang, W. Qi, Zh. Li, JJ. Bi, and WS. Wu
Volume 2013, Article ID 689214, 9 pages

Hindawi Publishing Corporation
Journal of Nanomaterials
Volume 2014, Article ID 202143, 2 pages
http://dx.doi.org/10.1155/2014/202143

Editorial
Functional Carbon Nanomaterials

Myoung-Woon Moon,[1] Ho-Young Kim,[2] Aiying Wang,[3] and Ashkan Vaziri[4]

[1] *Korea Institute of Science and Technology (KIST), Seoul 136-791, Republic of Korea*
[2] *Seoul National University, Seoul 151-744, Republic of Korea*
[3] *Ningbo Institute of Materials Technology and Engineering (NIMTE), Chinese Academy of Sciences, Ningbo 315201, China*
[4] *Northeastern University, Boston, MA 02155, USA*

Correspondence should be addressed to Myoung-Woon Moon; mwmoon@kist.re.kr

Received 4 January 2014; Accepted 4 January 2014; Published 10 February 2014

Copyright © 2014 Myoung-Woon Moon et al. This is an open access article distributed under the Creative Commons Attribution License, which permits unrestricted use, distribution, and reproduction in any medium, provided the original work is properly cited.

Carbon nanomaterials have increasingly gained interest due to their capability of forming various allotropes including nanotubes, fullerenes, diamond, amorphous carbon, and more recently, graphene. Carbon nanomaterials or nanostructures offer exceptional flexibility in tailoring various properties for specific purposes due to their chemical inertness. For example, they have resistance to acidic or basic media, structural stability at high temperatures in the absence of air, and tunable chemical nature of hydrophobicity. Different physical forms of carbon materials in nanoscale, including thin films, graphene foams or sponges, carbon nanotube forests, carbon fibers, carbon nanowalls, and porous carbon materials, can lead to a variety of functions. In addition to chemical and physical modifications, the functions of carbon nanomaterials can be altered by adding or doping metal elements such as gold, platinum, or silver. Carbon nanomaterials have been widely applied for use in energy, environment, water, biomedicine, and other fields.

The major goals of this special issue are to find novel fabrication methods for functional carbon nanomaterials and the modification or nanostructuring of carbon surfaces for novel functionalization in up-to-date applications. This issue includes research papers covering a wide range of current progress on the modification with physical and chemical methods and characterization for functional carbon nanomaterials and nanostructures, as well as the related applications in hard coatings, energy storage and conversion, water filtration, catalysts, and decontamination. The combined study on novel experimental preparation of carbon nanomaterials such as carbon nanotubes, amorphous carbon films, and fullerenes and the theoretical investigations of functional carbon nanomaterials with first-principles/ab initio calculation are presented. Moreover, in this special issue, some papers are particularly invited to address the above mentioned issues.

One paper of this special issue presents the functional coating of W-incorporated diamond-like carbon (W-C : H) films fabricated by a hybrid beams system consisting of a DC magnetron sputtering and a linear ion source. It shows that the films mainly exhibited the feature of amorphous carbon when W concentration in the films was less than 4.38 at.%, where the incorporated W atoms would be bonded with C atoms and resulted in the formation of nanoparticles along with a minimum value of residual compressive stress, a higher hardness, and better tribological properties.

Most papers in this special issue provide the functionalization of carbon nanotubes with doping and special modifications. Another paper explores field emission properties of carbon nanotubes (CNTs) with boron doping and H_2O adsorption using ab initio calculations. They investigated the electron field emission performance of CNTs simultaneously adsorbed with one H_2O molecule and doped with one boron atom (BCNT + H_2O). The results indicate that the electrons are localized at the top of BCNT + H_2O and the electronic density of states (DOS) around the Fermi level is enhanced. A different paper addresses nitrogen-doped CNTs synthesized by pyrolysis of (4-{[(pyridine-4-yl)methylidene]amino}phenyl) ferrocene in a solution of either acetonitrile or toluene as carbon source. Acetonitrile was found to produce mainly N-CNTs with "bamboo" morphology while toluene formed a mixture of pristine CNTs

and N-CNTs in the ratio of 1:1. The authors of another paper addressed adsorption of Eu(III) on multiwalled CNTs in terms of effects of pH, ionic strength, solid-liquid ratio, and water-soluble fullerene. The sorption process was influenced strongly by pH changes and ionic strength. An additional paper of this issue reports a comparative investigation of the antibacterial activity of two water-soluble fullerene derivatives bearing protonated amine (AF) and deprotonated carboxylic groups appended to the fullerene cage via organic linkers. It reveals that the water-soluble cationic fullerene derivative AF possesses promising antibacterial activity, which might be utilized in the development of novel types of chemical disinfectants.

One more paper addresses decontamination of surfaces exposed to carbon-based nanotubes and nanomaterials. Contamination of surfaces by nanomaterials can happen due to accidental spillage and release or gradual accumulation during processing or handling. The article proposes and investigates a potential method for surface decontamination of carbon-based nanomaterials using solvent cleaning and wipes. The results show that the removal efficiencies for single- and multiwalled carbon nanotubes from silicon wafers sprayed with water-surfactant solutions prior to mechanical wiping are greater than 90% and 95%, respectively. The need for further studies to understand the mechanisms of nanomaterial removal from surfaces and development of standard techniques for surface decontamination of nanomaterials is highlighted.

Acknowledgments

The editors would like to thank the authors for their contributions to this special issue and the reviewers for their time and dedication.

Myoung-Woon Moon
Ho-Young Kim
Aiying Wang
Ashkan Vaziri

Research Article

Decontamination of Surfaces Exposed to Carbon-Based Nanotubes and Nanomaterials

Paul Su,[1] Babak Haghpanah,[2] William W. Doerr,[1] Zahra Karimi,[2] Syed Hassan,[2] Louis Gritzo,[1] Ahmed A. Busnaina,[2] and Ashkan Vaziri[2]

[1] *FM Global, Norwood, MA 02062, USA*
[2] *Department of Mechanical and Industrial Engineering, Northeastern University, Boston, MA 02115, USA*

Correspondence should be addressed to Paul Su; pocheng.su@fmglobal.com

Received 10 October 2013; Accepted 12 December 2013; Published 16 January 2014

Academic Editor: Aiying Wang

Copyright © 2014 Paul Su et al. This is an open access article distributed under the Creative Commons Attribution License, which permits unrestricted use, distribution, and reproduction in any medium, provided the original work is properly cited.

Contamination of surfaces by nanomaterials can happen due to accidental spillage and release or gradual accumulation during processing or handling. Considering the increasingly wide use of nanomaterials in industry and research labs and also taking into account the diversity of physical and chemical properties of different nanomaterials (such as solubility, aggregation/agglomeration, and surface reactivity), there is a pressing need to define reliable nanomaterial-specific decontamination guidelines. In this paper, we propose and investigate a potential method for surface decontamination of carbon-based nanomaterials using solvent cleaning and wipes. The results show that the removal efficiency for single- and multiwalled carbon nanotubes from silicon wafers sprayed with water-surfactant solutions prior to mechanical wiping is greater than 90% and 95%, respectively. The need for further studies to understand the mechanisms of nanomaterial removal from surfaces and development of standard techniques for surface decontamination of nanomaterials is highlighted.

1. Introduction

Nanomaterials (NMs) are becoming more involved in an increasingly wide range of applications such as in composites, electronics, and automotive, biomedical, and personal care products due to their novel properties and functions [1–3]. Over the last decade, the global production of NMs has experienced a huge growth. For instance, the global production of carbon nanotubes (CNTs) was increased from ca. 280 metric tons in 2006 [4] to ca. 1000 metric tons in 2010 [5] and is anticipated to reach thousands of metric tons in the following decade [4, 6, 7]. The increasing production and application of NMs highlight the need for development of preventive measures and regulations to minimize NM exposure in case of accidental release inside the workplace [2, 8–14].

The potential toxicity of nanomaterials has raised concern about health and safety issues related to the production and use of NMs and their environmental impact as well as potential for contaminated property damage or business interruption due to accidental release of nanomaterials [2, 8–21]. Preliminary toxicology studies on nanomaterials, including in vitro cytotoxicity [22–24], small animal toxicology [25], and extrapolation of these data to the human scale, reveal the potentially toxic nature of these materials to human biological systems [26–29]. There are several inherent physiochemical factors including NM size, shape, chemical composition, surface charge, surface modifications, and adsorption capacity that can possibly affect the toxicity of nanomaterials [12]. Physical and environmental phenomena such as dissolution, agglomeration, and disagglomeration are the other factors that determine the toxic interaction of nanomaterials with biological systems [28–30]. The three exposure possibilities to NMs are respiration, dermal penetration through skin contact with contaminated surfaces, and digestion [31, 32]. Thus, effective decontamination measures for removal of nanomaterials from contaminated surfaces, air, and possibly water supplies are needed. With regard to NM air decontamination, high efficiency particulate air (HEPA) filters can trap air suspended NMs with high efficiency through various filtration mechanisms [33, 34]. As a first attempt to introduce approaches to remove NMs from contaminated water, Yang et al. reported that the CNTs suspended in the aqueous

environment can be transformed into large micron size aggregates in the presence of calcium ion (Ca^{2+}) and then effectively removed via paper filtration [35]. Concerning the removal of NM from surfaces of solids, the strong attachment of NMs to substrates by van der Waals forces [36–45] and also their increased contact area make it difficult to remove NMs [46, 47]. Their removal has to be through a physical force that could be applied directly (wipe or brush) or through a fluid (such as ultrasonic, megasonics, or a fluid jet) [48–59]. A few studies [9, 34, 60–62] have provided some basic surface cleaning recommendations for research laboratories and workplace in case of accidental release and spillage of nanomaterials. These recommendations include using vacuum cleaners fitted with HEPA filters on the exhaust to collect the NMs and prevent their dispersion in the air [63]; cleaning the liquid spills by applying absorbent materials/liquid traps [60, 61]; use of walk-off mats such as a clean room mat or "sticky mats" at access/egress points to limit propagation of particles outside the premises [34, 60, 61]; and avoiding the use of energetic methods such as dry sweeping and compressed air for removing the deposited nanomaterials [60–62]. After any visible NM contamination is removed, it is suggested to use wet or electrostatic microfiber cleaning cloths to remove residual NMs from the surfaces while causing minimal dispersion into the air [64].

In this paper, we focus on the surface decontamination of carbon-based NMs which are regarded as one of the most common types of NMs. We propose chemical (solvents, surfactants, etc.) cleaning as a potential method for surface decontamination of carbon-based NMs. In Section 2, we provide an overview of the current state of literature for common categories of solving media and summarize the solubility data for most carbon-based NMs. In Section 3, we discuss our preliminary results on surface decontamination of silicon wafers covered with single- and multiwalled CNTs using a simple wiping procedure and we quantify the removal efficiency of different solvents using scanning microscope imaging of samples before and after cleaning. Finally, conclusions will be derived and the need for further studies will be discussed in Section 4.

2. Chemical Cleaning

Chemical cleaning (or solvent cleaning) is used conventionally for the removal of residues, contaminants, or soils deposited on or attached to a substrate surface. The basic concept of chemical cleaning is to dissolve or suspend the contaminants and to eliminate them by the removal of the cleaning media. Studies on the solubility of nanomaterials have shown that many engineered NMs have minimal solubility and dispersibility in water or many common solvents [65–68]. For example, CNTs are shown to be neither soluble nor wettable by water or many other solvents, making them hard to be physically dispersed which in addition to cleaning is critical for obtaining individual CNTs for research and other applications [69–71]. Therefore, various surfactants [65, 69, 72–76], solvents [77–82], and polymers [83–85], as well as DNA [86–88] have been explored to noncovalently dissolve and disperse CNTs into a liquid phase. Figure 1 summarizes the solubility of single-walled CNT in various solvents as reported in the literature. In general, surfactants (short for surface active agents) are more effective for dissolving higher quantities of single-walled and multiwalled CNTs in water compared to most available solvents. The use of surfactants for the cleaning process is particularly of high interest for a number of reasons; water is a safe and convenient substance and surfactants are cheap, commercially available, and easy to use. The highest solubility is currently reported for an aqueous solution of gum arabic (15% wt), where 3% wt. (~30 mg/mL) solubility was obtained using sonication at 50 W and 43 kHz for a relatively short duration of 15–20 minutes [85]. We have also explored the available data on solubility of other common carbon-based NMs. In Figure 2, we have summarized the available results on the solubility of C_{60} fullerene in different solvents. Motivations for studying the solubility of fullerenes in solvents include exploring chemical reactions pathways for fullerene, their purification methods, and extracting higher fullerenes [66, 89–101]. Also, the aqueous solubility of fullerenes with the use of surfactants has been investigated for potential biological applications and the results are included in Figure 2 [102–106]. The differences in the reported solubility of fullerenes in a specific solvent in different studies can be attributed to the effects of temperature, illumination, or sonication during the solving process. Extraordinary temperature dependence is observed in the solubility of fullerene C_{60} in some solvents, reaching its maximum magnitude near 280 K and decreasing remarkably by increasing the temperature above this value [97, 107, 108]. In addition, there are studies investigating the solubility of higher-order fullerenes [90, 91, 93, 96–98] or combinations of different-order fullerenes [93] in various solvents. Studies performed on the solubility of fullerenes in aqueous media suggest that the solubility rates of fullerene in water-surfactants are several orders of magnitude less than the solubility rates obtained by successful solvents.

Since CNTs are one of the most common carbon-based NMs, we have discussed the efficiency of different solvents for dissolving CNTs in the following sections in more details.

2.1. Surfactants as the Cleaning Media. Surfactants can weaken the strong bond between particles and substrate by reduction of the surface tension, prevention of particle readhesion by creating a repulsive zone between the particles and substrate, and suspension of the particles in the solution by their amphiphilic mechanism [110]. When surfactants are available in adequate concentrations in the solution, they get adsorbed on the surface of CNTs, forming cylindrical micelles or hemimicelles which make CNTs soluble in water [111]. It is necessary that the amount of surfactant dissolved in the aqueous media should be far exceeding the surfactant critical micelle concentration to ensure that enough surfactant molecules can be absorbed onto the surface of the nanotubes to make them suspended and dissolved in water. For example, Sun et al. [76] obtained the optimum concentration of some surfactants for suspending CNTs as equal to 10 mg/mL. However, critical micelle concentrations for these surfactants from the literature are far less than

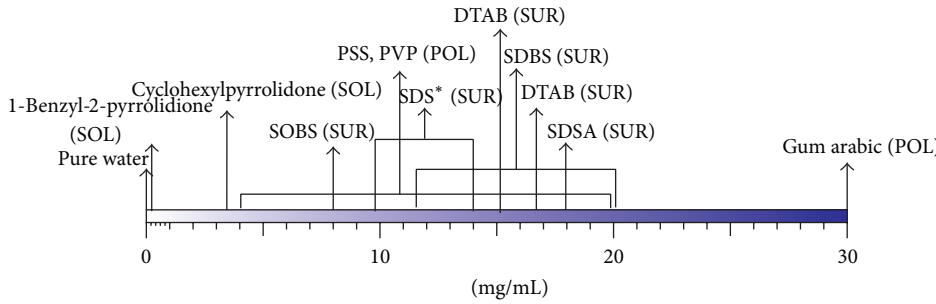

1,2-Dichlorobenzene (SOL), chloroform (SOL), 1-methylnaphthalene (SOL), 1-bromo-2-methylnaphthalene (SOL), and DMA (SOL) < 0.1 mg/mL

*The reported value is for MWCNTs

Figure 1: High concentration surfactant-, polymer-, and solvent-based suspensions of SWCNT as reported in the literature [69, 72, 75–81].

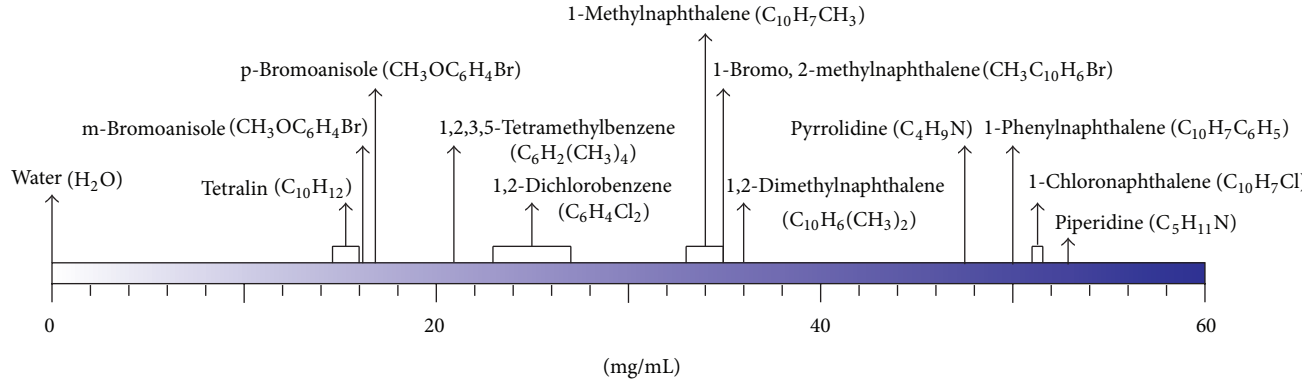

Figure 2: Solubility of C_{60} in the most effective C_{60} solvents at 298° K, as reported in the literature [66, 89, 99–101, 108, 109].

10 mg/mL [76]. In the use of surfactants as the cleaning media combined use of surfactants and mechanical removal might be necessary to fully overcome the adherence of NMs to substrates [110, 112].

Islam et al. [69] investigated the solubility of single-walled CNTs in water with different anionic, cationic, and nonionic surfactants by using a long-duration (16–24 hr) sonication procedure. They showed that the anionic surfactants sodium dodecylbenzene sulfonate (NaDDBS) and the close chemical relative, sodium 4-n-octylbenzene sulfonate (NaOBS), had high solubility of single-walled carbon nanotubes, with the solubility of up to 20 mg/mL and 8 mg/mL of CNTs, respectively. Using a different solubilization technique, Moore et al. [75] reported the relatively high ability of NaDDBS, and a close relative sodium dodecylsulfonate (SDSA), and sodium dodecyl sulfate (SDS) to individually suspend nanotubes in water [113]. However, of much interest for the purposes of cleaning, they showed that the difunctional block copolymer nonionic surfactants with high molecular weight have high suspendbility (19.2–28.2 mg/mL) but relatively lower individual dispersion quality compared to other surfactants. They concluded that the high dispersion rate of copolymers such as Pluronic F 98 and PEO-PBO-PEO triblock copolymer (EBE) is related to the enhanced steric stabilization by long polymeric groups. The solubility of multiwalled carbon nanotubes in SDS was studied by Zhou et al. [40]. They reported 1.4 wt% (14 mg/mL) as the maximum concentration of multiwalled CNTs that can be homogenously dispersed in the aqueous solution. It is noteworthy that the reported quantities for a single surfactant in different studies might be significantly different due to various factors related to the amount of surfactant used, test temperature, mechanical forcing and CNT type and manufacturing method.

2.2. Polymers as the Cleaning Media. Polymers appear as promising options for dissolving CNTs in aqueous media in high concentrations with relatively low agitation [75, 83–85]. O'Connell et al. [84] studied the solution of SWNTs in water by noncovalently associating them with linear polymers such as polyvinylpyrrolidone (PVP) and polystyrene sulfonate (PSS). They suggested that the high concentration solution of CNTs (2% wt., ~20 mg/mL) can be obtained by the robust association/wrapping of polymer layers with/around the nanotubes.

2.3. Solvents as the Cleaning Media. The use of solvents as cleaning agents to remove nanomaterials is questionable for a number of reasons. First, many of the solvents proposed to disperse nanotubes have some level of toxicity. Second, the solubility/dispersibility of many of the proposed solvents is

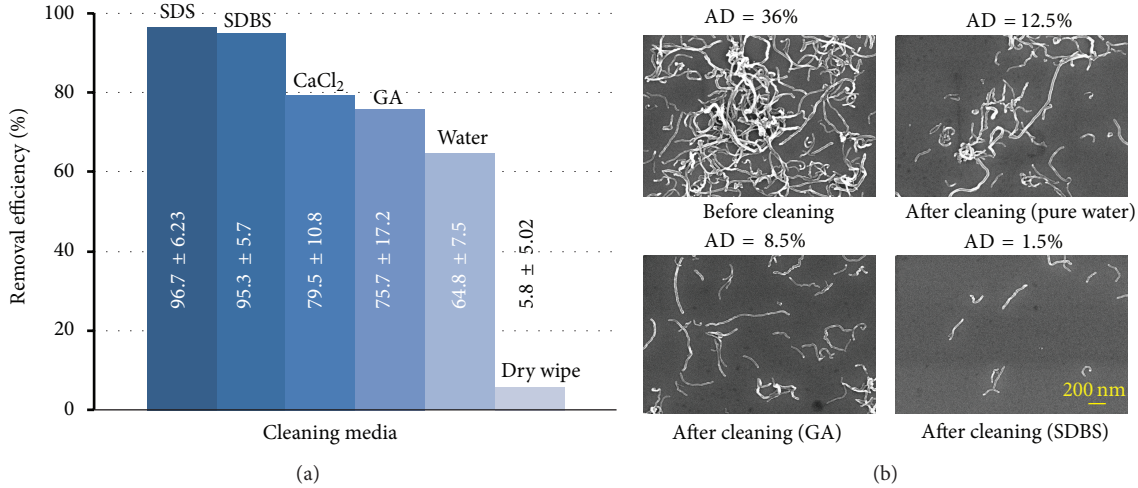

FIGURE 3: (a) MWCNT removal efficiency of SDS, SDBS, $CaCl_2$, gum arabic (GA), water, and dry wiping as discussed in Section 3. (b) Sample SEM image of the surface of multiwalled carbon nanotubes deposited silicon wafers before cleaning (AD = 36%) and after wipe cleaning with pure water (AD = 12.5%), gum Arabic (AD = 8.5%), and SDBS surfactant (AD = 1.5%). The average precleaning areal density was approximately 34% for all samples.

below 0.1 mg/mL, far less than the solubility of surfactants. Parra-Vasquez et al. [81] investigated the solubility of SWNTs obtained by different methods of production in superacids (e.g., fuming sulfuric and chlorosulfonic acids) and showed that high concentrations (>100 mg/mL) of SWNTs are spontaneously dispersed in acids within minutes. However, the use of acids as the cleaning media in the cleanup process does not seem reasonable because of the hazards in handling and usage and removal of acids and also the potential damage to the substrate.

3. Experimental Investigation: Removal Efficiency of CNT Chemical Cleaning

In this section, experimental investigations were performed to assess the removal efficiency of CNTs deposited on the surface of silicon wafers using different cleaning media. The CNTs used for this study were combustion chemical vapor deposition (CCVD) grown, acid purified carbon nanotubes dispersed in polyvinylpyrrolidone (PVP) surfactant. The average length and diameter of the MWCNTs used in this study were measured to be 250 nm and 15 nm, respectively. The averaged length and diameter of SWNCTs were 200 nm and 1.2 nm, respectively. In the experiments, carbon nanotubes in the form of pristine liquid solution were deposited on surface of silicon wafers ((111) orientation, nitrogen/phosphorus doped, P/E surface, and with mechanical grading) using the spin coating process. The wafers were 3″ in diameter and the spin coating was performed for 1 min at 3000 RPM. After spin coating, the CNT deposited wafers were heated at 105°C for 90 sec. in order to dry the wafer surface completely. A total number of 30 images with equal magnification and resolution were taken from different spots of each wafer surface using scanning electron microscope (SEM) imaging. The CNT surface aerial concentration for each image was then determined using an image processing program incorporated in MATLAB software. Average CNT aerial density from 30 different images of each wafer was obtained and used in the analysis. The average aerial density of the wafers, denoted by AD, was approximately 34% for SWCNTs and 36% for MWCNTs after the spin coating.

First, we have assessed the multiwalled CNT removal efficiency of two surfactants (i.e., SDBS (sodium dodecylbenzene sulfonate) and SDS (sodium dodecyl sulfate)), one polymer (gum arabic), one mineral salt (calcium chloride), and pure water in a simple wipe cleaning method. The concentrations of SDBS, SDS, $CaCl_2$, and gum arabic (GA) were 1.5%, 4%, 11%, and 10% wt, respectively. The mineral salt calcium chloride was specifically chosen since it was shown to be capable of transforming dispersed CNT in aqueous environment into aggregates [35]. The CNT-coated wafers were first treated by different cleaning media and then cleaned with a piece of nonwoven polyester/cellulose fabric. In the experiments, first the cleaning medium was sprayed on the surface of the wafer. After 2 minutes, the wafer was manually wiped once unidirectionally. The estimated hand pressure and wiping duration were 2 kPa and 5 sec., respectively. The wafer was dried using nitrogen gas after the cleaning. After cleaning, the wafers were imaged using SEM and the average final area density for each wafer was obtained by postprocessing the images as explained above. The removal efficiency was defined as the difference between the initial and the final average CNT aerial densities. Figure 3(a) shows the quantitative comparison of MWNT surface removal efficiency by different cleaning media used in this study. Figure 3(b) shows the SEM images of MWCNT-coated wafer surfaces before and after cleaning using different cleaning media. The two surfactants used in the experiments, SDS and SDBS, showed the highest MWCNT removal rates among all the solvent cleaning media with removal efficiency greater than 95%. The high removal efficiency in using the surfactant as the cleaning media can be attributed to the role of

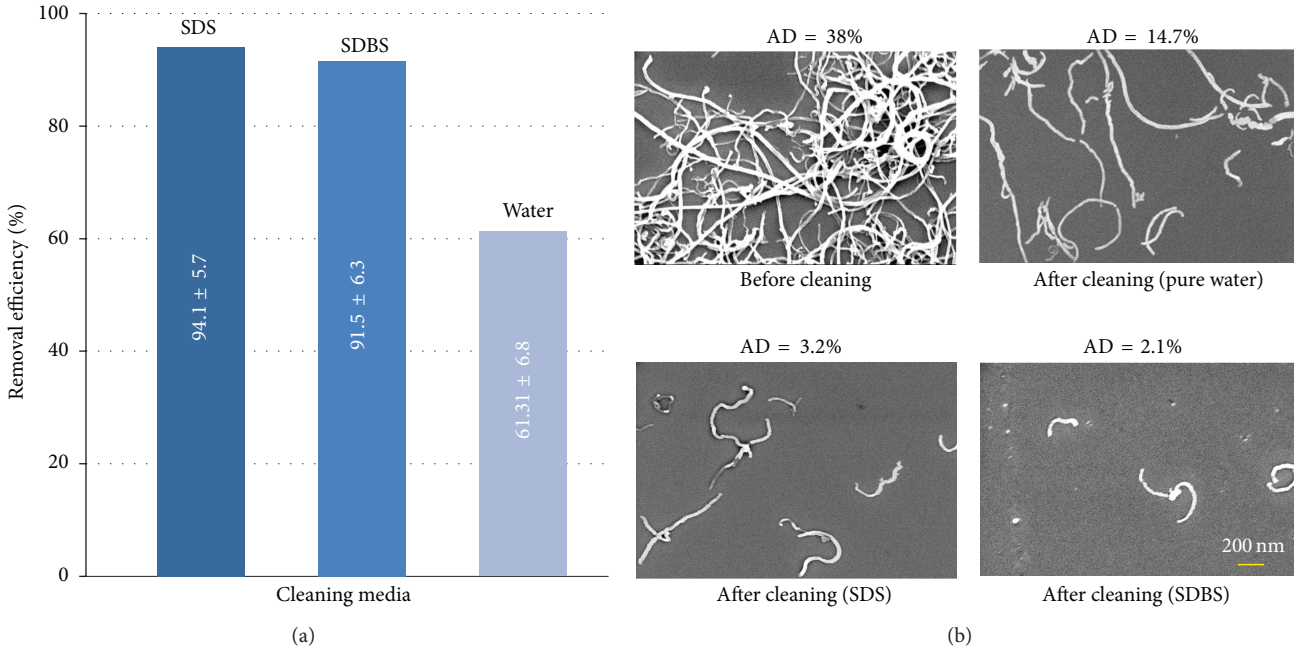

Figure 4: (a) SWCNT removal efficiency of SDS, SDBS and water as discussed in Section 3. (b) Sample SEM image of the surface of SWNTs deposited silicon wafers before cleaning (AD = 38%) and after wipe cleaning with pure water (AD = 14.7%), SDBS (AD = 3.2%), and SDS surfactant (AD = 2.1%). The average precleaning areal density was approximately 36% for all samples.

surfactant micelles in suspending the CNTs in aqueous media and increasing the soaking ability of water by decreasing the water surface tension. Pure water has the removal efficiency of almost 65% on the silicon wafer substrate. Gum arabic and $CaCl_2$ have comparable removal efficiency of approximately 76% and 80%, respectively, standing between the removal efficiency of pure water and that of surfactants solutions.

As the next step, we measured the single-walled CNT removal efficiency of two surfactants (i.e., SDBS (sodium dodecylbenzene sulfonate) and SDS (sodium dodecyl sulfate)), and pure water in the same wipe cleaning method. The two surfactants were chosen since they showed the highest efficiency for the removal of MWCNTs from the surface of silicon wafer in the last section. The same deposition and wiping methods were used. In Figure 4(a) a quantitative comparison of SWNT surface removal efficiency by different cleaning media is given. The two surfactants showed high SWCNT removal capability with efficiency greater than 90%. Wiping after pure water spray resulted in a removal efficiency of approximately 61%. Figure 4(b) shows sample SEM images of SWCNT-coated wafer surfaces before and after cleaning.

4. Conclusions

We proposed solvent cleaning as a technique for surface decontamination of carbon-based NMs such as CNTs, which can potentially be used for removal of nanomaterial adhered to surfaces caused by unwanted spillage and release or the gradual accumulation during the processing or handling. The role of cleaning media (i.e., surfactants, solvents, etc.) in facilitating the mechanical removal of single- and multiwalled CNTs from contaminated surfaces was discussed. The challenges associated with this technique include the high levels of agglomeration of CNTs and extremely low solubility in water and many common solvents, which tend to lower the efficiency of this method. Based on our pilot study presented in Section 3, the removal efficiency of single- and multiwalled carbon nanotubes using two different water-surfactant solutions from a highly smooth surface of a silicon wafer through wiping is greater than 90% and 95%, respectively. The higher removal efficiency for multiwalled carbon nanotubes can be attributed to the larger value of the binding energy density holding the nanotube aggregates together for MWCNTs compared to SWCNTs [114]. Surfactants are economical, commercially available, and easy to use. These factors make surfactants a good candidate for the removal of CNTs deposited on surfaces. However, more studies are needed to determine the effectiveness of CNT removal using the solvent cleaning technique for CNTs obtained by various production methods, with different chemical modifications or attached on different substrates.

Conflict of Interests

The authors declare that there is no conflict of interests regarding the publication of this article.

Acknowledgments

The authors thank Dr. Sivasubramanian Somu for the insightful discussion and Ms. Joy McNally for assistance in providing the journal articles referenced in this work. This work was supported in part by FM Global and by the U.S. Air Force

Office of Scientific Research under AFOSR YIP Grant Award, #FA FA9550-10-1-0145, under the technical supervision of Dr. Joycelyn Harrison. The authors also acknowledge the support of the Center of High-Rate Nanomanufacturing at Northeastern University for the experimental part of the study.

References

[1] The project on emerging nanotechnologies, Nanotechnology Consumer Products Inventory, http://www.nanotechproject.org/inventories/consumer/analysis_draft/.

[2] A. Dowling, *Nanoscience and Nanotechnologies: Opportunities and Uncertainties*, The Royal Society and the Royal Academy of Engineering, London, UK, 2004.

[3] S. S. Oh, D. H. Kim, M.-W. Moon et al., "Indium nanowires synthesized at an ultrafast rate," *Advanced Materials*, vol. 20, no. 6, pp. 1093–1098, 2008.

[4] S. Glotzer, *International Assessment of Research and Development in Simulation-Based Engineering and Science*, Imperial College Press, London, UK, 2010.

[5] "News briefing," *Nature*, vol. 461, pp. 702–703, 2009.

[6] Progress and perspectives in the carbon nanotube world, http://www.azonano.com/details.asp?articleID=2619.

[7] A. M. Thayer, "Carbon nanotubes by the metric ton: anticipating new commercial applications, producers increase capacity," *Chemical & Engineering News*, vol. 85, no. 46, pp. 29–38, 2007.

[8] National Institute for Occupational Safety and Health-NIOSH, "Approaches to safe nanotechnology—managing the health and safety concerns associated with engineered nanomaterials," 2009, http://www.cdc.gov/niosh/docs/2009-125/.

[9] US Department of Energy, "Approaches to Nanomaterial ES&H," Department of Energy, Nanoscale Science Centers, 2008, http://science.energy.gov/~/media/bes/pdf/doe_nsrc_approach_to_nanomaterial_esh.pdf.

[10] "Report, L.s.E.R.T., Nanotechnology: Recent Developments, Risks and Opportunities," 2007, http://www.lloyds.com/~/media/Lloyds/Archive/Lloyds%20Market%20Gallery/Lloyds%20Market%20Gallery/ER_Nanotechnology_Report.pdf.

[11] A. Hett, *Nanotechnology: Small Size—Large Impact*, Risk Dialogue Series, Swiss Reinsurance, Zurich, Switzerland, 2005.

[12] US Environmental Protection Agency-EPA, Nanotechnology white paper, 2007, http://www.epa.gov/osa/pdfs/nanotech/epa-nanotechnology-whitepaper-0207.pdf.

[13] National Institute for Occupational Safety and Health-NIOSH, "Progress toward safe nanotechnology in the workplace," 2007.

[14] A. C. Lin, "Size matters: regulating nanotechnology," *Harvard Environmental Law Review*, vol. 31, no. 2, pp. 349–408, 2007.

[15] P. Su, *It Is a Small World*, Reason, FM Global Research, Norwood, Mass, USA, 2010.

[16] National Institute for Occupational Safety and Health-NIOSH, "Interim guidance for worker medical screening, hazard surveillance pertaining to engineered nanoparticles," 2009, http://www.cdc.gov/niosh/docs/2009-116/.

[17] Y. Ju-Nam and J. R. Lead, "Manufactured nanoparticles: an overview of their chemistry, interactions and potential environmental implications," *Science of the Total Environment*, vol. 400, no. 1–3, pp. 396–414, 2008.

[18] National Institute for Occupational Safety and Health-NIOSH, Strategic plan for NIOSH nanotechnology research and guidance, http://www.cdc.gov/niosh/docs/2010-105/.

[19] C. A. Poland, R. Duffin, I. Kinloch et al., "Carbon nanotubes introduced into the abdominal cavity of mice show asbestos-like pathogenicity in a pilot study," *Nature Nanotechnology*, vol. 3, no. 7, pp. 423–428, 2008.

[20] V. J. Feron, J. H. E. Arts, C. F. Kuper, P. J. Slootweg, and R. A. Woutersen, "Health risks associated with inhaled nasal toxicants," *Critical Reviews in Toxicology*, vol. 31, no. 3, pp. 313–347, 2001.

[21] A. D. Maynard, P. A. Baron, M. Foley, A. A. Shvedova, E. R. Kisin, and V. Castranova, "Exposure to carbon nanotube material: aerosol release during the handling of unrefined single-walled carbon nanotube material," *Journal of Toxicology and Environmental Health A*, vol. 67, no. 1, pp. 87–107, 2004.

[22] G. Jia, H. Wang, L. Yan et al., "Cytotoxicity of carbon nanomaterials: single-wall nanotube, multi-wall nanotube, and fullerene," *Environmental Science & Technology*, vol. 39, no. 5, pp. 1378–1383, 2005.

[23] C. Kirchner, T. Liedl, S. Kudera et al., "Cytotoxicity of colloidal CdSe and CdSe/ZnS nanoparticles," *Nano Letters*, vol. 5, no. 2, pp. 331–338, 2005.

[24] N. Lewinski, V. Colvin, and R. Drezek, "Cytotoxicity of nanopartides," *Small*, vol. 4, no. 1, pp. 26–49, 2008.

[25] C.-W. Lam, J. T. James, R. McCluskey, and R. L. Hunter, "Pulmonary toxicity of single-wall carbon nanotubes in mice 7 and 90 days after intractracheal instillation," *Toxicological Sciences*, vol. 77, no. 1, pp. 126–134, 2004.

[26] S. F. Hansen, E. S. Michelson, A. Kamper, P. Borling, F. Stuer-Lauridsen, and A. Baun, "Categorization framework to aid exposure assessment of nanomaterials in consumer products," *Ecotoxicology*, vol. 17, no. 5, pp. 438–447, 2008.

[27] Z. D. Ok, J. C. Benneyan, and J. A. Isaacs, "Nanotechnology environmental, health, and safety issues: brief literature review since 2000," in *Proceedings of the IEEE International Symposium on Sustainable Systems and Technology (ISSST '09)*, pp. 1–5, Phoenix, Ariz, USA, May 2009.

[28] P. J. A. Borm, D. Robbins, S. Haubold et al., "The potential risks of nanomaterials: a review carried out for ECETOC," *Particle and Fibre Toxicology*, vol. 3, no. 1, article 11, 2006.

[29] R. Hardman, "A toxicologic review of quantum dots: toxicity depends on physicochemical and environmental factors," *Environmental Health Perspectives*, vol. 114, no. 2, pp. 165–172, 2006.

[30] J. Liu, D. M. Aruguete, M. Murayama, and M. F. Hochella Jr., "Influence of size and aggregation on the reactivity of an environmentally and industrially relevant nanomaterial (PbS)," *Environmental Science & Technology*, vol. 43, no. 21, pp. 8178–8183, 2009.

[31] R. J. Aitken, K. S. Creely, and C. L. Tran, *Nanoparticles: An Occupational Hygiene Review*, Institute of Occupational Medicine, Edinburgh, UK, 2004.

[32] AFSSET, "Nanomaterials: Effects on the Environment and Human Health," 2006, http://www.afssa.fr/ET/DocumentsET/afsset-summary-nanomaterials.pdf.

[33] L. Golanski, A. Guiot, and F. Tardif, "Efficiency of fibrous filters and personal protective equipments against nanoaerosols," Tech. Rep., Euripean Strategy for Nanosafety, 2008.

[34] AFSSET, "Nanomaterials and occupational safety," 2008, http://www.afssa.fr/ET/DocumentsET/08_07_ED_Nanomateriaux_2_Avis_EV.pdf.

[35] S.-T. Yang, H. Wang, Y. Wang, Y. Wang, H. Nie, and Y. Liu, "Removal of carbon nanotubes from aqueous environment with filter paper," *Chemosphere*, vol. 82, no. 4, pp. 621–626, 2011.

[36] T. S. Chow, "Size-dependent adhesion of nanoparticles on rough substrates," *Journal of Physics Condensed Matter*, vol. 15, no. 2, pp. L83–L87, 2003.

[37] S. Joo and D. F. Baldwin, "Adhesion mechanisms of nanoparticle silver to substrate materials: identification," *Nanotechnology*, vol. 21, no. 5, Article ID 055204, 2010.

[38] J. D. Whittaker, E. D. Minot, D. M. Tanenbaum, P. L. McEuen, and R. C. Davis, "Measurement of the adhesion force between carbon nanotubes and a silicon dioxide substrate," *Nano Letters*, vol. 6, no. 5, pp. 953–957, 2006.

[39] L. Qu, L. Dai, M. Stone, Z. Xia, and L. W. Zhong, "Carbon nanotube arrays with strong shear binding-on and easy normal lifting-off," *Science*, vol. 322, no. 5899, pp. 238–242, 2008.

[40] W. Zhou, Y. Huang, B. Liu et al., "Adhesion between carbon nanotubes and substrate: mimicking the gecko foot-hair," *Nano*, vol. 2, no. 3, pp. 175–179, 2007.

[41] B. Yurdumakan, N. R. Raravikar, P. M. Ajayan, and A. Dhinojwala, "Synthetic gecko foot-hairs from multiwalled carbon nanotubes," *Chemical Communications*, no. 30, pp. 3799–3801, 2005.

[42] S. Hu, T. H. Kim, J. G. Park, and A. A. Busnaina, "Effect of different deposition mediums on the adhesion and removal of particles," *Journal of the Electrochemical Society*, vol. 157, no. 6, pp. H662–H665, 2010.

[43] D. S. Rimai, D. J. Quesnel, and A. A. Busnaina, "The adhesion of dry particles in the nanometer to micrometer-size range," *Colloids and Surfaces A*, vol. 165, no. 1–3, pp. 3–10, 2000.

[44] A. A. Busnaina and T. Elsawy, "The effect of relative humidity on particle adhesion and removal," *The Journal of Adhesion*, vol. 74, no. 1–4, pp. 391–409, 2000.

[45] J. Tang and A. A. Busnaina, "The effect of time and humidity on particle adhesion and removal," *The Journal of Adhesion*, vol. 74, no. 1–4, pp. 411–419, 2000.

[46] S. Krishnan, A. A. Busnaina, D. S. Rimai, and L. P. Demejo, "The adhesion-induced deformation and the removal of submicrometer particles," *Journal of Adhesion Science and Technology*, vol. 8, no. 11, pp. 1357–1370, 1994.

[47] A. Busnaina, J. Taylor, and I. Kashkoush, "Measurement of the adhesion and removal forces of submicrometer particles on silicon substrates," *Journal of Adhesion Science and Technology*, vol. 7, no. 5, pp. 441–455, 1993.

[48] P. Karimi, T. Kim, J. Aceros, J. Park, and A. A. Busnaina, "The removal of nanoparticles from sub-micron trenches using megasonics," *Microelectronic Engineering*, vol. 87, no. 9, pp. 1665–1668, 2010.

[49] K. Bakhtari, R. O. Guldiken, P. Makaram, A. A. Busnaina, and J.-G. Park, "Experimental and numerical investigation of nanoparticle removal using acoustic streaming and the effect of time," *Journal of the Electrochemical Society*, vol. 153, no. 9, pp. G846–G850, 2006.

[50] K. Bakhtari, R. O. Guldiken, A. A. Busnaina, and J.-G. Park, "Experimental and analytical study of submicrometer particle removal from deep trenches," *Journal of the Electrochemical Society*, vol. 153, no. 9, pp. C603–C607, 2006.

[51] O. Guldiken, K. Bakhtari, A. Busnaina, and J. Park, "Metrology and removal of nanoparticles from 500 micron deep trenches," *Solid State Phenomena*, vol. 103-104, pp. 137–140, 2005.

[52] N. Moumen and A. A. Busnaina, "Removal of submicrometre alumina particles from silicon oxide substrates," *Surface Engineering*, vol. 17, no. 5, pp. 422–424, 2001.

[53] A. A. Busnaina and F. Dai, "The removal of submicron particles in liquid-based cleaning," *The Journal of Adhesion*, vol. 67, no. 1–4, pp. 181–193, 1998.

[54] A. A. Busnaina and G. W. Gale, "Removal of silica particles from silicon substrates using megasonic cleaning," *Particulate Science and Technology*, vol. 15, no. 3-4, pp. 361–369, 1997.

[55] G. W. Gale and A. A. Busnaina, "Removal of particulate contaminants using ultrasonics and megasonics: a review," *Particulate Science and Technology*, vol. 13, no. 3-4, pp. 197–211, 1995.

[56] D. S. Rimai and A. A. Busnaina, "Adhesion and removal of particles from surfaces," *Particulate Science and Technology*, vol. 13, no. 3-4, pp. 249–270, 1995.

[57] A. A. Busnaina, I. I. Kashkoush, and G. W. Gale, "An experimental study of megasonic cleaning of silicon wafers," *Journal of the Electrochemical Society*, vol. 142, no. 8, pp. 2812–2817, 1995.

[58] A. Busnaina and I. Kashkoush, "The effect of time, temperature and particle size on submicron particle removal using ultrasonic cleaning," *Chemical Engineering Communications*, vol. 125, no. 1, pp. 47–61, 1993.

[59] I. Kashkoush and A. Busnaina, "Submicron particle removal using ultrasonic cleaning," *Particulate Science and Technology*, vol. 11, no. 1-2, pp. 11–24, 1993.

[60] British Standard Institute, "Nanotechnologies—part 1: good practices guide for specifying manufactured nanomaterials," 2007, http://www3.imperial.ac.uk/pls/portallive/docs/1/34683697.PDF.

[61] British Standard Institute, "Nanotechnologies—part 2: guide to safe handling and disposal of manufactured nanomaterials," 2007, http://www3.imperial.ac.uk/pls/portallive/docs/1/34683696.PDF.

[62] BAUA, "Guidance for the handling and use of nanomaterials at the workplace," 2007.

[63] M. Klenke, "First results for safe procedures for handling nanoparticles," Tech. Rep., European Strategy for Nanosafety, 2008.

[64] D. Fleury, J. A. S. Bomfim, S. Metz, J. X. Bouillard, and J.-M. Brignon, "Nanoparticle risk management and cost evaluation: a general framework," *Journal of Physics*, vol. 304, no. 1, Article ID 012084, 2011.

[65] L. Vaisman, H. D. Wagner, and G. Marom, "The role of surfactants in dispersion of carbon nanotubes," *Advances in Colloid and Interface Science*, vol. 128–130, pp. 37–46, 2006.

[66] R. S. Ruoff, D. S. Tse, R. Malhotra, and D. C. Lorents, "Solubility of C_{60} in a variety of solvents," *The Journal of Physical Chemistry*, vol. 97, no. 13, pp. 3379–3383, 1993.

[67] W. W. Yu, E. Chang, R. Drezek, and V. L. Colvin, "Water-soluble quantum dots for biomedical applications," *Biochemical and Biophysical Research Communications*, vol. 348, no. 3, pp. 781–786, 2006.

[68] B. L. Frankamp, N. O. Fischer, R. Hong, S. Srivastava, and V. M. Rotello, "Surface modification using cubic silsesquioxane ligands. Facile synthesis of water-soluble metal oxide nanoparticles," *Chemistry of Materials*, vol. 18, no. 4, pp. 956–959, 2006.

[69] M. F. Islam, E. Rojas, D. M. Bergey, A. T. Johnson, and A. G. Yodh, "High weight fraction surfactant solubilization of single-wall carbon nanotubes in water," *Nano Letters*, vol. 3, no. 2, pp. 269–273, 2003.

[70] S.-W. Kim, S. Kim, J. B. Tracy, A. Jasanoff, and M. G. Bawendi, "Phosphine oxide polymer for water-soluble nanoparticles," *Journal of the American Chemical Society*, vol. 127, no. 13, pp. 4556–4557, 2005.

[71] C. X. Song, V. Labhasetwar, H. Murphy et al., "Formulation and characterization of biodegradable nanoparticles for intravascular local drug delivery," *Journal of Controlled Release*, vol. 43, no. 2-3, pp. 197–212, 1997.

[72] J. Yu, N. Grossiord, C. E. Koning, and J. Loos, "Controlling the dispersion of multi-wall carbon nanotubes in aqueous surfactant solution," *Carbon*, vol. 45, no. 3, pp. 618–623, 2007.

[73] H. Wang, W. Zhou, D. L. Ho et al., "Dispersing single-walled carbon nanotubes with surfactants: a small angle neutron scattering study," *Nano Letters*, vol. 4, no. 9, pp. 1789–1793, 2004.

[74] O. Matarredona, H. Rhoads, Z. Li, J. H. Harwell, L. Balzano, and D. E. Resasco, "Dispersion of single-walled carbon nanotubes in aqueous solutions of the anionic surfactant NaDDBS," *The Journal of Physical Chemistry B*, vol. 107, no. 48, pp. 13357–13367, 2003.

[75] V. C. Moore, M. S. Strano, E. H. Haroz et al., "Individually suspended single-walled carbon nanotubes in various surfactants," *Nano Letters*, vol. 3, no. 10, pp. 1379–1382, 2003.

[76] Z. Sun, V. Nicolosi, D. Rickard, S. D. Bergin, D. Aherne, and J. N. Coleman, "Quantitative evaluation of surfactant-stabilized single-walled carbon nanotubes: dispersion quality and its correlation with zeta potential," *The Journal of Physical Chemistry C*, vol. 112, no. 29, pp. 10692–10699, 2008.

[77] J. L. Bahr, E. T. Mickelson, M. J. Bronikowski, R. E. Smalley, and J. M. Tour, "Dissolution of small diameter single-wall carbon nanotubes in organic solvents?" *Chemical Communications*, no. 2, pp. 193–194, 2001.

[78] B. J. Landi, H. J. Ruf, J. J. Worman, and R. P. Raffaelle, "Effects of alkyl amide solvents on the dispersion of single-wall carbon nanotubes," *The Journal of Physical Chemistry B*, vol. 108, no. 44, pp. 17089–17095, 2004.

[79] S. D. Bergin, Z. Sun, P. Streich, J. Hamilton, and J. N. Coleman, "New solvents for nanotubes: approaching the dispersibility of surfactants," *The Journal of Physical Chemistry C*, vol. 114, no. 1, pp. 231–237, 2010.

[80] K. D. Ausman, R. Piner, O. Lourie, R. S. Ruoff, and M. Korobov, "Organic solvent dispersions of single-walled carbon nanotubes: toward solutions of pristine nanotubes," *The Journal of Physical Chemistry B*, vol. 104, no. 38, pp. 8911–8915, 2000.

[81] A. N. G. Parra-Vasquez, N. Behabtu, M. J. Green et al., "Spontaneous dissolution of ultralong single-and multiwalled carbon nanotubes," *ACS Nano*, vol. 4, no. 7, pp. 3969–3978, 2010.

[82] S. D. Bergin, V. Nicolosi, P. V. Streich et al., "Towards solutions of single-walled carbon nanotubes in common solvents," *Advanced Materials*, vol. 20, no. 10, pp. 1876–1881, 2008.

[83] J. N. Coleman, A. B. Dalton, S. Curran et al., "Phase separation of carbon nanotubes and turbostratic graphite using a functional organic polymer," *Advanced Materials*, vol. 12, no. 3, pp. 213–216, 2000.

[84] M. J. O'Connell, P. Boul, L. M. Ericson et al., "Reversible water-solubilization of single-walled carbon nanotubes by polymer wrapping," *Chemical Physics Letters*, vol. 342, no. 3-4, pp. 265–271, 2001.

[85] R. Bandyopadhyaya, E. Nativ-Roth, O. Regev, and R. Yerushalmi-Rozen, "Stabilization of individual carbon nanotubes in aqueous solutions," *Nano Letters*, vol. 2, no. 1, pp. 25–28, 2002.

[86] R. Haggenmueller, S. S. Rahatekar, J. A. Fagan et al., "Comparison of the quality of aqueous dispersions of single wall carbon nanotubes using surfactants and biomolecules," *Langmuir*, vol. 24, no. 9, pp. 5070–5078, 2008.

[87] S. Badaire, C. Zakri, M. Maugey et al., "Liquid crystals of DNA-stabilized carbon nanotubes," *Advanced Materials*, vol. 17, no. 13, pp. 1673–1676, 2005.

[88] M. Zheng, A. Jagota, M. S. Strano et al., "Structure-based carbon nanotube sorting by sequence-dependent DNA assembly," *Science*, vol. 302, no. 5650, pp. 1545–1548, 2003.

[89] W. A. Scrivens and J. M. Tour, "Potent solvents for C_{60} and their utility for the rapid acquisition of ^{13}C NMR data for fullerenes," *Journal of the Chemical Society, Chemical Communications*, no. 15, pp. 1207–1209, 1993.

[90] M. T. Beck, "Solubility and molecular state of C_{60} and C_{70} in solvents and solvent mixtures," *Pure and Applied Chemistry*, vol. 70, no. 10, pp. 1881–1887, 1998.

[91] T. Tomiyama, S. Uchiyama, and H. Shinohara, "Solubility and partial specific volumes of C_{60} and C_{70}," *Chemical Physics Letters*, vol. 264, no. 1-2, pp. 143–148, 1997.

[92] V. N. Bezmel'nitsyn, A. V. Eletskii, and M. V. Okun', "Fullerenes in solutions," *Physics-Uspekhi*, vol. 41, no. 11, article 1091, 1998.

[93] K. N. Semenov, N. A. Charykov, V. A. Keskinov, A. K. Piartman, A. A. Blokhin, and A. A. Kopyrin, "Solubility of light fullerenes in organic solvents," *Journal of Chemical & Engineering Data*, vol. 55, no. 1, pp. 13–36, 2010.

[94] Y. Marcus, A. L. Smith, M. V. Korobov, A. L. Mirakyan, N. V. Avramenko, and E. B. Stukalin, "Solubility of C_{60} fullerene," *The Journal of Physical Chemistry B*, vol. 105, no. 13, pp. 2499–2506, 2001.

[95] N. Sivaraman, R. Dhamodaran, I. Kaliappan, T. G. Srinivasan, P. R. Vasudeva Rao, and C. K. Mathews, "Solubility of C_{60} in organic solvents," *The Journal of Organic Chemistry*, vol. 57, no. 22, pp. 6077–6079, 1992.

[96] N. Sivaraman, R. Dhamodaran, I. Kaliappan, T. G. Srinivasan, V. P. R. Rao, and C. K. Mathews, "Solubility of C_{70} in organic solvents," *Fullerene Science and Technology*, vol. 2, no. 3, pp. 233–246, 1994.

[97] X. Zhou, J. Liu, Z. Jin, Z. Gu, Y. Wu, and Y. Sun, "Solubility of fullerene C_{60} and C_{70} in toluene, O-xylene and carbon disulfide at various temperatures," *Fullerene Science and Technology*, vol. 5, no. 1, pp. 285–290, 1997.

[98] M. V. Korobov, A. L. Mirakyan, N. V. Avramenko, G. Olofsson, A. L. Smith, and R. S. Ruoff, "Calorimetric studies of solvates of C_{60} and C_{70} with aromatic solvents," *The Journal of Physical Chemistry B*, vol. 103, no. 8, pp. 1339–1346, 1999.

[99] D. Heymann, "Solubility of C_{60} in alcohols and alkanes," *Carbon*, vol. 34, no. 5, pp. 627–631, 1996.

[100] S. Talukdar, P. Pradhan, and A. Banerji, "Electron donor-acceptor interactions of C_{60} with n-and π-donors : a rational approach towards its solubility," *Fullerene Science and Technology*, vol. 5, no. 3, pp. 547–557, 1997.

[101] N. V. Avramenko, E. B. Stukalin, and M. V. Korobov, "Thermodynamic properties of the molecular complexes of C_{60} with monosubstituted naphthalenes," *Journal of Thermal Analysis and Calorimetry*, vol. 82, no. 1, pp. 125–127, 2005.

[102] I. Ramakanth and A. Patnaik, "Characteristics of solubilization and encapsulation of fullerene C_{60} in non-ionic Triton X-100 micelles," *Carbon*, vol. 46, no. 4, pp. 692–698, 2008.

[103] A. Beeby, J. Eastoe, and R. K. Heenan, "Solubilisation of C_{60} in aqueous micellar solution," *Journal of the Chemical Society, Chemical Communications*, no. 2, pp. 173–175, 1994.

[104] Y. N. Yamakoshi, T. Yagami, K. Fukuhara, S. Sueyoshi, and N. Miyata, "Solubilization of fullerenes into water with polyvinylpyrrolidone applicable to biological tests," *Journal of*

the Chemical Society, Chemical Communications, no. 4, pp. 517–518, 1994.

[105] D. T. Lai, M. A. Neumann, M. Matsumoto, and J. Sunamoto, "Complexation of C_{60} fullerene with cholesteryl group-bearing pullulan in aqueous medium," *Chemistry Letters*, vol. 29, no. 1, pp. 64–65, 2000.

[106] H. Hungerbuehler, D. M. Guldi, and K. D. Asmus, "Incorporation of C_{60} into artificial lipid membranes," *Journal of the American Chemical Society*, vol. 115, no. 8, pp. 3386–3387, 1993.

[107] R. S. Ruoff, R. Malhotra, D. L. Huestis, D. S. Tse, and D. C. Lorents, "Anomalous solubility behaviour of C_{60}," *Nature*, vol. 362, no. 6416, pp. 140–141, 1993.

[108] R. J. Doome, S. Dermaut, A. Fonseca, M. Hammida, and J. B. Nagy, "New evidences for the anomalous temperature-dependent solubility of C_{60} and C_{70} fullerenes in various solvents," *Fullerene Science and Technology*, vol. 5, no. 7, pp. 1593–1606, 1997.

[109] M. T. Beck, G. Mandi, and S. Keki, "Solubility and molecular state of C_{60} in organic solvents," in *Recent Advances in the Chemistry and Physics of Fullerenes and Related Materials. 187th Electrochemical Society Meeting*, pp. 1510–1518, Electrochemical Society, Reno, Nev, USA, 1995.

[110] D. Ng, P. Y. Huang, Y. R. Jeng, and H. Liang, "Nanoparticle removal mechanisms during post-CMP cleaning," *Electrochemical and Solid-State Letters*, vol. 10, no. 8, pp. H227–H231, 2007.

[111] K. Yurekli, C. A. Mitchell, and R. Krishnamoorti, "Small-angle neutron scattering from surfactant-assisted aqueous dispersions of carbon nanotubes," *Journal of the American Chemical Society*, vol. 126, no. 32, pp. 9902–9903, 2004.

[112] D. Ng, S. Kundu, M. Kulkarni, and H. Liang, "Role of surfactant molecules in post-CMP cleaning," *Journal of the Electrochemical Society*, vol. 155, no. 2, pp. H64–H68, 2008.

[113] M. J. O'Connell, S. H. Bachilo, C. B. Huffman et al., "Band gap fluorescence from individual single-walled carbon nanotubes," *Science*, vol. 297, no. 5581, pp. 593–596, 2002.

[114] Y. Y. Huang and E. M. Terentjev, "Dispersion of carbon nanotubes: mixing, sonication, stabilization, and composite properties," *Polymers*, vol. 4, no. 1, pp. 275–295, 2012.

Research Article

The Activity of [60]Fullerene Derivatives Bearing Amine and Carboxylic Solubilizing Groups against *Escherichia coli*: A Comparative Study

Dmitry G. Deryabin,[1,2] Olga K. Davydova,[1] Zulfiya ZH. Yankina,[1] Alexey S. Vasilchenko,[1,3] Sergei A. Miroshnikov,[2] Alexey B. Kornev,[4] Anastasiya V. Ivanchikhina,[4] and Pavel A. Troshin[4]

[1] *Department of Microbiology, Orenburg State University, Pobedy Avenue 13, Orenburg 460018, Russia*
[2] *All-Russia Research Institute of Beef Cattle Breeding, 9 Yanvarya Street 29, Orenburg 460000, Russia*
[3] *Institute of Cellular and Intracellular Symbiosis, RAS, Pionerskaya Street 11, Orenburg 460000, Russia*
[4] *Institute for Problems of Chemical Physics of RAS, Academician Semenov Avenue 1, Chernogolovka, Moscow Region 142432, Russia*

Correspondence should be addressed to Dmitry G. Deryabin; dgderyabin@yandex.ru

Received 5 September 2013; Accepted 13 November 2013; Published 15 January 2014

Academic Editor: Myoung-Woon Moon

Copyright © 2014 Dmitry G. Deryabin et al. This is an open access article distributed under the Creative Commons Attribution License, which permits unrestricted use, distribution, and reproduction in any medium, provided the original work is properly cited.

We report a comparative investigation of the antibacterial activity of two water-soluble fullerene derivatives bearing protonated amine (AF) and deprotonated carboxylic (CF) groups appended to the fullerene cage via organic linkers. The negatively charged fullerene derivative CF showed no tendency to bind to the bacterial cells and, consequently, no significant antibacterial activity. In contrast, the compound AF loaded with cationic groups showed strong and partially irreversible binding to the negatively charged *Escherichia coli* K12 TG1 cells and to human erythrocytes, also possessing negative zeta potential. Adsorption of AF on the bacterial surface was visualized by atomic force microscopy revealing the formation of specific clusters (AF aggregates) surrounding the bacterial cell. Incubation of *E. coli* K12 TG1 with AF led to a dose-dependent bactericidal effect with LD_{50} = 79.1 μM. The presence of human erythrocytes in the test medium decreased the AF antibacterial activity. Thus we reveal that the water-soluble cationic fullerene derivative AF possesses promising antibacterial activity, which might be utilized in the development of novel types of chemical disinfectants.

1. Introduction

Investigation of carbon-based nanomaterials (CBN) has made a great impact on the research in the fields of physics, material chemistry and technology, and also life sciences. Water-soluble forms of carbon have been studied intensively worldwide during recent decades. We would like to refer to [1], dedicated to the studies of biological activity of CBN [1]. Toxicity and biocompatibility of CBN were two major points addressed in this journal. Several review papers discussing the biological activities of CBN appeared later [2–4].

Fullerenes, the spherical carbon cages, and their functional derivatives attracted particular attention due to their unusual molecular structures and properties. Recent publications proved lower toxicity of fullerenes compared to other types of CBN, especially carbon nanotubes [5, 6]. It is known that pristine fullerenes such as C_{60} and C_{70} are very hydrophobic and possess virtually zero solubility in water. Classical fullerene derivatives bearing one organic addend appended to the fullerene cage typically have a strong tendency to aggregate in aqueous solutions [7]. Such aggregation lowers their activity significantly and hinders their practical applications. The problem can be solved by using chemically functionalized fullerene derivatives bearing a sufficient number of hydrophilic (or, even better, ionic) functional groups that significantly improve the solubility of these compounds in water [8, 9].

A number of studies have reported effective gene delivery [10] and antioxidative [11], neuroprotective [12], antitumour

[13], and antiviral [14] activities of fullerenes and their derivatives, which makes further exploration of this exciting family of CBN promising. Interesting results were obtained while studying antimicrobial activity of fullerenes [15]. It was proposed that membrane targeting [16], respiratory chain inhibition [17], and photosensitizing effects [18] of fullerene derivatives are responsible for the observed antibacterial action. Functionalizing the carbon cage with hydrophilic functional groups brings up new biological properties. For example, alkylated C_{60}-bis(N,N-dimethylpyrrolidinium iodide) adducts inhibited bacterial growth effectively [19]. Similarly, a carboxylic derivative of [60]fullerene bearing malonic acid fragments on the carbon cage protected mice from bacteria-induced meningitis without direct bacterial inhibition [20]. It should be emphasized that mechanisms of the observed antibacterial activity and selectivity of different types of fullerene derivatives are not currently well understood.

Recently we have succeeded in the selective synthesis of different types of water-soluble fullerene derivatives possessing 4–8 organic addends attached to the cages of C_{60} and C_{70} fullerenes [21–24]. These compounds became available on a large (multigram) scale sufficient for performing a thorough investigation of their biological activities [25, 26]. In the present work, we performed a comparative study of antibacterial activity of two different water-soluble derivatives of [60]fullerene bearing protonated amine (AF) and carboxylate (CF) groups appended to the fullerene cage via organic linkers (Figure 1).

2. Experimental

2.1. Fullerene Derivatives. The fullerene derivatives AF, bearing four protonated 4-(2-pyridyl)piperazine-1-yl groups, and CF, comprising five residues of phenylacetic acid, were synthesized according to the previously published procedures [25, 26]. Spectroscopic characteristics of the prepared samples were identical to the previously reported data [25, 26].

2.2. Preparation and Characterization of Aqueous Fullerene Suspensions. Aqueous suspensions of fullerene derivatives (4 mg/mL) were prepared in deionized water, filtered through syringe filters, and poured into vials that were prewashed several times with filtered water in order to remove dust particles. The suspensions were then incubated for about 2 hours at 20°C, thus allowing the colloidal systems to reach an equilibrium. The temperature control accuracy was 0.1°C.

The size of fullerene aggregates in aqueous suspension was measured using dynamic light scattering (DLS) with a Photocor Complex (Photocor Instruments Inc., USA) setup equipped with a He-Ne laser ($\lambda = 679.5$ nm). The mutual diffusion coefficients of fullerene aggregates were computed from the DLS data using the DynaLS program (Alango, Israel). Hydrodynamic diameters of the fullerene aggregates were calculated from the mutual diffusion coefficients using the Einstein-Stokes formula for diffusion coefficients of spherical particles.

Electrophoresis of fullerene derivatives was performed in a 1.5% agarose gel at a constant voltage of 150 V and current of 100 mA, so that the electric field strength was 5 V/cm. After 20 min of electrophoresis, migration of compounds was evaluated by visible and UV light on a transilluminator (Vilber Lourmat, France). The Smoluchowski equation was used to calculate the ζ-potential from the electrophoretic mobility.

Adsorption and fluorescence spectra of fullerene derivatives in aqueous suspensions were recorded with a Fluorat-02 Panorama spectrofluorometer (Lumex, Russia) in a spectral range of 220–400 nm.

2.3. Bacterial Strain and Cultures Preparation. The experiments involving bacterial cells were performed using the *Escherichia coli* K12 TG1 strain. The applicability of this strain for evaluation of bactericidal activity of a wide range of carbon-based nanomaterials has been demonstrated previously [26]. The bacteria were grown in LB-broth (Sigma-Aldrich, USA) for 18–24 hours at 37°C, after which the cells were harvested by centrifugation at 1000 g for 10 min, washed once with the distilled water, and diluted to achieve the optical density of 0.5 absorption units at 640 nm, which corresponds to the concentration of 3.5×10^9 colony-forming units (CFU) per 1 mL.

The human erythrocytes were collected from blood (0 Rh+) by centrifugation at 1000 g for 10 min and washing the precipitate with 0.85% NaCl solution twice. The final concentration of erythrocytes was 7×10^8 cells/mL, which is equal to the surface area of 0.02 m^2/mL.

2.4. Investigation of Adsorption/Desorption of Fullerene Derivatives on the Cell Surfaces. Fullerene derivatives AF and CF were introduced to the cell suspensions to prepare a series of samples with 2, 1, 0.5, 0.25, 0.12, 0.06, and 0.03 μM concentrations of the compounds. After incubation at 37°C for 60 minutes, the prokaryotic and eukaryotic cells modified with the fullerene derivatives were separated by centrifugation at 1000 g for 10 min. The concentration of unbound fullerene derivative in the supernatant was determined using fluorimetry in the case of AF and photometry in the case of CF. The value of the adsorption was calculated using

$$A = \frac{(C_0 - C_e)}{S}, \quad (1)$$

where C_0 is the starting concentration of the fullerene derivative, C_e is the equilibrium concentration of the fullerene derivative after partial adsorption to the cell membranes (determined in supernatant), and S is the surface area of the cells.

The evaluation of the fullerene derivative desorption from the bacterial cells surfaces was performed by dispersing the *E. coli* K12 TG1 cells in the solutions of AF ($C_0 = 1\,\mu$M) and CF ($C_0 = 10\,\mu$M); is incubation of these dispersions for 60 min is followed by centrifugation. The precipitated bacterial biomass was separated and dispersed again in an equal volume of distilled water, while the supernatant liquor

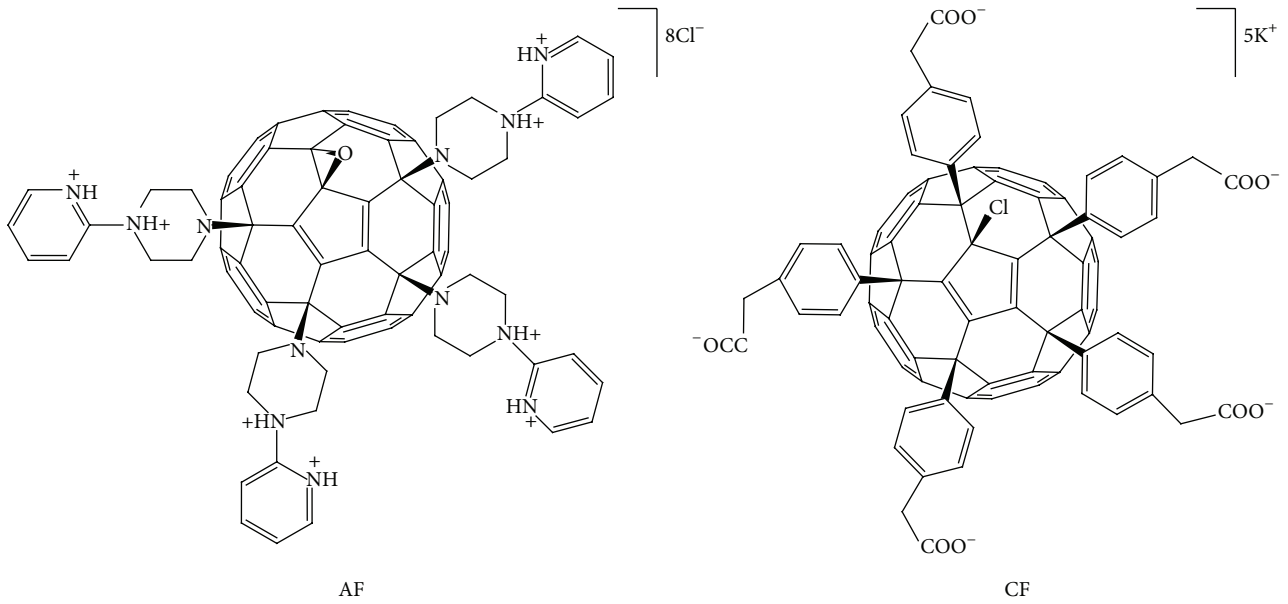

Figure 1: Molecular structures of the fullerene derivatives AF and CF.

was analysed using fluorimetry or photometry to reveal the concentrations of the AF and CF, respectively. The bacterial cells that were redispersed in distilled water were subjected again to centrifugation and the concentration of the fullerene derivative in the supernatant liquid was determined. Washing the bacterial biomass with distilled water was repeated ten times and each time the fullerene derivative concentration in the supernatant was determined in order to reconstruct the desorption profiles.

2.5. Atomic Force Microscopy. Visualization of the bacterial cells in the intact form or after incubation with the fullerene derivatives was performed using an atomic force microscope (SMM-2000; Proton-MIET, Russia). An aliquot (20 μL) of the suspension comprising either intact cells of *E. coli* K12 TG1 or their mixtures with AF and CF was applied to the freshly prepared mica at 95% relative humidity and 20–22°C. The samples were scanned in a contact mode using V-shaped silicon nitride cantilevers MSCT-AUNM (Veeco Instruments Inc., USA) with a spring constant of 0.01 N/m and a tip curvature of 150–250 Å. Quantitative morphometrical analysis of the images was performed using standard software provided with the microscope.

2.6. Bactericidal Activity of Fullerene Derivatives. The test samples comprised a suspension of *E. coli* K12 TG1 at a concentration of 3.5×10^9 CFU/mL and the fullerene derivatives were added in concentrations ranging from 25 to 200 μM. In a separate series of experiments, *E. coli* was incubated with fullerene derivatives in the presence of human erythrocytes at a concentration 7×10^8 cells/mL. This concentration of erythrocytes provided an equal surface area compared to the total area of the bacterial cell membranes (0.02 m^2/mL). Lysis of erythrocytes was induced by addition of 0.05% saponin prior to plating the prepared cultures in the BCP-agar medium.

The 100 μL aliquots taken from the experimental samples 60 min after the fullerene derivative addition and the control samples comprising no fullerene derivatives were diluted with 900 μL of distilled water. Small portions of the obtained test samples (10 μL) were inoculated on the plates with BCP-agar (Bio-Merieux, France). The percentage of the bacterial cells retaining their viability during incubation with fullerenes (calculated as the total number of CFU in an experimental sample divided by the number of CFU in the control series) was determined after an additional 18–24 h incubation of the samples at 37°C. The dose of the fullerene derivative causing the death of 50% of the microbial cells (LD_{50}) was obtained from these experiments.

3. Results and Discussion

3.1. Characterization of Aqueous Fullerene Suspensions. The attachment of the cationic (protonated amine, AF) or anionic (COO–, CF) functional groups to the [60]fullerene cage significantly increased the solubility of the fullerene derivatives in water. The resulting aqueous solutions of AF and CF (concentration 4 mg/mL) were transparent and had a bright orange-brown colour. No fullerene precipitation was observed in the course of the experiments indicating that the prepared aqueous systems were rather stable with respect to aggregation and sedimentation of the dissolved/dispersed compounds.

The dynamic light scattering (DLS) experiments allowed the determination of the hydrodynamic sizes of the fullerene nanoparticles in aqueous suspensions. The DLS experiments showed that both [60]fullerene derivatives form aggregates in aqueous solutions with diameters of 2–200 nm (AF) and 70–100 nm (CF) (Figure 2). Larger particles of 10^4–10^6 nm (AF)

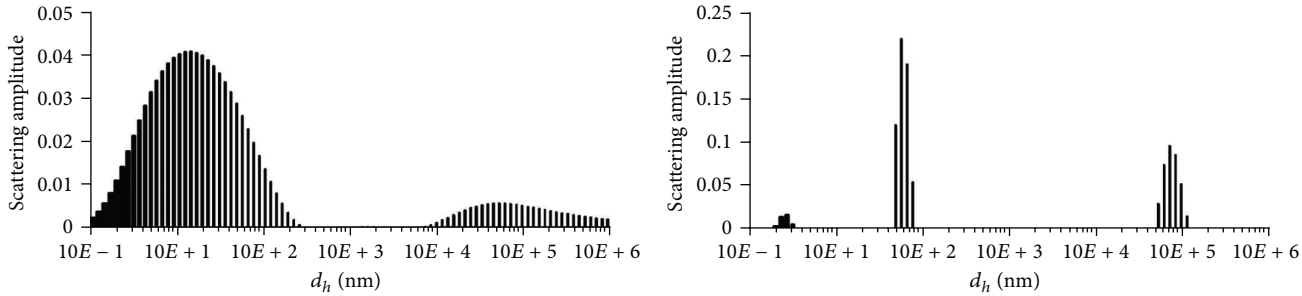

Figure 2: DLS profiles for aqueous suspensions of AF (a) and CF (b) fullerene derivatives.

and ~10^5 nm (CF) correspond, most likely, to some larger aggregates composed of the fullerene derivative aggregates.

The DLS measurements indicated that the fullerene aggregates formed in aqueous systems have rather high polydispersity, particularly in the case of AF. These data correspond well to the previous reports describing spherical and irregularly shaped fullerene-based nanoparticles as revealed by DLS, TEM, and high-resolution TEM [26–30]. Very similar nanoclusters were also observed in this work using atomic force microscopy (AFM) (see Section 3.4); therefore, DLS and AFM measurements showed that fullerene derivatives AF and CF undergo aggregation in aqueous solutions. Taking into account the typical size of these aggregates, the bicomponent systems comprising the fullerene derivative and water should be called a colloidal solution or even suspension rather than a true solution.

3.2. Detection of Electric Charge and Zeta Potentials of Fullerene Derivatives. The agarose gel electrophoresis performed for the water-soluble fullerene derivatives AF and CF showed that they represent highly charged cationic and anionic species (Table 1). Motion of the carboxylic fullerene derivative towards the anode was clearly detectable with the naked eye. Movement of the amino fullerene towards the cathode was visualized with a UV transilluminator owing to the reasonably strong fluorescence of the AF compound (see Section 3.3).

The calculated zeta potentials (ζ) of AF and CF were +41.5 mV and −52.2 mV, respectively. It is known that aqueous fullerene suspensions are stable if the zeta potentials of the dispersed particles are smaller than −15 mV or higher than +15 mV [31]. Very pronounced cationic and anionic properties of AF and CF, respectively, reflected in the values of their zeta potentials, explain the high solubility of these compounds in water. It should also be noted that compounds of AF and CF have rather large dipole moments since organic addends bearing ionic groups are located at one hemisphere of the fullerene cage.

Moreover, the functionalized part of the fullerene cage becomes hydrophilic, while the opposite side of the carbon sphere remains hydrophobic. Therefore, peculiarities of the molecular structures of AF and CF enable electrostatic dipole-dipole and hydrophobic-hydrophilic interactions. Thus, van der Waals attraction forces [32] bring the molecules of the fullerene derivatives together forming suspensions of solvated nanoparticles rather than true molecular solutions.

3.3. Spectroscopic Study of Fullerene Derivatives. An aqueous suspension of CF exhibits one distinct adsorption band with the maximum at 230 nm, while the AF suspension shows two bands with maxima at 240 and 300 nm (Figure 3(a)).

It is surprising that the amino fullerene showed unusually strong fluorescence with maxima at 360 nm under excitation with ultraviolet light at 240 or 300 nm. An excitation of AF solution at 240 nm produced 1.8 times higher fluorescence intensity compared to the excitation at 300 nm. The fluorescence intensity linearly depended on the concentration of AF in the range of 0–2 μM (Figure 3(b)).

The fluorescence was observed previously for pristine [60]fullerene and its derivatives. Compared to the week fluorescence of pristine C60 (λ_{max} = 689 nm) [33], the functionalized fullerenes show stronger emission bands shifted to the short-wave spectral range. For instance, blue-shifted fluorescence was reported for the fullerene derivatives bearing eight or ten pyridyl groups attached to the carbon cage [34].

In this study we used the fluorescence spectroscopy to perform an accurate investigation of AF adsorption and desorption on the surface of prokaryotic or eukaryotic cells. In the case of the nonfluorescent CF derivative, a photometric method was used for determination of its concentration in the experimental solutions.

3.4. Adsorption of the Fullerene Derivatives on the Surface of Prokaryotic or Eukaryotic Cells. The prokaryotic (*E. coli*) or eukaryotic (human erythrocyte) cells were incubated with the suspensions of the fullerene derivative AF at concentrations ranging from 0.03 to 1 μM. Then the cells loaded with the fullerene derivative were separated by centrifugation and the supernatant liquid was subjected to fluorescence analysis.

The fluorescence measurements revealed the residual amount of amino fullerene that was not adsorbed by the cells. These experiments show that AF has similarly strong but not identical affinity to both types of cell surfaces. An increase in the AF concentration resulted in a stronger binding of this compound to the cell membranes reflected by higher binding indexes (Table 2).

Table 1: Fullerene derivatives electrophoretic mobility and zeta-potentials.

Compound	Mobility in the electric field (the cathode side is on the left; the anode side is on the right)	Zeta potential, ζ, mV
AF	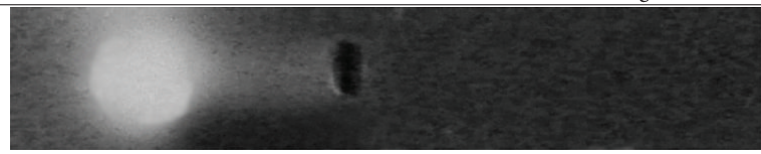	+41.5
CF	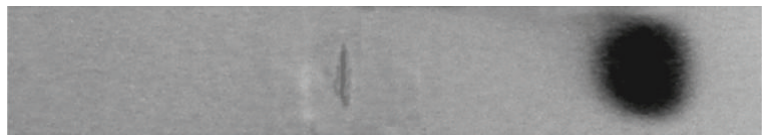	−52.2

Table 2: AF adsorption values on *E. coli* K12 TG1 cells and human erythrocytes.

Concentration of AF, μM			Adsorption values, μM/m^2	
Initial	Bound to cells			
	E. coli	Erythrocytes	*E. coli*	Erythrocytes
0.03	0.03 ± 0.01	0.02 ± 0.01	1.50	1.00
0.06	0.06 ± 0.01	0.06 ± 0.01	3.00	3.00
0.12	0.11 ± 0.02	0.10 ± 0.02	5.50	5.00
0.25	0.18 ± 0.01	0.16 ± 0.01	9.00	8.00
0.50	0.40 ± 0.02	0.23 ± 0.03	20.00	11.50
1.00	0.54 ± 0.17	0.39 ± 0.11	27.00	19.50

It is seen from Table 2 that AF when used in high concentrations has somewhat stronger affinity to the *E. coli* cells compared to the human erythrocytes. For example, the maximal adsorption values of 27.0 μM/m^2 and 19.5 μM/m^2 were obtained for *E. coli* and erythrocytes, respectively, when AF was added at an initial concentration of 1 μM.

Similar experiments were also performed for CF incubated with prokaryotic and eukaryotic cells. Due to the lower affinity of CF to the cell membranes, its initial concentration was increased to 10 μM. However, the fullerene derivative CF showed very weak adsorption on bacterial and erythrocyte cell surfaces, as characterized by maximal adsorption values of 1.91 μM/m^2 and 2.64 μM/m^2, respectively.

The binding of AF to the bacterial cells was confirmed by atomic force microscopy. Contact mode AFM allowed us to visualize the cells of *E. coli* before (Figure 4(a)) and after (Figure 4(b)) incubation with AF.

The analysis of the morphological characteristics of the bacterial cell incubated with AF showed a significant increase in the surface roughness. This change was caused by the granules (35–160 nm in diameter) that accumulated on the cell surface. We believe that these granules are represented by nanoclusters composed of AF molecules, which were also revealed by the DLS measurements (see above). In addition, the *E. coli* cells changed their length, width, and height, thus supporting additionally the action of the AF derivative. It is important to note that no signs of leakage of the cytosolic content of the bacterial cells to the environment were observed. This observation implies that the membrane disruption is not the leading mechanism of antibacterial activity of fullerenes [35, 36] in contrast to the action of other types of CBN [37].

Analysis of the morphological characteristics of *E. coli* cells incubated with CF did not reveal any significant changes in the cell surface roughness or size (Figure 4(c)). At the same time, scanning the substrate (mica) around the bacterial cells revealed freely located round-shaped features with a mean diameter of 217.90 ± 89.71 nm. These features might be attributed to the aggregates of the CF molecules also evident from the DLS data.

The sharply different behaviour of AF and CF with respect to the prokaryotic (bacterial) and eukaryotic (erythrocyte) cells can be explained mainly by the electrostatic forces. Indeed, the cationic AF (ζ = +41.5 mV) should have strong Coulomb attraction to the negatively charged *E. coli* cells (ζ = −50.0 mV) [38] and somewhat weaker attraction to the less negatively charged human erythrocytes (ζ = −13.5 mV) [39]. At the same time, the anionic fullerene derivative CF bearing a negative charge itself (ζ = −52.2 mV) cannot interact effectively with the surface of the prokaryotic and eukaryotic cells due to the Coulomb repulsion. The proposed mechanism relying on electrostatic interactions between the fullerene derivatives (or their aggregates) and cell membranes can explain both antibacterial [40] and cytotoxic [41, 42] effects of the fullerene derivatives. However, one should keep in mind that electrostatic interactions could be just an initial step of a complicated cascade of processes that occur when prokaryotic or eukaryotic cells are incubated with the fullerene derivatives.

3.5. Desorption of Fullerene Derivatives from the E. coli Cell Surface. In order to check the strength and reversibility of the AF and CF binding to the bacterial cell surface, we analysed the desorption of these compounds using a very simple experiment (see Section 2). The obtained AF and CF desorption values are shown in Table 3.

It was shown that the binding of the amino fullerene AF to the bacterial cells is strong and partially irreversible. It is seen from Table 3 that only 64.7 ± 1.6% of initially adsorbed AF was desorbed from the bacterial cells after 10 washing cycles. Moreover, excretion of fullerene occurs gradually and the last cycles showed very little and decreasing desorption of AF,

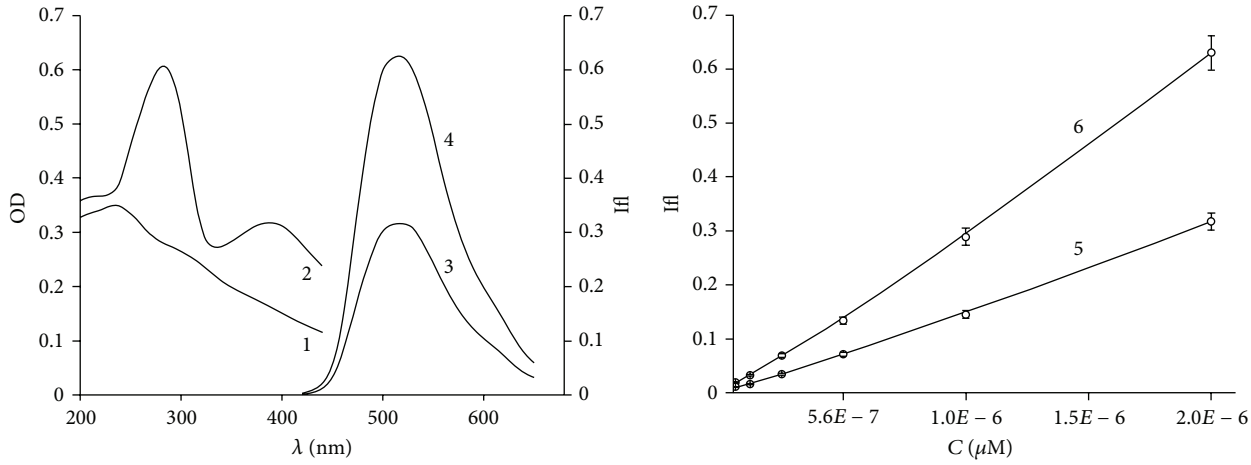

Figure 3: Optical spectra of the fullerene derivatives. (a) Adsorption spectra of CF, $C = 2 * 10^{-6}$ M (1), and AF, $C = 2 * 10^{-5}$ M (2), and the fluorescence spectra of AF obtained under excitation at 300 nm (3) and 240 nm (4). (b) Dependence of AF fluorescence intensity on the concentration of AF in the solution for $\lambda_{ex.} = 300$ nm (5) and $\lambda_{ex.} = 240$ nm (6).

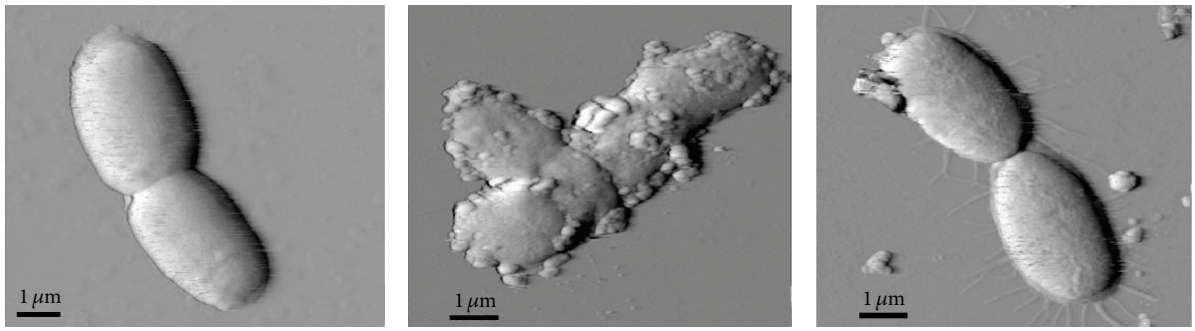

Figure 4: AFM images of *E. coli* K12 TG1 before (a) and after incubation with AF (b) and CF (c).

thus indicating that the remaining amount of this fullerene derivative is absorbed irreversibly. It can be estimated from these data that each *E. coli* cell absorbed irreversibly about 10^5 molecules of AF.

The observed partially irreversible absorption of AF suggests the possibility of its penetration into the microbial cell, which was reported previously for some other fullerene derivatives [43]. The transmembrane AF diffusion could develop due to the concentration gradient and subsequently lead to the electrostatic binding of AF to the intracellular structures and molecules bearing negative charges (including DNA) [44].

This is our assumption at the present stage; further research will be performed to check this idea experimentally.

Similar desorption experiments were performed with CF. The obtained desorption values shown in Table 3 illustrate that four washing cycles removed 94.7 ± 5.5% of CF applied in a very high initial concentration of 10 μM. Most of the fullerenes (80.9 ± 3.3%) were already washed out at the first cycle. This observation suggests that interactions of CF with the bacterial cells are very weak, which is in line with the experimental results described above.

3.6. Antibacterial Activity of Fullerene Derivatives against E. coli. The bactericidal effect of fullerene derivatives was evaluated by investigating the loss of the viability of *E. coli* K12 TG1 cells after a 60-minute incubation with different concentrations of AF and CF. Carboxylic fullerene derivative CF did not cause any bactericidal effect at concentrations of up to 400 μM. In contrast, the amino fullerene derivative showed notable bactericidal activity. The incubation of *E. coli* with AF led to the time- and concentration-dependent death of the bacterial cells (Table 4). The characteristic LD_{50} value of 79.1 μM was calculated from the obtained data. Use of higher concentrations of this compound (400 μM and higher) resulted in the death of at least 99% of *E. coli* cells. These results suggest that AF might be considered as a novel and promising type of chemical bactericide.

Table 3: Fullerene derivatives desorption from *E. coli* K12 TG1 cells.

Number of the consecutive washing (separation/redispersion) cycles	Fullerene derivative desorption, %	
	AF	CF
1	16.5 ± 1.0	80.9 ± 3.3
2	13.7 ± 0.7	6.7 ± 0.5
3	8.3 ± 0.5	5.4 ± 0.4
4	7.1 ± 0.5	1.7 ± 0.1
5	4.9 ± 0.4	0
6	4.2 ± 0.3	0
7	3.7 ± 0.2	0
8	2.7 ± 0.2	0
9	2.2 ± 0.1	0
10	1.4 ± 0.1	0
Total	64.7 ± 1.6	94.7 ± 5.5

Table 4: Percentage of the *E. coli* K12 TG1 cells that lost their vitality after 60 min of incubation with AF in the absence and in the presence of human erythrocytes.

Concentration of AF, μM	Bactericidal effect, %	
	E. coli	*E. coli* + erythrocytes
25	12.0 ± 3.7	1.8 ± 4.4
50	31.9 ± 3.1	5.6 ± 4.3
100	58.1 ± 2.4	6.0 ± 4.3
200	77.6 ± 1.4	66.8 ± 1.8

The selectivity of the antibacterial action of AF was investigated in a three-component test mixture comprising fullerene derivative, *E. coli* cells, and human erythrocytes. The concentrations of the cells in the test samples were adjusted to equalize the total areas (0.02 m^2/mL) of the *E. coli* and the erythrocyte cell surfaces. Indeed, the bactericidal activity of AF was essentially decreased in the presence of human erythrocytes in the test samples together with the *E. coli* cells (Table 4). The effect of the erythrocytes suppressing the antibacterial activity of AF was the most pronounced for concentrations ≤100 μM.

This observation is explained by nonspecific AF binding to the bacterial cells and erythrocytes. Such a concurrent pathway decreases the bactericidal activity of AF and increases LD_{50} value more than twofold for the system comprising both *E. coli* cells and human erythrocytes. The observed tendency of AF to bind to the erythrocytes hinders *in vivo* applications of this compound for fullerene-mediated therapy. Nevertheless, AF still can be considered as a promising chemical disinfectant for various types of surfaces.

4. Conclusion

Highly water-soluble derivatives of [60]fullerene bearing cationic (protonated amine, AF) or anionic (COO–, CF) functional groups appended to the fullerene cage have been investigated. It was shown that both fullerene derivatives form nanoclusters in aqueous solutions with hydrodynamic diameters of 2–200 nm (AF) and 70–100 nm (CF) as revealed by the DLS measurements.

The obtained experimental data implied that initial interactions of the fullerene derivatives and their nanoclusters with prokaryotic and eukaryotic cells are governed mainly by electrostatic Coulomb forces. Moreover, electrostatic interactions explain the appearance of the antibacterial activity of fullerene derivatives. Indeed, the cationic fullerene derivative AF (having zeta potential $\zeta = +41.5$ mV) undergoes strong binding to the negatively charged *E. coli* cells ($\zeta = -50$ mV) due to the attractive electrostatic interactions that result in the appreciable bactericidal activity of this compound. In contrast, the anionic fullerene derivative CF ($\zeta = -52.2$ mV) does not bind to the bacterial cell membranes because of the repulsive Coulomb interactions and subsequently shows no bactericidal effect. The binding of the amino fullerene (AF) clusters to the bacterial cells and also the absence of such binding in the case of CF were visualized by atomic force microscopy.

The fullerene derivative AF induced time- and concentration-dependent death of the bacterial *E. coli* cells characterized by an LD_{50} value of 79.1 μM. However, the antibacterial activity mechanism of [60]fullerene and fullerene derivatives is unclear and still debated [45]. Like Aquino et al. [46] we confirmed AF influence on the bacteria viability without cell membrane disruption. On the other hand, our results reaffirm AF intercalation into the cell wall that enables membrane stress [40], subsequent respiratory chain inhibition [47], and ROS-dependent toxicity [48].

The bactericidal activity of AF decreased significantly in the presence of human erythrocytes. Indeed, human erythrocytes also bear a negative charge ($\zeta = -13.5$ mV), which facilitates their electrostatic interactions with the positively charged AF molecules (and/or nanoclusters). The efficient binding of AF (and, presumably, other positively charged fullerene derivatives) to both prokaryotic (*E. coli*) and eukaryotic (erythrocyte) cells hinders *in vivo* applications of such compounds for fullerene-mediated therapy. Nevertheless, AF can still be considered as a promising chemical disinfectant for various types of surfaces. In contrast, CF (and probably other anionic fullerene-based compounds) shows no ability to bind to the bacterial cells or erythrocytes and might have big potential for *in vivo* studies and, possibly, for some biomedicinal applications.

Conflict of Interests

The authors declare that there is no conflict of interests regarding the publication of this paper.

Acknowledgments

The authors acknowledge the financial support provided by the Russian Ministry of Science and Education (Contract

no. P327), the Russian Foundation for Basic Research (12-03-33031), the Russian President Science Foundation (MK-6177.2013.3), and the Presidium of the Russian Academy of Sciences (Research Programs no. 8 "Development of methods for synthesis of new compounds and materials" and no. 24 "Fundamental research in the field of nanotechnology and nanomaterials").

References

[1] R. H. Hurt, M. Monthioux, and A. Kane, "Toxicology of carbon nanomaterials: status, trends, and perspectives on the special issue," *Carbon*, vol. 44, no. 6, pp. 1028–1033, 2006.

[2] S. Bosi, T. D. Ros, G. Spalluto, and M. Prato, "Fullerene derivatives: an attractive tool for biological applications," *European Journal of Medicinal Chemistry*, vol. 38, no. 11-12, pp. 913–923, 2003.

[3] R. Brayner, "The toxicological impact of nanoparticles," *Nano Today*, vol. 3, no. 1-2, pp. 48–55, 2008.

[4] M. S. Mauter and M. Elimelech, "Environmental applications of carbon-based nanomaterials," *Environmental Science and Technology*, vol. 42, no. 16, pp. 5843–5859, 2008.

[5] C.-W. Lam, J. T. James, R. McCluskey, S. Arepalli, and R. L. Hunter, "A review of carbon nanotube toxicity and assessment of potential occupational and environmental health risks," *Critical Reviews in Toxicology*, vol. 36, no. 3, pp. 189–217, 2006.

[6] J. Kolosnjaj-Tabi, H. Szwarc, and F. Moussa, "*In vivo* toxicity studies of pristine carbon nanotubes: a review," in *The Delivery of Nanoparticles*, A. A. Hashim, Ed., chapter 2, pp. 37–58, InTech, Vienna, Austeria, 2012.

[7] S. Nath, H. Pal, A. V. Sapre, and J. P. Mittal, "Solvatochromism. Aggregation and photochemical properties of fullerenes, C_{60} and C_{70}, in solution," *Journal of Photoscience*, vol. 10, no. 1, p. 105, 2003.

[8] F. Langa and J. -F. Nierengarten, *Fullerenes: Principles and Applications*, Nanoscience & Nanotechnology, Royal Society of Chemistry, Cambridge, UK, 2007.

[9] P. A. Troshin, O. A. Troshina, R. N. Lyubovskaya, and V. F. Razumov, "Functional derivatives of fullerenes: synthesis and applications in the fields of organic electronics and biomedicine," Ivanovo: IvSU, 2010.

[10] S. C. Chueh, M. K. Lai, M. S. Lee, L. Y. Chiang, T. I. Ho, and S. C. Chen, "Decrease of free radical level in organ perfusate by a novel water-soluble carbon-sixty, hexa(sulfobutyl)fullerenes," *Transplantation Proceedings*, vol. 31, no. 5, pp. 1976–1977, 1999.

[11] R. Maeda-Mamiya, E. Noiri, H. Isobe et al., "*In vivo* gene delivery by cationic tetraamino fullerene," *Proceedings of the National Academy of Sciences of the United States of America*, vol. 107, no. 12, pp. 5339–5344, 2010.

[12] L. L. Dugan, D. M. Turetsky, C. Du et al., "Carboxyfullerenes as neuroprotective agents," *Proceedings of the National Academy of Sciences of the United States of America*, vol. 94, no. 17, pp. 9434–9439, 1997.

[13] Y. Tabata, Y. Murakami, and Y. Ikada, "Antitumor effect of poly(ethylene glycol)-modified fullerene," *Fullerene Science and Technology*, vol. 5, no. 5, pp. 989–1007, 1997.

[14] F. Kasermann and C. Kempf, "Photodynamic inactivation of enveloped viruses by buckminsterfullerene," *Antiviral Research*, vol. 34, no. 1, pp. 65–70, 1997.

[15] D. Y. Lyon, J. D. Fortner, C. M. Sayes, V. L. Colvin, and J. B. Hughes, "Bacterial cell association and antimicrobial activity of a C_{60} water suspension," *Environmental Toxicology and Chemistry*, vol. 24, no. 11, pp. 2757–2762, 2005.

[16] J. P. Kamat, T. P. A. Devasagayam, K. I. Priyadarsini, and H. Mohan, "Reactive oxygen species mediated membrane damage induced by fullerene derivatives and its possible biological implications," *Toxicology*, vol. 155, no. 1–3, pp. 55–61, 2000.

[17] T. Mashino, N. Usui, K. Okuda, T. Hirota, and M. Mochizuki, "Respiratory chain inhibition by fullerene derivatives: hydrogen peroxide production caused by fullerene derivatives and a respiratory chain system," *Bioorganic and Medicinal Chemistry*, vol. 11, no. 7, pp. 1433–1438, 2003.

[18] S. K. Sharma, L. Y. Chiang, and M. R. Hamblin, "Photodynamic therapy with fullerenes *in vivo*: reality or a dream?" *Nanomedicine*, vol. 6, no. 10, pp. 1813–1825, 2011.

[19] T. Mashino, D. Nishikawa, K. Takahashi et al., "Antibacterial and antiproliferative activity of cationic fullerene derivatives," *Bioorganic and Medicinal Chemistry Letters*, vol. 13, no. 24, pp. 4395–4397, 2003.

[20] N. Tsao, P. P. Kanakamma, T.-Y. Luh, C.-K. Chou, and H.-Y. Lei, "Inhibition of *Escherichia coli*-induced meningitis by carboxyfullerence," *Antimicrobial Agents and Chemotherapy*, vol. 43, no. 9, pp. 2273–2277, 1999.

[21] A. A. Yurkova, E. A. Khakina, S. I. Troyanov et al., "Arbuzov chemistry with chlorofullerene $C_{60}Cl_6$: a powerful method for selective synthesis of highly functionalized [60]fullerene derivatives," *Chemical Communications*, vol. 48, no. 71, pp. 8916–8918, 2012.

[22] E. A. Khakina, A. A. Yurkova, A. A. Peregudov et al., "Highly selective reactions of $C_{60}Cl_6$ with thiols for the synthesis of functionalized [60]fullerene derivatives," *Chemical Communications*, vol. 48, no. 57, pp. 7158–7160, 2012.

[23] A. B. Kornev, E. A. Khakina, S. I. Troyanov et al., "Facile preparation of amine and amino acid adducts of [60]fullerene using chlorofullerene $C_{60}Cl_6$ as a precursor," *Chemical Communications*, vol. 48, no. 44, pp. 5461–5463, 2012.

[24] A. B. Kornev, A. S. Peregudov, V. M. Martynenko, J. Balzarini, B. Hoorelbeke, and P. A. Troshin, "Synthesis and antiviral activity of highly water-soluble polycarboxylic derivatives of [70]fullerene," *Chemical Communications*, vol. 47, no. 29, pp. 8298–8300, 2011.

[25] O. A. Troshina, P. A. Troshin, A. S. Peregudov, J. Kozlovskiy, and R. N. Balzarini, "Photoaddition of N-substituted piperazines to C_{60}: an efficient approach to the synthesis of water-soluble fullerene derivatives," *Chemistry*, vol. 12, no. 21, pp. 5569–5577, 2006.

[26] O. A. Troshina, P. A. Troshin, A. S. Peregudov, V. I. Kozlovskiy, J. Balzarini, and R. N. Lyubovskaya, "Chlorofullerene $C_{60}Cl_6$: a precursor for straightforward preparation of highly water-soluble polycarboxylic fullerene derivatives active against HIV," *Organic and Biomolecular Chemistry*, vol. 5, no. 17, pp. 2783–2791, 2007.

[27] S. Kang, M. Herzberg, D. F. Rodrigues, and M. Elimelech, "Antibacterial effects of carbon nanotubes: size does matter!," *Langmuir*, vol. 24, no. 13, pp. 6409–6413, 2008.

[28] D. Bouchard, X. Ma, and C. Isaacson, "Colloidal properties of aqueous fullerenes: isoelectric points and aggregation kinetics of C_{60} and C_{60} derivatives," *Environmental Science & Technology*, vol. 43, no. 17, pp. 6597–6603, 2009.

[29] G. Wang, G. Zhao, and L. Yan, "Relationship between toxicity and molecular volume of dioxins, organic phosphorous compounds and n-alkanols," *Chinese Science Bulletin*, vol. 49, no. 14, pp. 1437–1441, 2004.

[30] S. S. Gayathri and A. Patnaik, "Aggregation of a C_{60}-didodecyloxybenzene dyad: structure, dynamics, and mechanism of vesicle growth," *Langmuir*, vol. 23, no. 9, pp. 4800–4808, 2007.

[31] Y. Kanbur and Z. Küçükyavuz, "Synthesis and characterization of surface modified fullerene," *Fullerenes, Nanotubes and Carbon Nanostructures*, vol. 20, no. 2, pp. 119–126.

[32] X. Ma and D. Bouchard, "Formation of aqueous suspensions of fullerenes," *Environmental Science & Technology*, vol. 43, no. 2, pp. 330–336, 2009.

[33] E. Yifeng, L. Bai, L. Fan, M. Han, X. Zhang, and S. Yang, "Electrochemically generated fluorescent fullerene[60] nanoparticles as a new and viable bioimaging platform," *Journal of Materials Chemistry*, vol. 21, pp. 819–823, 2011.

[34] Y. Matsuo, K. Tahara, K. Morita, K. Matsuo, and E. Nakamura, "Regioselective eightfold and tenfold additions of a pyridine-modified organocopper reagent to [60]fullerene," *Angewandte Chemie*, vol. 46, no. 16, pp. 2844–2847, 2007.

[35] D. Y. Lyon and P. J. Alvarez, "Fullerene water suspension (nC_{60}) exerts antibacterial effects via ROS-independent protein oxidation," *Environmental Science & Technology*, vol. 42, no. 21, pp. 8127–8132, 2008.

[36] M. HuiLi and X. J. Liang, "Fullerenes as unique nanopharmaceuticals for disease treatment," *Science China Chemistry*, vol. 53, no. 11, pp. 2233–2240, 2010.

[37] S. Liu, A. K. Ng, R. Xu et al., "Antibacterial action of dispersed single-walled carbon nanotubes on *Escherichia coli* and *Bacillus subtilis* investigated by atomic force microscopy," *Nanoscale*, vol. 2, no. 12, pp. 2744–2750, 2010.

[38] H. Schwegmann, A. J. Feitza, and F. H. Frimmela, "Influence of the zeta potential on the sorption and toxicity of iron oxide nanoparticles on *S. cerevisiae* and *E. coli*," *Journal of Colloid and Interface Science*, vol. 347, no. 1, pp. 43–48, 2010.

[39] N. Guzelsu, C. Wienstien, and S. P. Kotha, "A new streaming potential chamber for zeta potential measurements of particulates," *Review of Scientific Instruments*, vol. 81, no. 1, Article ID 015106, 2010.

[40] Y. J. Tang, J. M. Ashcroft, D. Chen et al., "Charge-associated effects of fullerene derivatives on microbial structural integrity and central metabolism," *Nano Letters*, vol. 7, no. 3, pp. 754–760, 2007.

[41] H. J. Johnston, G. R. Hutchison, F. M. Christensen, K. Aschberger, and V. Stone, "The biological mechanisms and physicochemical characteristics responsible for driving fullerene toxicity," *Toxicological Sciences*, vol. 114, no. 2, pp. 162–182, 2009.

[42] F. Rancan, S. Rosan, F. Boehm et al., "Cytotoxicity and photocytotoxicity of a dendritic C_{60} mono-adduct and a malonic acid C_{60} tris-adduct on Jurkat cells," *Journal of Photochemistry and Photobiology B*, vol. 67, no. 3, pp. 157–162, 2002.

[43] J. Wong-Ekkabut, S. Baoukina, W. Triampo, I.-M. Tang, D. P. Tieleman, and L. Monticelli, "Computer simulation study of fullerene translocation through lipid membranes," *Nature Nanotechnology*, vol. 3, no. 6, pp. 363–368, 2008.

[44] I. Nakanishi, S. Fukuzumi, T. Konishi et al., "Fullerenes for the new millennium," in *Proceedings of the International Symposium on Fullerenes, Nanotubes, and Carbon Nanoclusters*, P. V. Kamat, D. M. Guldi, and K. M. Kadish, Eds., vol. 11, The Electrochemical Society, Pennington, NJ, USA, 2001.

[45] M. Carini, L. Djordjevic, and T. D. Ros, "Fullerenes in biology and medicine," in *Handbook of Carbon Nano Materials*, vol. 3, pp. 1–48, World Scientific Publishing, 2012.

[46] A. Aquino, J. Chan, K. Giolma, and M. Loh, "The effect of a fullerene water suspension on the growth, cell viability, and membrane integrity of *Escherichia coli* B23," *Journal of Eexperimental Microbiology & Immunology*, vol. 14, pp. 13–20, 2010.

[47] T. Mashino, K. Okuda, T. Hirota, M. Hirobe, T. Nagano, and M. Mochizuki, "Inhibition of *E. coli* growth by fullerene derivatives and inhibition mechanism," *Bioorganic and Medicinal Chemistry Letters*, vol. 9, no. 20, pp. 2959–2962, 1999.

[48] G. P. Tegos, T. N. Demidova, D. Arcila-Lopez et al., "Cationic fullerenes are effective and selective antimicrobial photosensitizers," *Chemistry and Biology*, vol. 12, no. 10, pp. 1127–1135, 2005.

Hindawi Publishing Corporation
Journal of Nanomaterials
Volume 2013, Article ID 530959, 8 pages
http://dx.doi.org/10.1155/2013/530959

Research Article

Incorporated W Roles on Microstructure and Properties of W-C:H Films by a Hybrid Linear Ion Beam Systems

Peng Guo, Peiling Ke, and Aiying Wang

Key Laboratory of Marine Materials and Related Technologies, Zhejiang Key Laboratory of Marine Materials and Protective Technologies, Ningbo Institute of Materials Technology and Engineering, Chinese Academy of Sciences, Ningbo 315201, China

Correspondence should be addressed to Aiying Wang; aywang@nimte.ac.cn

Received 9 October 2013; Revised 21 November 2013; Accepted 21 November 2013

Academic Editor: Myoung-Woon Moon

Copyright © 2013 Peng Guo et al. This is an open access article distributed under the Creative Commons Attribution License, which permits unrestricted use, distribution, and reproduction in any medium, provided the original work is properly cited.

W-incorporated diamond-like carbon (W-C:H) films were fabricated by a hybrid beams system consisting of a DC magnetron sputtering and a linear ion source. The W concentration (1.08~31.74 at.%) in the film was controlled by varying the sputtering current. The cross-sectional topography, composition, and microstructure of the W-C:H films were investigated by SEM, XPS, TEM, and Raman spectroscopy. The mechanical and tribological properties of the films as a function of W concentration were evaluated by a stress-tester, nanoindentation, and ball-on-disk tribometer, respectively. The results showed that films mainly exhibited the feature of amorphous carbon when W concentration of the films was less than 4.38 at.%, where the incorporated W atoms would be bonded with C atoms and resulted in the formation of WC_{1-x} nanoparticles. The W-C:H film with 4.38 at.% W concentration showed a minimum value of residual compressive stress, a higher hardness, and better tribological properties. Beyond this W concentration range, both the residual stress and mechanical properties were deteriorated due to the growth of tungsten carbide nanoparticles in the carbon matrix.

1. Introduction

Diamond-like carbon film (DLC) is a metastable form of amorphous carbon with a certain dominant sp^3 bonding. Due to its unique properties such as high hardness, low friction coefficient, good chemical inertness, and the optical transparency in a wide range of VIS-IR, DLC film has been used as protective coatings in many industrial fields [1]. However, high residual stress is the major drawback of DLC films for its wider practical application [2–6]. Immense amounts of concrete research have shown that the incorporation of metal elements, such as Mo, Cu, Al, Cr, and W, is one of the good methods to decrease the internal stress of DLC films [7–12]. As one of the doped metal elements, W-incorporated DLC films (W-C:H) have been received considerable attention both in scientific research and industrial fields of carbon based materials [13–19]. The properties and structure of W-C:H films prepared by the process combining reactive magnetron sputtering with plasma source ion implantation were reported by Baba and coworkers [20]. Takeno et al. [21] investigated the electrical properties and structure of W-C:H films prepared by radio frequency plasma enhanced chemical vapor deposition, and a resistive superconducting transition was discovered in their report. Wang et al. [22] reported a rapid increase and a gradual decrease in the residual stress of DLC films prepared by end-Hall-type ion gun with increasing W concentration. But considering the characterization complexity of carbon bonds caused by the incorporated W atoms and the easier controlled synthesis with a wide range of W concentration, the new deposition technique of hybrid ion beam system is demanded and the relationship between properties and structure of W-C:H films as a function of W concentration lacked study.

Ion beam sources have been widely used in the field of science and industry such as substrate cleaning, DLC film deposition and surface modification [20, 23–29]. Anode layer type linear ion source (ALIS) is a kind of closed drift type linear ion sources promoted by the plasma acceleration technology of the aerospace thruster [30]. As a large-area surface treatment technique, the ALIS is a gridded ion source

with simple electrode structure, which can provide a higher ion beam current density and readily be scaled to any desired length [30–34].

In this work, a hybrid ion beam deposition system consisting of a DC magnetron sputtering and an ALIS is employed to fabricate the W-C:H films, the used method focused on the W-C:H films with different W concentration, and the films were prepared by a unique hybrid ion beam system. The mechanical properties and structure of the films as a function of W concentration were studied. The results indicated that the DLC films with relatively low stress and high hardness could be achieved by doping a low concentration of W atoms.

2. Experiment

Si (100) wafer of thickness 710 ± 15 μm was used as the substrate material. A thin Si (100) wafer of thickness 250 ± 5 μm was also used as substrate to accurately estimate the internal residual stress. The substrate was cleaned ultrasonically in acetone and dried in air before deposition. The W-C:H film was prepared on Si substrate by a hybrid ion beams deposition system consisting of a DC magnetron rectangular sputtering with a 100 mm (W) × 400 mm (L) W target (99.95%) and a 380 mm (L) anode layer type linear ion source (ALIS) [35]. The substrates were sputter-cleaned for 20 mins using Ar ions with a pulsed bias voltage of −100 V. The base pressure was evacuated to a vacuum of about 2×10^{-5} Torr. During film deposition process, hydrocarbon gas (C_2H_2) was introduced into the linear ion source to obtain the hydrocarbon ions for DLC deposition. The Ar sputtering gas was supplied to the magnetron sputter for W sputtering. The concentration of tungsten in the films was controlled by varying the sputtering current from 0.9 to 1.5 A. The C_2H_2 flux and Ar flux were kept at 10 and 70 sccm, respectively, and the work pressure was kept at about 4.0×10^{-3} Torr. Typical values of ALIS voltage and current were 1300 V and 0.2 A, respectively. A negative pulsed bias voltage of −100 V (350 KHz, 1.1 μs) was applied to the substrate. The deposition time was 40 mins. For comparison, the pure DLC film was also prepared using ALIS and a negative substrate bias of −100 V.

The thickness of the deposited films was measured by surface profilometer (Alpha-Step IQ, USA). The cross-morphology of the deposited films was observed by a cross-section SEM (Hitachi S-4800). An X-ray photoelectron spectroscopy (XPS, Thermo Scientific ESCALAB 250) with monochromated Al X-ray resource was used to characterize the chemical composition, atomic bonds, and microstructure of the films. High-resolution transmission electron microscopy (TEM, Tecnai F20), operated at 200 KeV with a point-to-point resolution of 0.24 nm, was used to clarify the microstructure. Raman spectroscopy (Renishaw inVia-reflex) equipped with a He-Ne laser of 532 nm exciting wavelength was used to measure the atomic bonds of the films at a detecting range from 600 to 2000 cm^{-1}.

The internal residual stress of the films was calculated using the Stoney equation, and the curvature of film/substrate composite was determined by a laser tester. Mechanical properties were measured using the nanoindenter (MTS-G200) with the depth to 200 nm, and the hardness was chosen in a depth of around 1/10 of the coating thickness in order to avoid the contribution of Si substrate to the results. The tribological behaviors of the Si coated by the films were measured on a rotary ball-on-disk tribometer at room temperature with a relative humidity of about 50% under dry sliding conditions. All the tests were performed at 0.12 ms^{-1} sliding speed for a distance of 400 m and the applied load was 5 N.

3. Results and Discussion

Figures 1(a) and 1(b) showed the change of W concentration and average growth rate of the films as a function of the sputtering current, respectively. The W/C atomic ratio of the films was determined based on the atomic sensitivity factors and area ratio of the C 1s to W 4f peaks in XPS spectra of the films. The W concentration of the films increased from 1.08 to 31.74 at.% as the sputtering current increased from 0.9 to 1.5 A, as shown in Figure 1(a), while the growth rate of films decreased slightly from about 17 to 15 nm/min, as seen in Figure 1(b), which may be induced by antisputtering effect of W atoms with higher kinetic energy at 1.5 A sputtering current [36]. Noted that, less than the sputtering current of 0.9 A, it was difficult to extract the accurate amount of W concentration from the XPS spectra because of the serious W target pollution by the ionized carbon precursors. Beyond the case of 1.5 A, the deposited films showed a typical W metallic luster.

Figure 2 showed the cross-sectional SEM images of the films with different W concentrations. And the films in Figure 2 were marked by double-headed arrows. The images demonstrated similar smooth surface when W concentration was less than 4.38 at.% and exhibited the feature of the amorphous structure, which suggested that W-C:H films with W concentration less than 4.38 at.% kept amorphous features. However, when the W concentration increased to 31.74 at.%, the film became rough with emergence of nanoscale particulates in the carbon matrix, as illustrated in Figure 2(d), due to the formation of tungsten carbide phase.

XPS provided the approach to analyze the chemical bonds of the deposited films by C 1s. Figure 3(a) displayed the XPS C 1s peaks of the pure DLC film and W-C:H films with different W concentrations. When the W concentration was less than 4.38 at.%, the C 1s spectra were divided into two peaks around 284.6 eV and 286.5 eV corresponding to the typical C–C/C–H and C–O/C=O binding energy, respectively [20, 37–39]. However, when the W concentration increased to 31.74 at.%, a shoulder peak with a lower binding energy of about 283.5 eV appeared, as shown in Figure 3(b). The peak at 283.1~283.6 eV is generally assigned to the W–C bonds [18, 20, 40], so it can be deduced that the tungsten carbide was formed in the films with a higher W concentration.

Figure 4 displayed the plan-view high-resolution TEM images and the corresponding SAED patterns of the pure DLC film and W-C:H films. Similar to the result of pure DLC, Figure 4(b) presented dense and smooth granular contrasts,

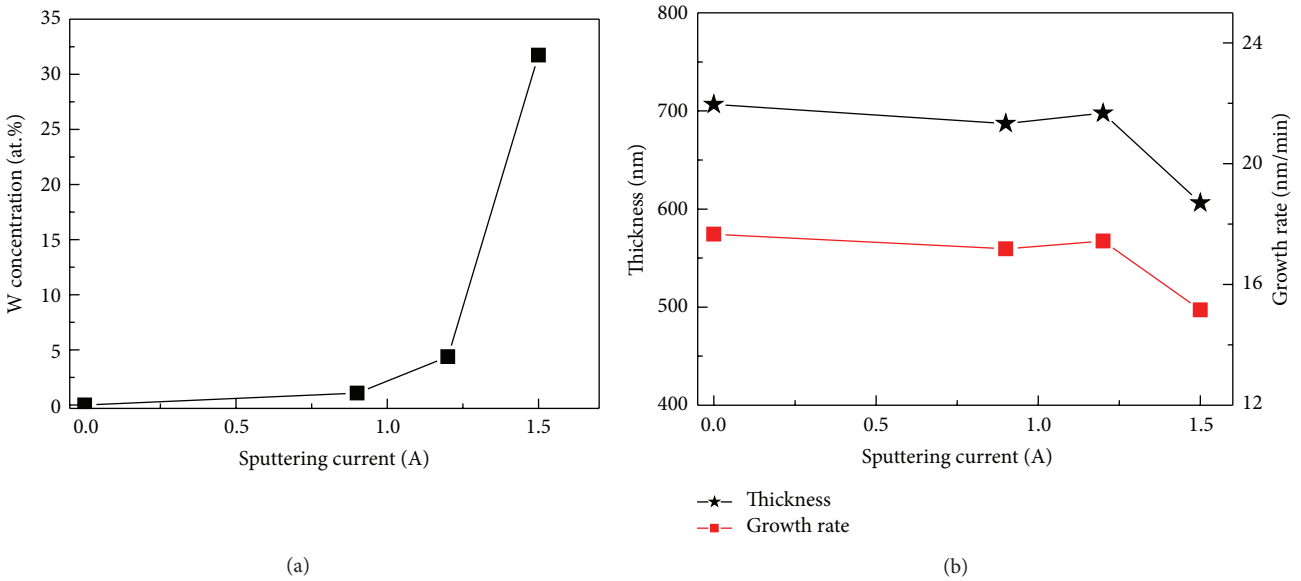

FIGURE 1: W concentration (a), growth rate and thickness (b) of the films as a function of sputtering current.

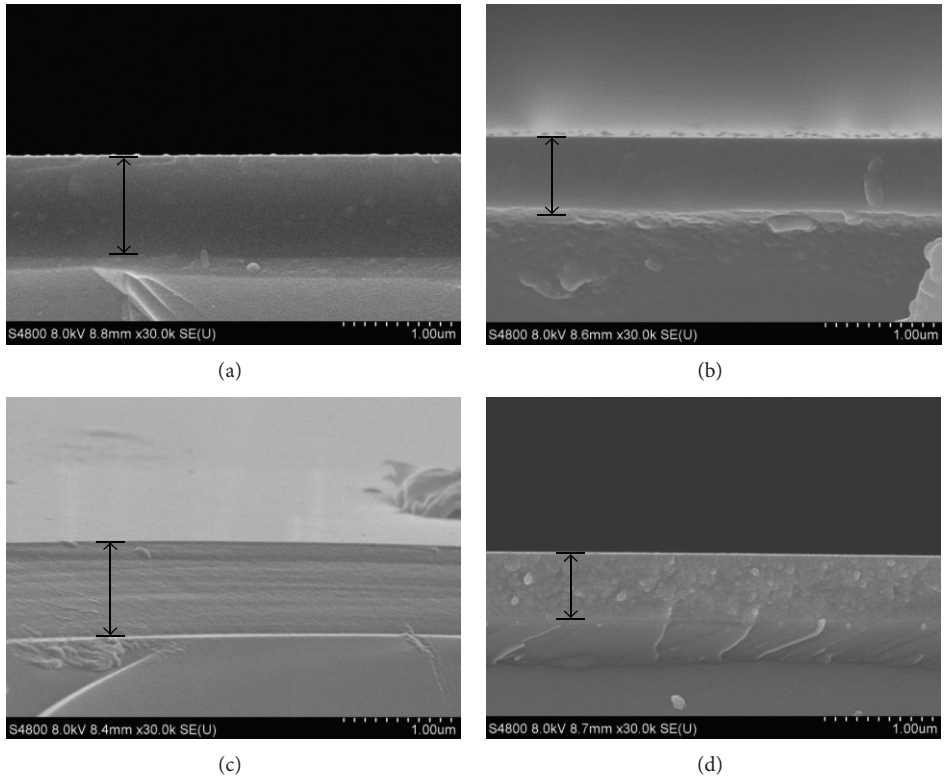

FIGURE 2: Cross-sectional SEM images of the pure DLC film (a); films with 1.08 at.% W (b), 4.38 at.% W (c), and 31.74 at.% W (d).

and the corresponding SAED patterns showed a broad and diffuse diffraction halo. It implied that the deposited films essentially formed a typical amorphous structure, and the W atoms were uniformly distributed and dissolved in the DLC matrix. But for the W-C:H film with 4.38 at.% W atoms (Figure 4(c)), a few nanoparticles with grain diameter about 5 nm were found in the film, and more nanoparticles with similar grain diameter could be observed obviously in W-C:H film with 31.74 at.% W atoms (Figure 4(d)); the corresponding diffraction ring of SAED pattern in Figure 4(d) became much sharper than that in Figure 4(c), suggesting more carbide particles of high crystallinity existed in these films. Figure 4(d) revealed the clear lattice fringes of the nanoparticles

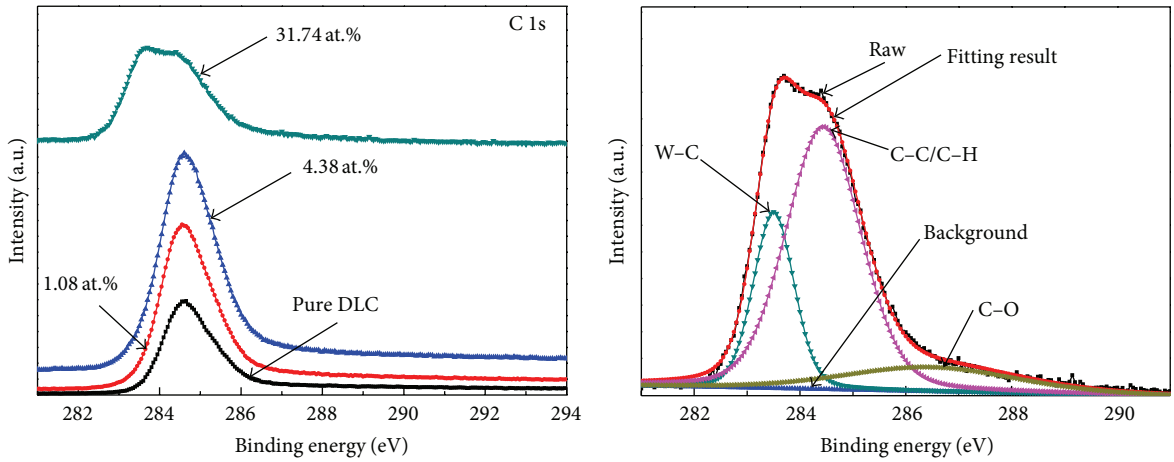

FIGURE 3: Typical C 1s high-resolution XPS spectra of the films with different W concentration (a), XPS spectra of the films with 31.74 at.% W (b).

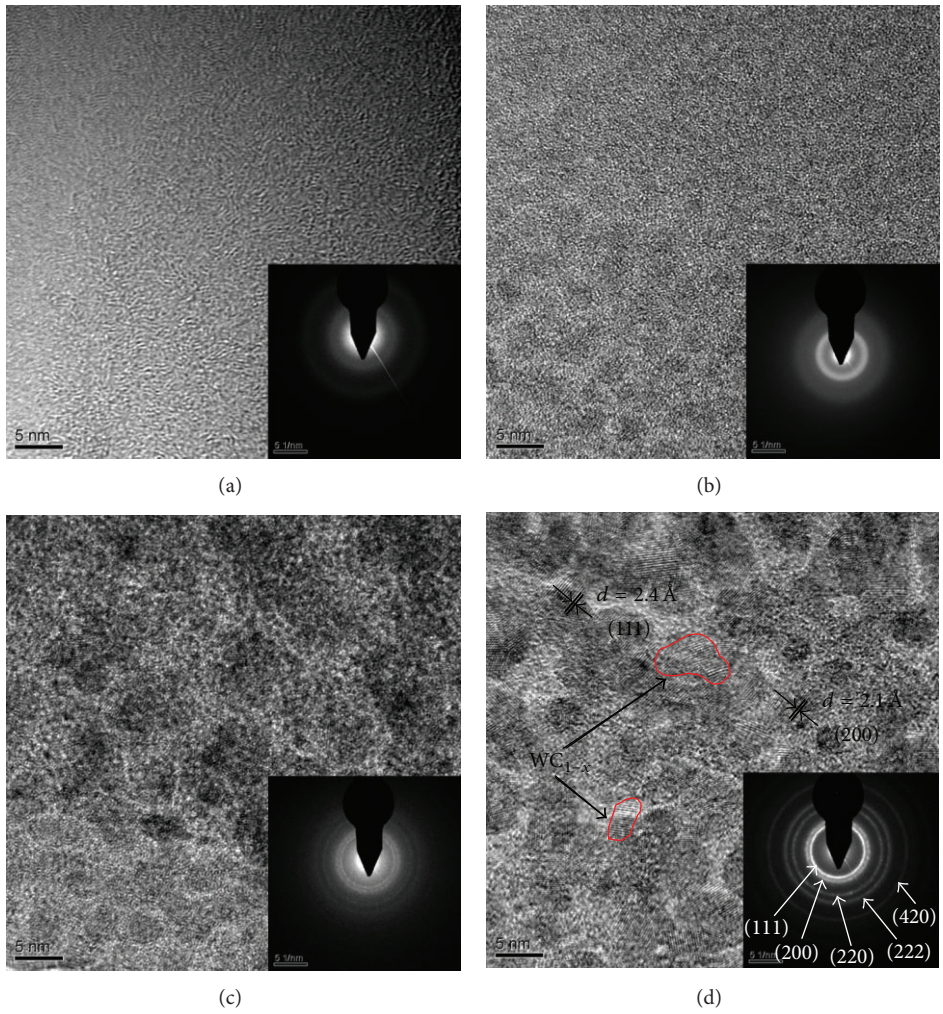

FIGURE 4: Plan-view high-resolution TEM images and corresponding SAED pattern of the pure DLC film (a); films with 1.08 at.% W (b), 4.38 at.% W (c), and 31.74 at.% W (d).

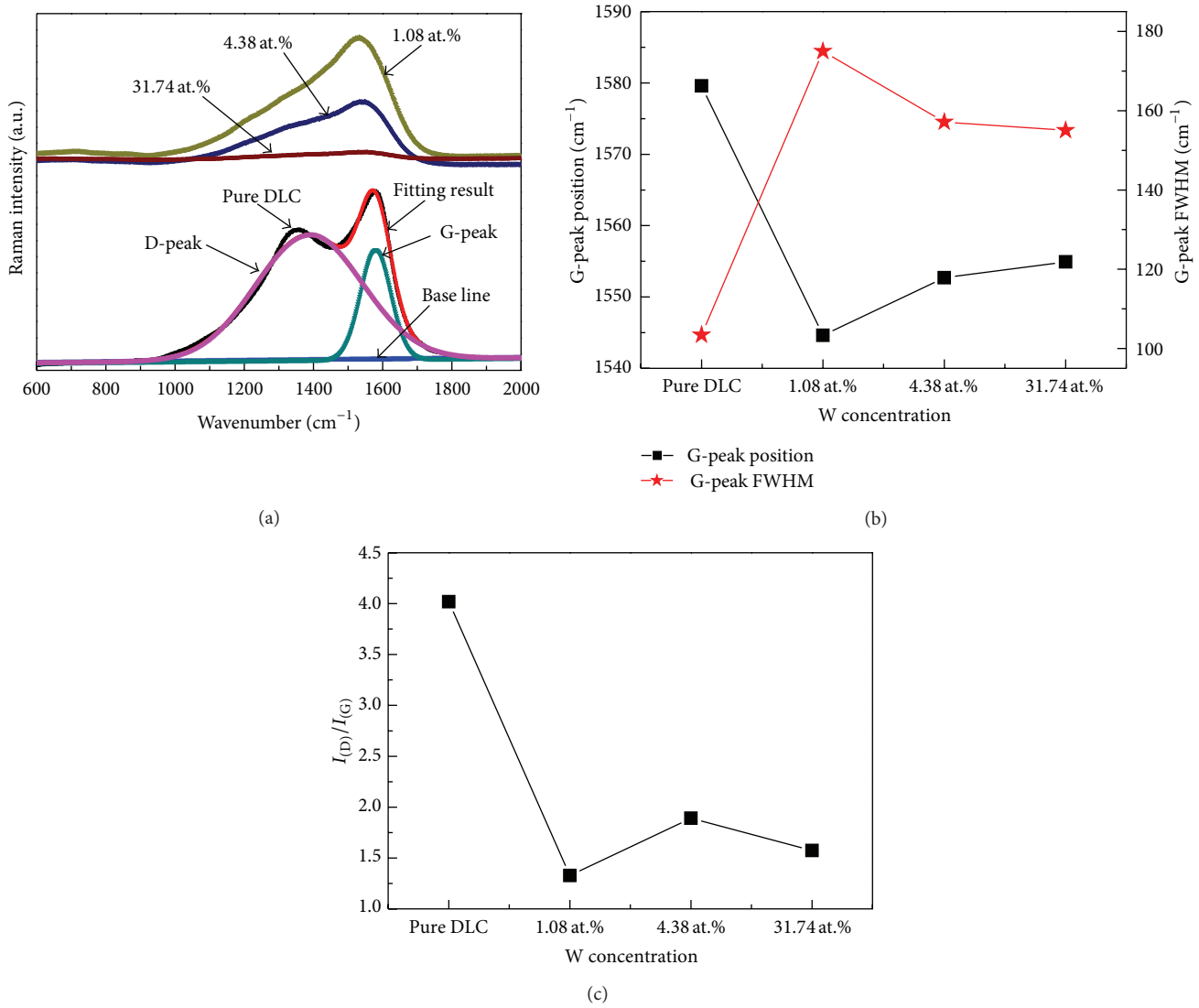

Figure 5: Typical Raman spectrum (a) and G FWHM and position (b), I_D/I_G (c) of films with different W concentration.

(marked red circles) uniformly embedded in the DLC matrix, the sharp crystalline diffraction rings observed in Figure 4(d) indicated the existence of polycrystalline phases, which were identified to be the (111), (200), (220), (222), and (420) reflections of the cubic (FCC) WC_{1-x} structure. The TEM results indicated that the dissolved W atoms began to form WC_{1-x} phase in the DLC matrix when W concentration of the films was in the range of 1.08~4.38 at.%, and the films with higher W concentration were nanocomposite of WC_{1-x} particles embedded in the DLC matrix.

Raman is usually employed to characterize the atomic bonds of carbon films. Figure 5(a) displayed the Raman spectra of the W-C:H films at various W concentrations. Obviously, all samples presented a broad asymmetric Raman scattering band in the range of 1000–1700 cm^{-1}, which was essentially as the typical carbon bond feature in hydrogenated amorphous carbons films. Raman spectroscopy can be generally deconvoluted into two peaks: one named G-peak at 1580 cm^{-1} arising from E_{2g} symmetry stretching vibration mode caused by the sp^2 atom and the other named shoulder D-peak at around 1360 cm^{-1} caused by the zone edge of A_{1g} breathing mode [1]. The experimental spectrum was fitted using two Gaussian peaks after background correction. According to the fitted G-peak position, the intensity ratio of D-peak to G-peak (I_D/I_G), and the full width half maximum (FWHM) of the G-peak, the bonding structure of DLC films such as bond disorder, sp^2/sp^3 ratio can be derived qualitatively [41–43]. Figure 5(b) showed that when W concentration increased from 1.08 to 31.74 at.%, the G peak position shifted monotonically from 1544.6 cm^{-1} to 1554.9 cm^{-1} and the I_D/I_G ratio also increased from 1.32 to 1.57 as in Figure 5(c), implying a higher sp^2/sp^3 ratio in the W-C:H films with higher W concentration; however, the G-peak FWHM decreased from 175 cm^{-1} to 155 cm^{-1}; it revealed that the degree of film structural disorder declined. But in comparison with the W-C:H films, the pure DLC film

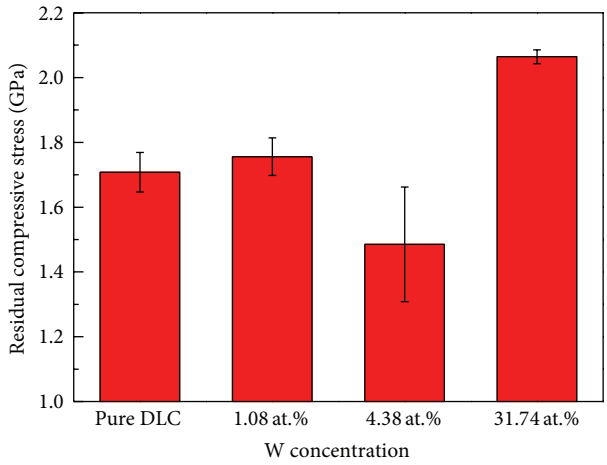

Figure 6: Residual compressive stress as a function of W concentration.

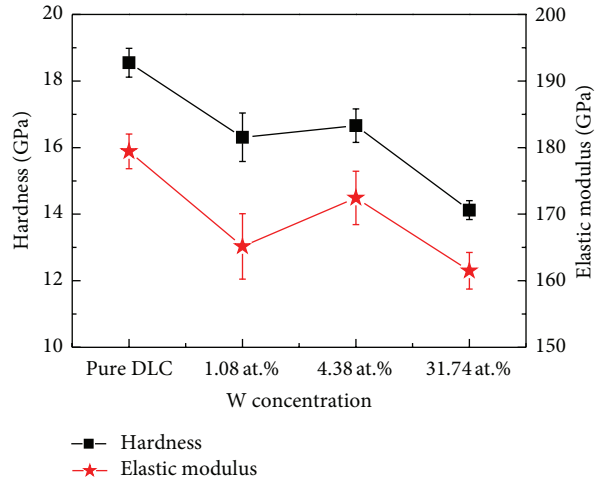

Figure 7: The hardness and elastic modulus as a function of the W concentration.

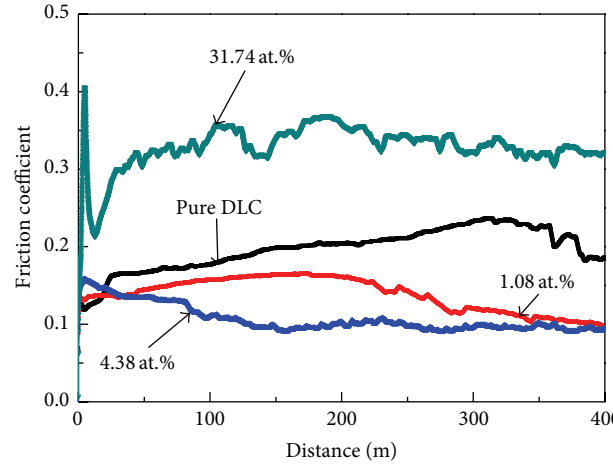

(a)

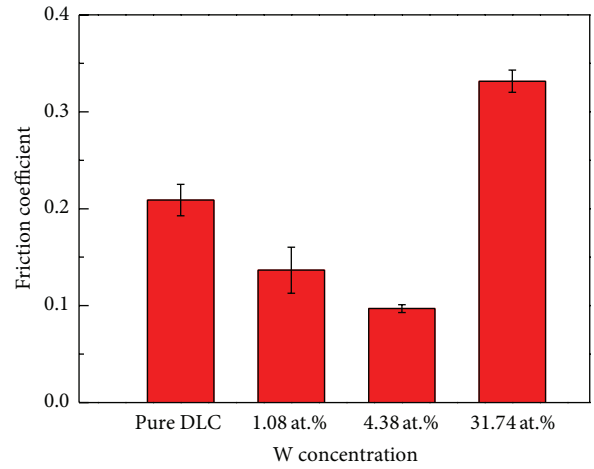

(b)

Figure 8: Friction coefficient (a) and average friction coefficient (b) in stable test condition of the films various W concentrations.

exhibited a higher sp^2/sp^3 ratio and less structural disorder, which may be due to the change of plasma caused by the collision between the W atoms with high energy and the carbon atoms; other researchers also discovered structure evolution due to influence of ion energy [44–46].

Figure 6 showed that the residual compressive stress in the pure DLC films was about 1.7 GPa and arrived at 2.06 GPa in W-C:H film with 31.74 at.% W concentration; a minimum value about 1.485 GPa was obtained when the W concentration was 4.38 at.%, indicating that the residual compressive stress in the DLC films could be reduced in a proper range of W concentration. The decline of the film residual compressive stress could be explained by two stages. Firstly, at the lower W doping level, part of the W atoms was distributed in the DLC matrix without bonding with carbon atom, which provides the pivot location for the bond distortion and reduced the film compressive stress [9, 22]. Moreover, the other few W atoms formed the nanocrystallites and embedded in the carbon matrix, which could also relax the stress by the diffusion and sliding of the grain boundary [11]. Since the W–C bond length was longer than that of the C–C bond; however, with further increasing the W concentration, more formation of W-C bond would induce the severe distortion of the atomic bond angles, which in turn increased the internal stress [9]. The present results agreed well with those reported by the others' work [17, 47].

Figure 7 depicted the hardness and elastic modulus as a function of the W concentration. It could be observed that, with more W atoms in the films, the hardness and elastic modulus of the films decreased from 18.5 GPa to 14.12 GPa and from 179.4 GPa to 161.5 GPa, respectively. Generally, the mechanical properties of DLC films mainly depend on the sp^3 carbon matrix [1], but the incorporation of W atoms and formation of nanoparticles in the DLC would break up the continuity of the carbon network, which would cause the decline of the hardness and elastic modulus. The similar phenomenon was also found in Cr-C:H and Ti-C:H films [48, 49].

The friction coefficient of the films with sliding distance evolution and coefficient in stable test condition were shown in Figure 8. It indicated that W-C:H films with W atoms less than 4.38 at.% had a lower friction coefficient compared with the pure DLC in the stable test condition. But when more W atoms were in the film, the friction coefficient of the film became larger than 0.3, exhibiting the feature of tungsten carbide in the DLC matrix. Similar to the Cr element as a strong carbide former candidate doped in DLC films, other phenomena were also discovered in Cr-C:H films with different Cr concentration [50], which could be attributed to the formed hard WC_{1-x} phase in the DLC matrix [24]. The tribological property related with the microstructure influenced by W concentration was in accord with the results analyzed by XPS, SEM, and TEM.

4. Conclusions

The W-C:H films were prepared by a DC reactive magnetron sputtering with W target (99.99%) in the Ar and C_2H_2 gas mixture. The concentration of tungsten in the films was varied from 1.08 at.% to 31.74 at.% by changing the sputtering current. The films mainly exhibited the feature of amorphous carbon when W concentration of the films was less than 4.38 at.%. The solubility of the W atoms in the DLC films was in the range of 1.08~4.38 at.%. W atoms would bond with C atoms, resulting in the formation of WC_{1-x} nanoparticles with the W concentration exceeding the solubility. The films with 4.38 at.% W concentration showed a minimum value residual compressive stress, a higher hardness value, and better tribological properties.

Acknowledgments

The present research was financially supported by the programs of the State Key Project of Fundamental Research of China (nos. 2012CB933003, 2013CB632302) and the National Natural Science Foundation of China (51371187).

References

[1] J. Robertson, "Diamond-like amorphous carbon," *Materials Science and Engineering R*, vol. 37, no. 4-6, pp. 129–281, 2002.

[2] M. Lejeune, M. Benlahsen, and R. Bouzerar, "Stress and structural relaxation in amorphous hydrogenated carbon films," *Applied Physics Letters*, vol. 84, no. 3, pp. 344–346, 2004.

[3] E. Liu, L. Li, B. Blanpain, and J. P. Celis, "Residual stresses of diamond and diamondlike carbon films," *Journal of Applied Physics*, vol. 98, no. 7, Article ID 073515, 2005.

[4] T. Ma, Y.-Z. Hu, H. Wang, and X. Li, "Microstructural and stress properties of ultrathin diamondlike carbon films during growth: molecular dynamics simulations," *Physical Review B*, vol. 75, no. 3, Article ID 035425, 2007.

[5] O. A. Podsvirov, P. A. Karaseov, A. Y. Vinogradov et al., "Residual stress in diamond-like carbon films: role of growth conditions and ion irradiation," *Journal of Surface Investigation*, vol. 4, no. 2, pp. 241–244, 2010.

[6] K.-S. Kim, S.-H. Lee, Y.-C. Kim, S.-C. Lee, P.-R. Cha, and K.-R. Lee, "Structural analysis for the stress variation of ta-C film with deposition energy: a molecular dynamics simulation," *Metals and Materials International*, vol. 14, no. 3, pp. 347–352, 2008.

[7] L. Ji, H. Li, F. Zhao, J. Chen, and H. Zhou, "Microstructure and mechanical properties of Mo/DLC nanocomposite films," *Diamond and Related Materials*, vol. 17, no. 11, pp. 1949–1954, 2008.

[8] W. Dai and A. Wang, "Synthesis, characterization and properties of the DLC films with low Cr concentration doping by a hybrid linear ion beam system," *Surface and Coatings Technology*, vol. 205, no. 8-9, pp. 2882–2886, 2011.

[9] A.-Y. Wang, K.-R. Lee, J.-P. Ahn, and J. H. Han, "Structure and mechanical properties of W incorporated diamond-like carbon films prepared by a hybrid ion beam deposition technique," *Carbon*, vol. 44, no. 9, pp. 1826–1832, 2006.

[10] C.-C. Chen and F. C.-N. Hong, "Structure and properties of diamond-like carbon nanocomposite films containing copper nanoparticles," *Applied Surface Science*, vol. 242, no. 3-4, pp. 261–269, 2005.

[11] W. Dai and A. Wang, "Deposition and properties of Al-containing diamond-like carbon films by a hybrid ion beam sources," *Journal of Alloys and Compounds*, vol. 509, no. 13, pp. 4626–4631, 2011.

[12] J. E. Krzanowski and J. L. Endrino, "The effects of substrate bias on phase stability and properties of sputter-deposited tungsten carbide," *Materials Letters*, vol. 58, no. 27-28, pp. 3437–3440, 2004.

[13] W. J. Meng and B. A. Gillispie, "Mechanical properties of Ti-containing and W-containing diamond-like carbon coatings," *Journal of Applied Physics*, vol. 84, no. 8, pp. 4314–4321, 1998.

[14] M. L. Terranova, V. Sessa, S. Piccirillo et al., "Temperature-dependent conduction of W-containing composite diamond films," *Applied Physics Letters*, vol. 79, no. 13, pp. 2007–2009, 2001.

[15] N. Yao, A. G. Evans, and C. V. Cooper, "Wear mechanism operating in W-DLC coatings in contact with machined steel surfaces," *Surface and Coatings Technology*, vol. 179, no. 2-3, pp. 306–313, 2004.

[16] J. Veverkova and S. V. Hainsworth, "Effect of temperature and counterface on the tribological performance of W-DLC on a steel substrate," *Wear*, vol. 264, no. 7-8, pp. 518–525, 2008.

[17] C. W. Moura e Silva, J. R. T. Branco, and A. Cavaleiro, "How can H content influence the tribological behaviour of W-containing DLC coatings," *Solid State Sciences*, vol. 11, no. 10, pp. 1778–1782, 2009.

[18] T. Takeno, T. Komiyama, H. Miki, T. Takagi, and T. Aoyama, "XPS and TEM study of W-DLC/DLC double-layered film," *Thin Solid Films*, vol. 517, no. 17, pp. 5010–5013, 2009.

[19] A. L. Mohd Tobi, J. Ding, S. Pearson, S. B. Leen, and P. H. Shipway, "The effect of gross sliding fretting wear on stress distributions in thin W-DLC coating systems," *Tribology International*, vol. 43, no. 10, pp. 1917–1932, 2010.

[20] K. Baba, R. Hatada, and Y. Tanaka, "Preparation and properties of W-containing diamond-like carbon films by magnetron plasma source ion implantation," *Surface and Coatings Technology*, vol. 201, no. 19-20, pp. 8362–8365, 2007.

[21] T. Takeno, H. Miki, T. Takagi, and H. Onodera, "Electrically conductive properties of tungsten-containing diamond-like carbon films," *Diamond and Related Materials*, vol. 15, no. 11-12, pp. 1902–1905, 2006.

[22] A.-Y. Wang, H.-S. Ahn, K.-R. Lee, and J.-P. Ahn, "Unusual stress behavior in W-incorporated hydrogenated amorphous carbon

films," *Applied Physics Letters*, vol. 86, no. 11, Article ID 111902, 2005.

[23] S. Faruque Ahmed, K.-R. Lee, J.-I. Yoon, and M.-W. Moon, "Nanoporous structures of polyimide induced by Ar ion beam irradiation," *Applied Surface Science*, vol. 258, no. 8, pp. 3841–3845, 2012.

[24] X. Han, F. Yan, A. Zhang et al., "Structure and tribological behavior of amorphous carbon films implanted with Cr+ ions," *Materials Science and Engineering A*, vol. 348, no. 1-2, pp. 319–326, 2003.

[25] M.-W. Moon, S. H. Lee, J.-Y. Sun, K. H. Oh, A. Vaziri, and J. W. Hutchinson, "Wrinkled hard skins on polymers created by focused ion beam," *Proceedings of the National Academy of Sciences of the United States of America*, vol. 104, no. 4, pp. 1130–1133, 2007.

[26] Š. Meškinis, R. Gudaitis, V. Kopustinskas, and S. Tamulevičius, "Electrical and piezoresistive properties of ion beam deposited DLC films," *Applied Surface Science*, vol. 254, no. 16, pp. 5252–5256, 2008.

[27] F. Schwarz, G. Thorwarth, and B. Stritzker, "Synthesis of silver and copper nanoparticle containing a-C:H by ion irradiation of polymers," *Solid State Sciences*, vol. 11, no. 10, pp. 1819–1823, 2009.

[28] R. Kometani, K. Yusa, S. Warisawa, and S. Ishihara, "Piezoresistive effect in the three-dimensional diamondlike carbon nanostructure fabricated by focused-ion-beam chemical vapor deposition," *Journal of Vacuum Science & Technology B*, vol. 28, no. 6, pp. F38–F41, 2010.

[29] S. Nakao, T. Soga, T. Sonoda, T. Asada, and N. Kishi, "Optical and electrical properties of nitrogen-doped diamond-like carbon films prepared by a bipolar-type plasma-based ion implantation," *Japanese Journal of Applied Physics*, vol. 51, no. 1, Article ID 01AC04, 2012.

[30] V. V. Zhurin, H. R. Kaufman, and R. S. Robinson, "Physics of closed drift thrusters," *Plasma Sources Science and Technology*, vol. 8, no. 1, pp. R1–R20, 1999.

[31] A. Anders, "Plasma and ion sources in large area coating: a review," *Surface and Coatings Technology*, vol. 200, no. 5-6, pp. 1893–1906, 2005.

[32] I. V. Bordenjuk, O. A. Panchenko, S. V. Sologub, and I. G. Brown, "Development of additional magnetron discharge in the drift region of an ion source with closed electron drift," *Problems of Atomic Science and Technology*, no. 6, pp. 168–170, 2008.

[33] D.-H. Park, J.-H. Kim, Y. Ermakov, and W.-K. Choi, "Linear ion source with closed drift and extended acceleration region," *Review of Scientific Instruments*, vol. 79, no. 2, Article ID 02B312, 2008.

[34] S. Lee, J.-K. Kim, and D.-G. Kim, "Effects of electrode geometry on the ion beam extraction of closed drift type anode layer linear ion source," *Review of Scientific Instruments*, vol. 83, no. 2, Article ID 02B703, 2012.

[35] W. Dai, H. Zheng, G. Wu, and A. Wang, "Effect of bias voltage on growth property of Cr-DLC film prepared by linear ion beam deposition technique," *Vacuum*, vol. 85, no. 2, pp. 231–235, 2010.

[36] H. Huang, G. H. Gilmer, and T. D. De La Rubia, "An atomistic simulator for thin film deposition in three dimensions," *Journal of Applied Physics*, vol. 84, no. 7, pp. 3636–3649, 1998.

[37] D. Bourgoin, S. Turgeon, and G. G. Ross, "Characterization of hydrogenated amorphous carbon films produced by plasma-enhanced chemical vapour deposition with various chemical hybridizations," *Thin Solid Films*, vol. 357, no. 2, pp. 246–253, 1999.

[38] P. Mérel, M. Tabbal, M. Chaker, S. Moisa, and J. Margot, "Direct evaluation of the sp3 content in diamond-like-carbon films by XPS," *Applied Surface Science*, vol. 136, no. 1-2, pp. 105–110, 1998.

[39] Y. Taki and O. Takai, "XPS structural characterization of hydrogenated amorphous carbon thin films prepared by shielded arc ion plating," *Thin Solid Films*, vol. 316, no. 1-2, pp. 45–50, 1998.

[40] J. Luthin and C. Linsmeier, "Carbon films and carbide formation on tungsten," *Surface Science*, vol. 454, no. 1, pp. 78–82, 2000.

[41] A. C. Ferrari and J. Robertson, "Interpretation of Raman spectra of disordered and amorphous carbon," *Physical Review B*, vol. 61, no. 20, pp. 14095–14107, 2000.

[42] A. C. Ferrari and J. Robertson, "Resonant raman spectroscopy of disordered, amorphous, and diamondlike carbon," *Physical Review B*, vol. 64, no. 7, Article ID 075414, 13 pages, 2001.

[43] C. Casiraghi, A. C. Ferrari, and J. Robertson, "Raman spectroscopy of hydrogenated amorphous carbons," *Physical Review B*, vol. 72, no. 8, Article ID 085401, 2005.

[44] I. Gerhards, C. Ronning, H. Hofsäss, M. Seibt, and H. Gibhardt, "Ion beam synthesis of diamond-like carbon thin films containing copper nanocrystals," *Journal of Applied Physics*, vol. 93, no. 2, pp. 1203–1207, 2003.

[45] J. L. Endrino, D. Horwat, R. Gago et al., "Electronic structure and conductivity of nanocomposite metal (Au, Ag, Cu, Mo)-containing amorphous carbon films," *Solid State Sciences*, vol. 11, no. 10, pp. 1742–1746, 2009.

[46] Y.-H. Chan, C.-F. Huang, K.-L. Ou, and P.-W. Peng, "Mechanical properties and antibacterial activity of copper doped diamond-like carbon films," *Surface and Coatings Technology*, vol. 206, no. 6, pp. 1037–1040, 2011.

[47] S. J. Park, K.-R. Lee, D.-H. Ko, and K. Y. Eun, "Microstructure and mechanical properties of WC-C nanocomposite films," *Diamond and Related Materials*, vol. 11, no. 10, pp. 1747–1752, 2002.

[48] V. Singh, J. C. Jiang, and E. I. Meletis, "Cr-diamondlike carbon nanocomposite films: synthesis, characterization and properties," *Thin Solid Films*, vol. 489, no. 1-2, pp. 150–158, 2005.

[49] T. Sonoda, S. Nakao, and M. Ikeyama, "Deposition of Ti/C nano-composite DLC films by magnetron DC sputtering with dual targets," *Vacuum*, vol. 84, no. 5, pp. 666–668, 2009.

[50] W. Dai, P. Ke, and A. Wang, "Microstructure and property evolution of Cr-DLC films with different Cr content deposited by a hybrid beam technique," *Vacuum*, vol. 85, no. 8, pp. 792–797, 2011.

Hindawi Publishing Corporation
Journal of Nanomaterials
Volume 2013, Article ID 404923, 6 pages
http://dx.doi.org/10.1155/2013/404923

Research Article

Field Emission Properties of Carbon Nanotubes with Boron Doping and H_2O Adsorption

Yijun Wang,[1] Liuding Wang,[2] and Cheng Yan[3]

[1] *School of Physics and Electronic Engineering, Xianyang Normal University, Xianyang 712000, China*
[2] *School of Science, Northwestern Polytechnical University, Xi'an 710129, China*
[3] *Science and Technology on Low-Light-Level Night Vision Laboratory, Xi'an 710065, China*

Correspondence should be addressed to Yijun Wang; 806605363@qq.com

Received 22 August 2013; Accepted 18 November 2013

Academic Editor: Ashkan Vaziri

Copyright © 2013 Yijun Wang et al. This is an open access article distributed under the Creative Commons Attribution License, which permits unrestricted use, distribution, and reproduction in any medium, provided the original work is properly cited.

Gas adsorption and atom doping usually present when preparing carbon nanotubes (CNTs) and can affect the field emission properties of carbon nanotubes. H_2O molecule and boron atom are the most important adsorbates, respectively. Using ab-initio calculations, we have investigated the electron field emission performance of CNTs simultaneously adsorbed with one H_2O molecule and doped with one boron atom (BCNT+H_2O) in this paper. The results indicate that the electrons localize at the top of BCNT+H_2O and the electronic density of states (DOS) around the Fermi level is enhanced obviously. It is expected that BCNT+H_2O will be more propitious to the field emission of electrons based on the calculations of DOS, HOMO/LUMO, and Mulliken charge population.

1. Introduction

Carbon nanotubes (CNTs) have attracted much attention due to their high aspect ratio and remarkable mechanical, electronic, and chemical properties [1–3]. The quasi-one-dimensional structures and unique electric properties make CNTs have a lot of potential applications in different fields [4–6]. Especially, because of the excellent field emission properties, CNTs have been promising candidates for flat-panel displays [7, 8]. Up to now, many experimental [9] and theoretical [10–12] studies have shown that the gas adsorption is of great advantage to the electron emission of the CNTs. For example, Kim et al. calculated the DOS and field emission properties of closed CNTs under electric field [13], Maiti et al. explained the reason why H_2O adsorption on the top of CNTs can improve the electron emission properties [14], and Zhang et al. pointed out that CNTs doped with boron and nitrogen are easy to emit electrons [15].

Naturally, some kinds of gas can markedly change the energy band structure of carbon nanotubes, whereas the work of simultaneous doping and adsorption is rarely reported until now. Therefore, it is very important to study the emission properties of CNTs doped with other atoms and adsorbed with gases under electric field. In this paper we adopted the density functional theory (DFT) to investigate the performances of BCNT+H_2O.

2. Models and Calculation Methods

A single-walled armchair (5, 5) CNT with a cap (Figure 1) is adopted. The cap is a hemisphere (30 carbon atoms) of C_{60} at one end of the CNT and the dangling bonds at the other end are saturated by hydrogen atoms. The position of boron dope is selected at the top layer of the CNT and the distance of H_2O adsorption from the top pentagon is about 0.3 nm. Therefore the whole system contains 93 atoms.

All the calculations were carried out by using first-principle DFT provided by DMOL^3 code [16]. The geometrical optimization was based on the local density approximation (LDA) during self-consistent field iteration with the Perdew-Wang parameterization of the local exchange correlation energy. The generalized gradient approximation (GGA) was adopted to calculate the total energy and various electronic properties with the Perdew-Wang-91 (PW91) function [17]. The all-electron Kohn-Sham wave functions were expanded

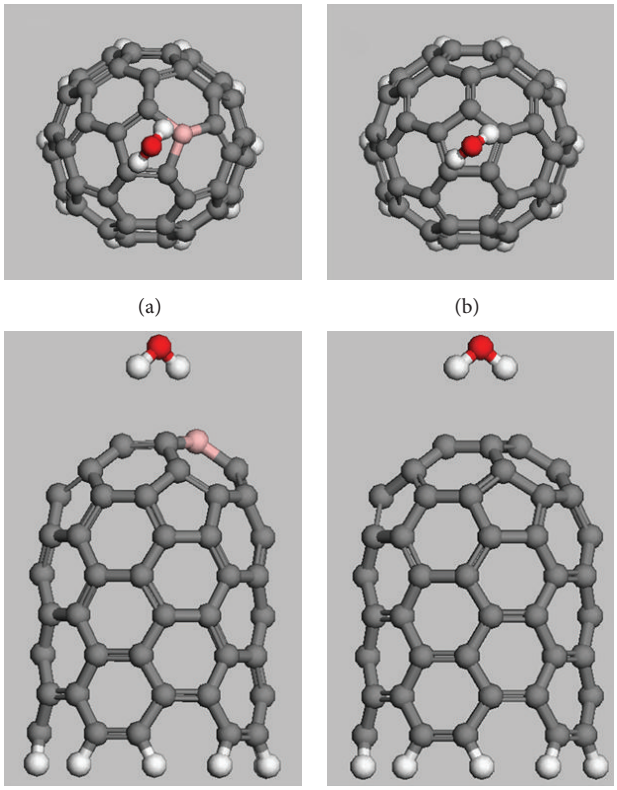

Figure 1: The structures of BCNT+H_2O and CNT+H_2O. (a) and (b) are the top views; (c) and (d) are the side views of BCNT+H_2O and CNT+H_2O, respectively.

in the local atomic orbital basis set with orbital cutoff of 4.5 Å. Self-consistent field procedure was done with a convergence criterion of 10^{-5} a.u. on the energy and electron density.

3. Results and Discussion

In order to study the electronic field emission properties of BCNT+H_2O, a uniform external electric field with the direction from the top to the end of the CNT is applied, whose intensities are $E = 0$ and $E = 10$ eV/nm, respectively. In real field emission conditions, a short tip of the structures is considered. The electric field gradient along CNTs axis is ignored and the whole structure is supposed to be in a uniform external electric field [17].

The adsorption distance and adsorption energy are shown in Table 1. The adsorption energy (W_{ad}) under the different electric field is defined in (1) and (2), respectively. Consider the following:

$$W_{ad(E=0)} = W_{CNTs(E=0)} + W_{H_2O(E=0)} - W_{CNT+H_2O(E=0)}, \quad (1)$$

$$W_{ad(E=10\,eV/nm)} = W_{CNTs(E=10\,eV/nm)} + W_{H_2O(E=0)} - W_{CNT+H_2O(E=10\,eV/nm)}, \quad (2)$$

Table 1: The adsorption distance (nm) and adsorption energy (eV) of CNT + H_2O and BCNT+H_2O systems with and without electric field (eV/nm).

Systems	$E = 0$ eV/nm		$E = 10$ eV/nm	
	Distance/nm	Energy/eV	Distance	Energy
CNT+H_2O	0.307	0.03	0.300	0.91
BCNT+H_2O	0.315	0.09	0.310	1.34

Table 2: Pseudogap (eV) and DOS (electron/eV) at E_f under different electric field (eV/nm).

Systems	$E = 0$ eV/nm		$E = 10$ eV/nm	
	DOS at E_f	Pseudogap	DOS at E_f	Pseudogap
CNT+H_2O	3.14	3.34	10.56	2.12
BCNT+H_2O	10.61	2.10	18.56	1.61

where the $W_{CNTs(E=0)}$, $W_{H_2O(E=0)}$, and $W_{CNT+H_2O(E=0)}$ are the total energy of the pure CNT, the adsorbate (a H_2O molecule), and the adsorbed CNT system, respectively, under the strength of electric field of 0 eV/nm, and where $W_{CNTs(E=10\,eV/nm)}$ and $W_{CNT+H_2O(E=10\,eV/nm)}$ have the same meaning under the strength of electric field of 10 eV/nm.

From Table 1, we can see that the adsorption distance is about 0.3 nm and the adsorption energy is very small for BCNT+H_2O and CNT+H_2O systems in the absence of electric field. When the electric field increases to 10 eV/nm, their adsorption energy is remarkably enhanced, while their adsorption distance decreases slightly. Moreover, Table 1 shows that the adsorption energy of BCNT+H_2O is much higher than that of CNT+H_2O under the same strength of electric field, which indicates that the structure of BCNT+H_2O is more stable [18] than that in a electron transmitter.

Figure 2 presents the DOS of the two systems under the different electric fields and the local density of states (LDOS) of the boron atom and the nearest three carbon atoms on the top of BCNT+H_2O under $E = 10$ eV/nm. Obviously, the DOS plots of the two systems shift towards the low energy direction and their corresponding peak positions of antibond states are more close to E_f when the electric fields increase from 0 to 10 eV/nm. This indicates that the probability of electron occurrence at antibond states increase, which is well consistent with Kim's conclusion [13].

To determine the pseudogap, an advanced peak separation technique [19] is adopted. Furthermore, the DOS at E_f is also calculated, as listed in Table 2. When the electric fields increase from 0 to 10 eV/nm, the DOS of the two systems at E_f enhances by a big margin. Especially the DOS of BCNT+H_2O is about 179% that of CNT+H_2O at $E = 10$ eV/nm. The reasons can be found from Figure 2(e) that the peak position of LDOS for BCNT+H_2O tip is very close to Fermi level, which leads to the enhancement of DOS at E_f. Moreover, we can infer that the external electric field significantly weakens the covalent bond and enhances

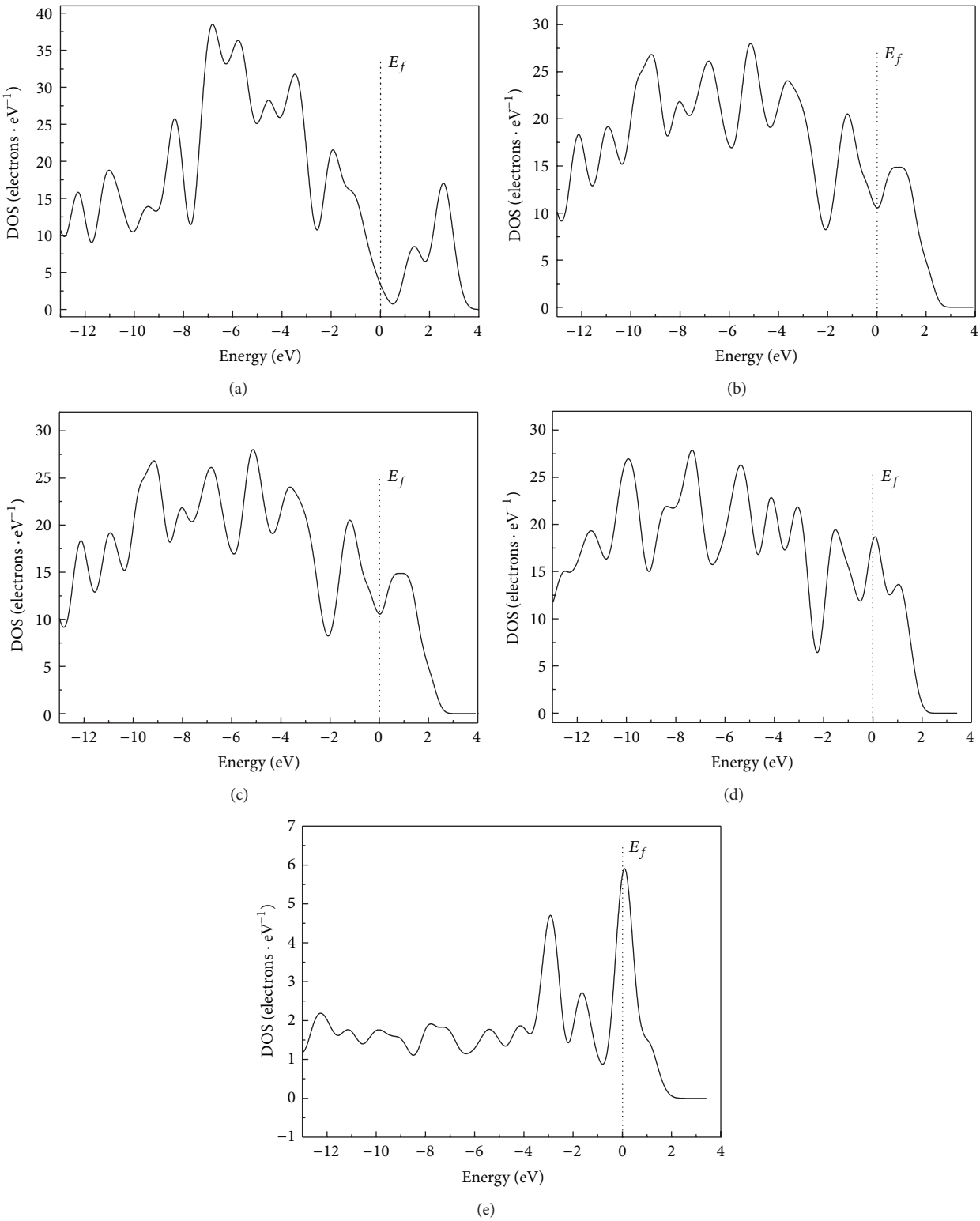

Figure 2: DOS plots of CNT+H_2O and BCNT+H_2O under the different electric field. (a) and (c) are DOS of CNT+H_2O and BCNT+H_2O without electric field, (b) and (d) are DOS of CNT+H_2O and BCNT+H_2O under $E = 10$ eV/nm, and (e) is LDOS of a boron and 3 carbon atoms of BCNT+H_2O under $E = 10$ eV/nm, respectively.

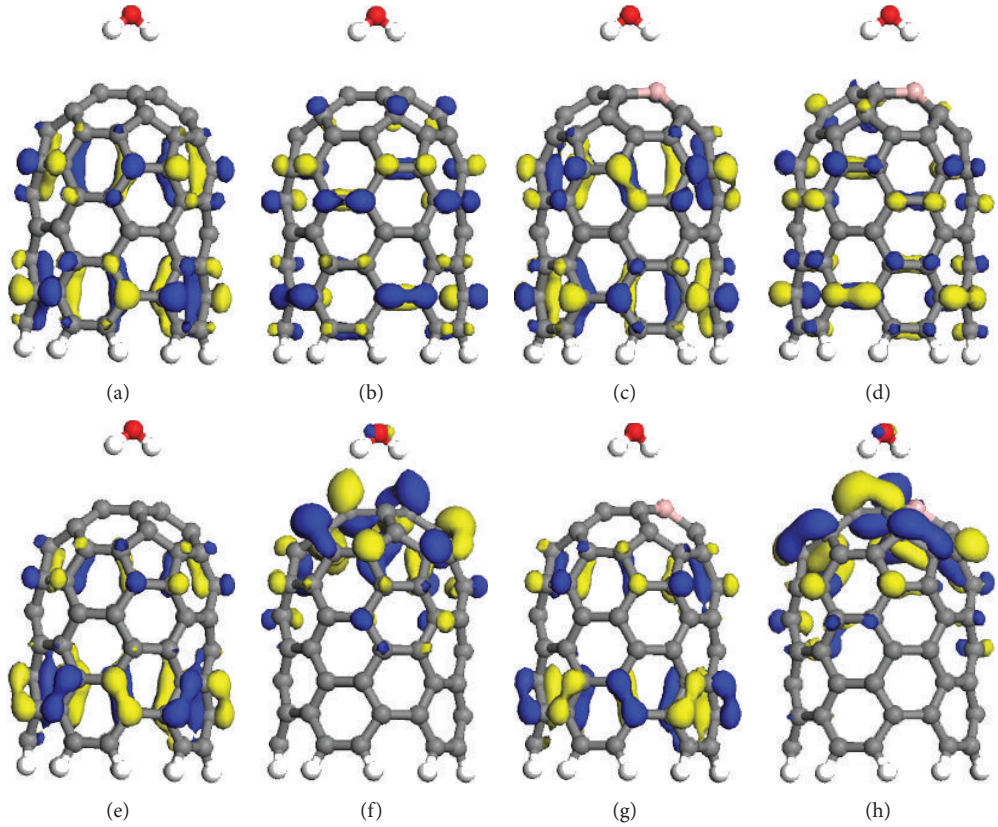

Figure 3: Side views of the charge density under different electric field: (a), (b) and (c), (d) refer to HOMO/LUMO of CNT+H_2O and BCNT+H_2O without electric field, respectively. (e), (f) and (g), (h) refer to HOMO/LUMO of CNT+H_2O and BCNT+H_2O under E = 10 eV/nm, respectively.

the metallic bond from the pseudogap of BCNT+H_2O compared with CNT+H_2O. Therefore, the calculated results and theoretical analysis above mentioned indicate consistently that the electron transmission in BCNT+H_2O is much easier and the corresponding field emission properties can be effectively improved compared with CNT+H_2O.

To further investigate the field emission property of BCNT+H_2O, we have performed the electronic orbital analysis. As shown in Figure 3, the HOMOs of CNT+H_2O and BCNT+H_2O are all localized at their body and the distribution is very similar no matter whether the electric field is applied or not. However, the LUMO of later is mainly localized at the tip of CNTs at E = 10 eV/nm.

This means that there are more electrons congregating on the top region of BCNT+H_2O. Once the stronger electric field is applied these electrons immediately emit to the surrounding space. It can be seen that the conclusions of orbital analysis are well consistent with that of the discussion above.

When a boron atom substitutes a carbon atom in the top layer, the charges distribution and the electronic structures change accordingly. Figure 4 exhibits the results of Mulliken population analysis for the CNT+H_2O and BCNT+H_2O in the presence of E = 10 eV/nm. We can see that the boron atom carries a little negative charge and each of the nearest three carbon atoms carries much more negative charges than other atoms located in the first and second layer [20]. The analysis results show that the boron doping can cause more electrons aggregation at the top. Essentially, the electron congregation becomes more obvious with the increase of applied electric field and extra electrons on the tip of system will congregate in the conduction band. Consequently the Fermi level shifts toward the vacuum level. This will lower the potential barrier of BCNT+H_2O tip and make the field emission more easily. All of these discussions indicate that BCNT+H_2O can enhance the electron field emission.

4. Conclusions

In summary, we investigate the electronic structure and physical mechanism of the fieldemission of the capped SWNT which are simultaneously adsorbed with one H_2O molecule and doped by a boron atom in the top layer. The calculations and analysis confirm that BCNT+H_2O has a higher DOS at E_f than CNT+H_2O. Although the HOMO of BCNT+H_2O changes hardly with and without the applied electric field, the LUMO is highly localized at the top. Furthermore, the Mulliken population analysis shows that a lot of electrons congregate at the cap of BCNT+H_2O. Naturally, present results of the LDOS, the pseudogap, the HOMO/LUMO, and Mulliken population analysis congruously indicate that

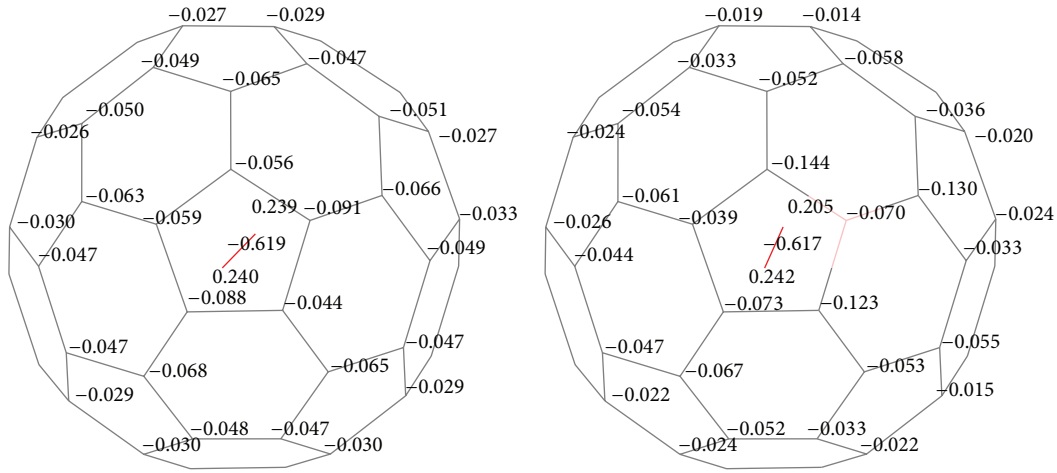

FIGURE 4: Mulliken population analysis of CNT+H_2O (a) and BCNT+H_2O (b) under $E = 10$ eV/nm.

BCNT+H_2O can effectively improve the fieldemission properties of carbon nanotubes compared with CNT+H_2O.

Conflict of Interests

The authors, hereby, declare that they do not have any conflict of interests.

Acknowledgments

This work was financially supported by the National Natural Science Foundation of China (11075135, 61307002), the Natural Science Foundation of Shaanxi Province (no. 2012JM1009), the Scientific Research Program of Shaanxi Provincial Education Department (no. 12JK0984), the Scientific Research Program (nos. 12XSYK014, 12XSYK017), and the Teaching Reform Research Program of Xianyang Normal University (no. 201200127), China.

References

[1] S. Iijima, "Helical microtubules of graphitic carbon," *Nature*, vol. 354, no. 6348, pp. 56–58, 1991.

[2] C. Hierold, O. Brand, G. K. Fedder, J. G. Korvink, and O. Tabata, *Carbon Nanotube Devices: Properties, Modeling, Integration and Applications*, vol. 8 of *Advanced Micro & Nanosystems*, Wiley-VCH, 2008.

[3] A. V. Eletskii, "Carbon nanotube-based electron field emitters," *Physics-Uspekhi*, vol. 53, no. 9, pp. 863–892, 2010.

[4] J. Ali, A. Kumar, S. Husain, M. Kumari, H. Harsh, and M. Husain, "Characterization and field emission studies of uniformly distributed multi-walled carbon nanotubes (MWCNTS) film grown by low-pressure chemical vapour deposition (LPCVD)," *Current Nanoscience*, vol. 7, no. 3, pp. 333–336, 2011.

[5] S. M. Lupekhin and A. A. Ibragimov, "Field emission of electrons from a single carbon fiber with a nanostructured emitting surface," *Technical Physics*, vol. 57, no. 1, pp. 119–123, 2012.

[6] E. F. Zharikova, L. I. Ochertyanova, I. V. Vasylenko et al., "Multi-walled carbon nanotubes with the pyridine-containing fragment and copper(II) ions," *Russian Chemical Bulletin*, vol. 61, no. 7, pp. 1430–1436, 2012.

[7] V. Guglielmotti, E. Tamburri, S. Orlanducci et al., "Macroscopic self-standing SWCNT fibres as efficient electron emitters with very high emission current for robust cold cathodes," *Carbon*, vol. 52, no. 2, pp. 356–362, 2013.

[8] N. Perea-López, B. Rebollo-Plata, J. A. Briones-León et al., "Millimeter-long carbon nanotubes: outstanding electron-emitting sources," *ACS Nano*, vol. 5, no. 6, pp. 5072–5077, 2011.

[9] X. P. Tang, A. Kleinhammes, H. Shimoda et al., "Electronic structures of single-walled carbon nanotubes determined by NMR," *Science*, vol. 288, no. 5465, pp. 492–494, 2000.

[10] S. Seenithurai, R. K. Pandyan, S. V. Kumar, and M. Mahendran, "H_2 adsorptionin Ni and passivated Ni doped 4 Å single walledcarbon nanotube," *International Journal of Hydrogen Energy*, vol. 38, no. 18, pp. 7376–7381, 2013.

[11] M. O. Ezzat, O. H. S. Al-Obaidi, and M. N. Mordi, "Theoretical study of benzylic oxidation and effect of para—substituents by using hyperchem program," *Journal of Proteomics and Bioinformatics*, vol. 4, no. 5, pp. 113–115, 2011.

[12] B. Lu and Z. Zhen, "Computational study of B- or N-doped single-walled carbon nanotubes as NH_3 and NO_2 sensors," *Carbon*, vol. 45, no. 10, pp. 2105–2110, 2007.

[13] C. Kim, B. Kim, S. M. Lee, C. Jo, and Y. H. Lee, "Electronic structures of capped carbon nanotubes under electric fields," *Physical Review B*, vol. 65, no. 16, pp. 165418–165423, 2002.

[14] A. Maiti, J. Andzelm, N. Tanpipat, and P. Von Allmen, "Effect of adsorbates on field emission from carbon nanotubes," *Physical Review Letters*, vol. 87, no. 15, Article ID 155502, 2001.

[15] G. Zhang, W. Duan, and B. Gu, "Effect of substitutional atoms in the tip on field-emission properties of capped carbon nanotubes," *Applied Physics Letters*, vol. 80, no. 14, pp. 2589–2591, 2002.

[16] B. J. Delley, "DMOL is available commercially from BIOSYM technologies," *Chemical Physics*, vol. 92, pp. 508–517, 1990.

[17] L. Qiao, W. T. Zheng, H. Xu, L. Zhang, and Q. Jiang, "Field emission properties of N-doped capped single-walled carbon nanotubes: a first-principles density-functional study," *Journal of Chemical Physics*, vol. 126, no. 16, Article ID 164702, 2007.

[18] Z. Li and C. Y. Wang, "First-principles study of field emission properties of gas adsorption on the carbon nanotubes," *Chemical Physics*, vol. 330, no. 3, pp. 417–422, 2006.

[19] L. D. Wang, J. Q. Zhou, Q. X. Cao, and Z. Chen, "Investigation of peak separation for X-ray diffraction profiles of spinodal decomposition by a kind of optimized Voigt function," *Journal of Materials Science and Technology*, vol. 19, no. 4, pp. 371–373, 2003.

[20] Y. J. Wang, L. D. Wang, M. Yang, and C. Yan, "Effects of B and N dopings and H_2O adsorption on structural stability and field emission properties of cone-capped carbon nanotubes," *Chinese Physics B*, vol. 20, no. 11, Article ID 117304, 2011.

Hindawi Publishing Corporation
Journal of Nanomaterials
Volume 2013, Article ID 750318, 7 pages
http://dx.doi.org/10.1155/2013/750318

Research Article

Nitrogen-Doped Carbon Nanotubes Synthesised by Pyrolysis of (4-{[(Pyridine-4-yl)methylidene]amino}phenyl)ferrocene

Godfrey Keru, Patrick G. Ndungu, and Vincent O. Nyamori

School of Chemistry and Physics, University of KwaZulu-Natal, Westville Campus, Private Bag X54001, Durban 4000, South Africa

Correspondence should be addressed to Vincent O. Nyamori; nyamori@ukzn.ac.za

Received 3 June 2013; Accepted 13 August 2013

Academic Editor: Myoung-Woon Moon

Copyright © 2013 Godfrey Keru et al. This is an open access article distributed under the Creative Commons Attribution License, which permits unrestricted use, distribution, and reproduction in any medium, provided the original work is properly cited.

Nitrogen-doped carbon nanotubes (N-CNTs) were synthesized by pyrolysis of (4-{[(pyridine-4-yl)methylidene]amino}phenyl) ferrocene in a solution of either acetonitrile or toluene as carbon source. This was achieved by testing three different growth temperatures (800, 850, and 900°C), and the 850°C was found to be the most favourable condition for N-CNT growth. At the lower temperature of 800°C, amorphous carbon was mainly formed while at the higher temperature of 900°C, the yield of carbon spheres (CSs) increased. Apart from the variation in temperature, the formation of other shaped carbon nanomaterials (SCNMs) was found to be carbon source dependent. Acetonitrile was found to produce mainly N-CNTs with "bamboo" morphology while toluene formed a mixture of pristine CNTs and N-CNTs in the ratio of 1 : 1. N-CNTs, and other SCNMs synthesized were characterized by means of TEM, SEM, Raman spectroscopy, TGA, and elemental analysis.

1. Introduction

The introduction of heteroatoms into the backbone of carbon nanotubes (CNTs) changes their structural, chemical, and electrical properties [1]. Doping CNTs with nitrogen creates superficial defects that alters the chemical properties of CNTs and creates a path to reactivity and applications [2]. Some of the potential applications of N-CNTs include lithium storage [3, 4], biosensors [5, 6], fuel cells [7, 8], drug delivery [9], catalytic support [10], field emission [4, 11], and electronic devices [12], among others.

Heteroatom doping was first reported by Stephan et al. [13]. They doped CNTs with nitrogen and boron by means of the arc discharge method. Currently, nitrogen doping is accomplished by either *in situ* or *ex situ* [14] methods whereby in the latter the walls of CNTs are functionalized with nitrogen-containing groups by use of molecules such as NH_3 [15] subsequent to CNT synthesis. Another useful example of *ex situ* technique which does not involve a simple molecule but a complex has been illustrated by Schilling and Bron [16], where they functionalised multi-walled CNTs with the aid of a nitrogen-containing complex, iron tetramethoxyphenylporphyrin chloride (FeTMMP-Cl). On the other hand, nitrogen doping using *in situ* synthesis has been reported by means of arc discharge [17], laser ablation [18], and chemical vapour deposition (CVD) [19] techniques. In general, the CVD method is preferred since it is more economical, relatively easier to produce and scale up the synthesis of N-CNTs. In this approach, the carbon source also provides the nitrogen source [2, 20]; however, the catalyst can also act as a source of nitrogen [9, 21]. Additional examples include the use of nitrogen source that is completely separate from the carbon source and the catalyst [22].

N-CNTs can be identified by the characteristic "bamboo" morphology that arises due to the presence of nitrogen, which introduces defects and pentagon rings in the graphene network that results in a positive curvature of the tubular layer [1]. The distance between each bamboo compartment has been found to be directly proportional to the amount of nitrogen doping with a smaller size compartment signifying a higher nitrogen doping level [23]. Organometallic complexes, especially ferrocene and its derivatives, have been used as both catalysts and as carbon sources for the synthesis of CNTs and other shaped carbon nanomaterials (SCNMs) [24]. The use of ferrocene and acetonitrile has also been investigated [25]; however, in this

paper we report on the use of an organometallic complex, (4-{[(pyridine-4-yl)methylidene]amino}phenyl)ferrocene, $[Fe(C_5H_5)(C_{17}H_{13}N_2)]$, which is a novel ferrocenyl derivative as a catalyst for the synthesis of N-CNTs. It does not only act as the source of active metal iron nanoparticle but also as nitrogen and carbon source in a solution of acetonitrile or toluene. This paper also explores the variation of growth temperature and how it affects the yield, type of SCNMs formed and level of nitrogen doping.

2. Experimental

All the chemicals used were of analytical grade and were used as received unless stated otherwise. The catalyst precursors were synthesized as previously reported: 4-nitrophenyl ferrocene [26] and 4-ferrocenylaniline by catalytic reduction of 4-nitrophenyl ferrocene as reported by Altaf et al. [27]. In brief, 2 g of 4-nitrophenyl ferrocene was dissolved in 100 mL of methanol, and 2.62 g of zinc powder was slowly added to the mixture while stirring. Then 4 mL of formic acid was added drop wise, and thereafter the mixture was heated to 70°C. The reaction was monitored by TLC, and the reaction product was isolated with a yield of 85%. (4-{[(Pyridine-4-yl) methylidene]amino}phenyl)ferrocene was prepared as reported earlier by our group [28] under solvent-free conditions. Briefly, this involved mixing 4-ferrocenylaniline (130 mg, 0.47 mmol) and pyridine-4-carboxyaldehyde (76 mg, 0.71 mmol) in a Pyrex tube fitted with a ground glass joint (Scheme 1). The solid mixture was thoroughly ground leading to a melt, which solidified once it was left to stand under vacuum. The red solid was then subjected to column chromatography using a solvent mixture of hexane : dichloromethane in the ratio of 8 : 2. The pure product was isolated and obtained as red crystals.

An amount of 2.5 wt.% of (4-{[(pyridine-4-yl)methylidene]amino}phenyl)ferrocene was used as a catalyst in the CVD floating catalyst method to synthesize N-CNTs. The setup of the reactor used was based on a previously reported design [29]. A quartz tube (inner diameter 27 mm and length 850 mm), used as the reactor vessel, was placed inside a muffle/tube furnace (model no. TSH12/50/610, Elite Thermal Systems Ltd) fitted with a main zone temperature controller (Eurotherm 2416). The temperature was controlled and set to the desired maximum reaction temperature (T_{max}), that is, 800, 850, or 900°C. The purging and reducing gas was 10% H_2 in argon (v/v) set at a flow rate of 100 mL/min. When the desired temperature (T_{max}) was attained, a solution of 2.5 wt.% catalyst and the carbon source was injected at a rate of 0.8 mL/min with the aid of a New Era Inc., syringe pump (model no. NE 300). The carbonaceous materials obtained from the uniform hot zone were collected and weighed. The products were characterized by means of transmission electron microscopy (TEM), scanning electron microscopy (SEM), Raman spectroscopy, thermogravimetric analysis, and elemental analysis.

3. Results and Discussion

The catalyst, (4-{[(pyridine-4-yl)methylidene]amino}phenyl)ferrocene was easily synthesized under solvent-free conditions to obtain an excellent yield (162 mg, 94%) and characterized as before [28]. The catalyst was further utilized in a solution of either toluene or acetonitrile as the carbon source to synthesize shaped carbon nanomaterials (SCNMs) by means of the floating catalyst CVD method. Apart from the catalyst, acetonitrile was also used as an additional nitrogen source, and the results obtained are shown in Table 1.

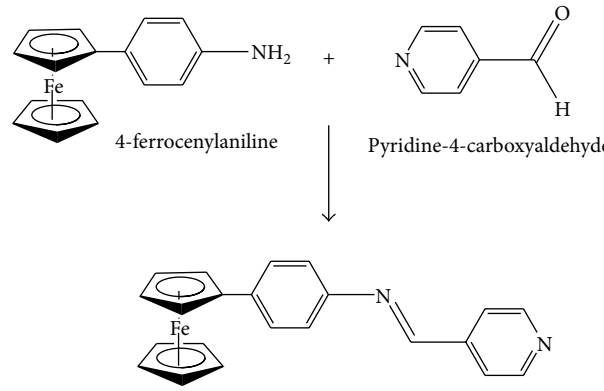

(4-{[(pyridine-4-yl)methylidene]amino}phenyl)ferrocene

Scheme 1: Solvent-free synthesis of (4-{[(pyridine-4-yl)methylidene]amino}phenyl)ferrocene.

From the results, three types of SCNMs were formed, that is, CNTs, amorphous carbon (Ac), and carbon spheres (CSs). These results are in agreement with the findings of Nxumalo et al. [30] who reported formation of similar products by pyrolysis of ferrocenylaniline or a mixture of ferrocene and aniline in different proportions by using toluene as the carbon source at 900°C. However, in their case they also obtained carbon fibres. It is evident that the resultant products and their distribution are dependent not only on the catalyst and carbon source used, but also on the choice of reaction conditions such as reaction temperature (T_{max}), reaction time, gas flow rate, and pressure [31]. Figure 1 shows the TEM images of a representative samples of the SCNMs obtained.

The TEM images in Figure 1 show that the CNTs formed have "bamboo" shaped compartments which usually signifies nitrogen doping. Bamboo compartments arise due to formation of pentagonal rings in the graphene network, which induces positive curvature in the graphene layer [1]. Inclusion of nitrogen or oxygen in the carbon graphene network is relatively easy. This is more so due to similarities in their hybridisation and bond length, that is, C=C, C=O, and C=N being 1.38 Å, 1.36 Å, and 1.34 Å, respectively. However, the C=N bond length is shorter than that of C=C, and hence it distorts the order in the graphene matrix by introducing pentagons which cause strain in the structure [32]. These distortions created by the nitrogen atoms cause defects and are seen to be more concentrated in the inner layer than other layers, and hence the bamboo morphology is more pronounced inside the tube [33].

3.1. Effect of Carbon Source. The effect of the carbon source on the size of individual bamboo compartments, wall thickness

Table 1: Products obtained by pyrolysis of (4-{[(pyridine-4-yl)methylidene]amino}phenyl)ferrocene (2.5 wt.%) in a solution of toluene or acetonitrile.

Temperature (°C)	Carbon source	Yield (mg)	Composition of the product*	Avg. ID (nm)	Avg. OD (nm)
800	Toluene	176	40% T; 60% Ac	10.19	60.19
	Acetonitrile	100	60% T; 40% Ac	31.309	50.64
850	Toluene	300	50% T; 45% CS; 5% Ac	15.62	68.31
	Acetonitrile	178	85% T; 15% Ac	54.248	60.709
900	Toluene	570	2% T; 98% CS	25.36	73.76
	Acetonitrile	240	20% T; 80% CS	65.69	76.47

*The composition of the products is based on acceptable counting procedures using electron micrographs; at least 50 images were used in each case and over 200 SCNMs were counted per sample.
T: carbon nanotubes; Ac: amorphous carbon; CS: carbon spheres; Avg. ID: average inner diameter; Avg. OD: average outer diameter.

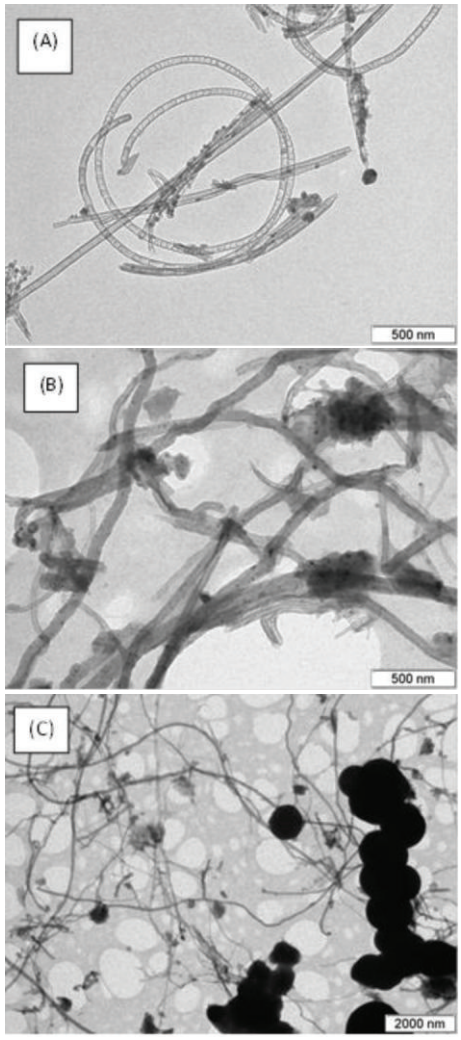

Figure 1: TEM images of SCNMs synthesized from a solution of (A) acetonitrile at 850°C, (B) acetonitrile at 800°C, and (C) toluene at 850°C.

and general morphology of CNTs was investigated. This was accomplished by comparing the type of CNTs formed when a solution of acetonitrile or toluene was used as the carbon source. Figure 2 shows some TEM images of N-CNTs grown from a solution of either acetonitrile or toluene.

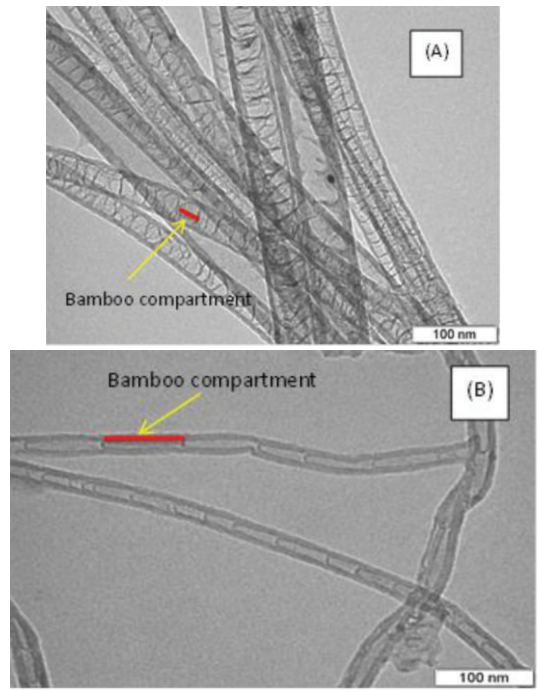

Figure 2: TEM images of N-CNTs synthesized at 850°C from a solution of (A) acetonitrile and (B) toluene. The red lines and arrows on the images indicate the individual bamboo compartments.

The sizes of each bamboo compartment were different and this has a direct relationship with the amount of nitrogen from the nitrogen source. N-CNTs synthesized from a solution of acetonitrile formed shorter bamboo compartments compared with the ones formed from a solution of toluene. A possible explanation could be that more nitrogen atoms are incorporated into the structure since apart from the ferrocenyl derivative which contains nitrogen, the acetonitrile solvent also introduces additional nitrogen which would also be involved in the doping process. These findings concur with those of Nxumalo et al. [30], who observed a decrease in bamboo compartment size and more individual compartments in each tube, which was an indication of the increased extent of nitrogen doping. Chen et al. [8] also reported a positive correlation between higher nitrogen content in the carbon source and higher nitrogen doping in the N-CNTs.

In addition to the bamboo compartment size, the use of acetonitrile formed N-CNTs with bigger internal diameters and smaller wall thicknesses. The increased internal diameter and reduced wall thickness could be due to the level of nitrogen doping. Our findings concur with those of Ionescu et al. [34] who reported an increase in internal N-CNT diameter and decrease in wall thickness with increased nitrogen doping.

Some of the CNTs synthesised in a solution of toluene lacked bamboo structures, indicating that effective nitrogen doping did not readily take place in the graphene network. The number of N-CNTs (with bamboo structures) and pristine CNTs was in the ratio 1 : 1. This was determined by counting tubes in at least 50 images. Koós and coworkers [31] made a similar observation when they synthesized N-CNTs in a solution of toluene in 5% benzylamine. This suggests that nitrogen doping significantly depends on both choice of carbon source and catalyst [35]. It was noted that N-CNTs synthesized from a solution of acetonitrile were well aligned (Figure 3(a)). On the other hand, the pristine CNTs (as determined by lack of bamboo structures) synthesised from a solution of toluene were observed to have kinks, were wavy, and not aligned (Figure 3(b)). A possible reason could be that products derived from the latter approach were not only less ordered, but also intermingled with a mixture of pristine CNTs and N-CNTs, and hence distorting the alignment of the tubes [31].

3.2. Effect of Growth Temperature. Varying the growth temperature was found to have an effect on the level of nitrogen doping, yield, and the graphitic nature or crystallinity of N-CNTs.

3.2.1. The Nitrogen-Doping Percentage. Elemental analysis (CHNS) was used to study the relationship between growth temperature and nitrogen-doping. It was observed that the nitrogen-doping percentage increased from zero to 2.21% in N-CNTs synthesized in a solution of toluene as the growth temperature increased from 800 to 850°C. When a solution of acetonitrile was used, a similar, but more effective, doping trend was observed; that is, the nitrogen-doping percentage increased from 3.96% to 17.57% in the same temperature range. However, a different trend was observed when the growth temperature was increased to 900°C when acetonitrile was used as a carbon source. The doping percentage decreased to 3.47%. A possible explanation of this reduction could be that as the growth temperature was raised to 900°C, elemental nitrogen that is usually incorporated into the graphene structure did not react but escaped through the exhaust system, and this was evident from the water trap showing more vigorous bubbling. Our findings concur with Tang et al. [35], who reported that the level of nitrogen-doping decreased by half when the temperature was increased from 800 to 900°C. The highest nitrogen doping was noted at 850°C in a solution of acetonitrile indicating a direct relationship between nitrogen doping, growth temperature and amount of nitrogen in the carbon sources. Furthermore, in terms of the extent of nitrogen doping, the elemental analysis at 850°C strongly correlates with the TEM observations (Figure 2) and results discussed above.

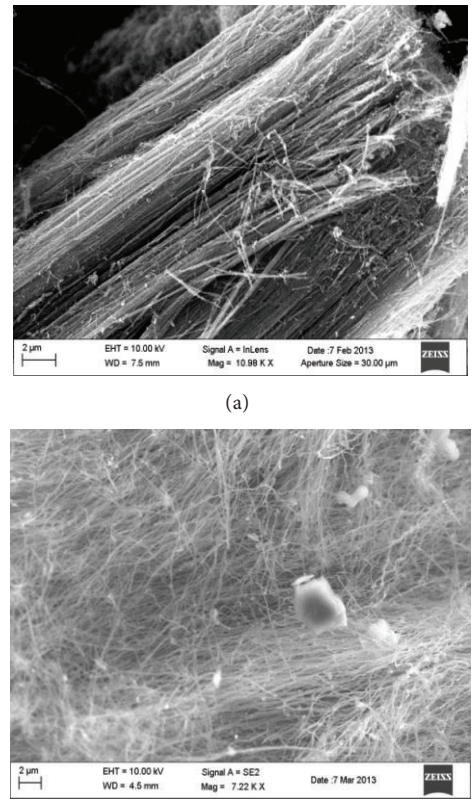

Figure 3: SEM images of CNTs synthesized at 850°C from a solution of (a) acetonitrile and (b) toluene showing the former to be well aligned and the latter to be wavy.

3.2.2. N-CNT Yield and General Morphology. Generally the yield of N-CNTs increased with growth temperature for both acetonitrile and toluene. A solution of toluene gave a higher yield (176, 300, and 570 mg) compared with acetonitrile (100, 178, and 240 mg) at 800, 850, and 900°C, respectively (Table 1). It was also evident that the type of SCNMs formed changed with growth temperature. At 800°C, a lot of Ac formed but the amount decreased as the growth temperature increased to 900°C. However, the percentage of CS increased with growth temperature. A possible reason could be due to agglomeration of catalyst nanoparticles into bigger particles at higher temperatures (note that catalyst concentration was kept constant) and hence favouring the growth of other nanomaterials other than CNTs [36]. Seah et al. [37] also observed a similar trend at high temperature, and attributed this to higher catalyst/carbon ratio would also lead to catalyst particles agglomerating at a higher rate, hence, becoming too large and thus resulting in unfavourable conditions for 2 CNT growth.

The morphology of the N-CNTs such as the outer diameter (OD) was observed to change with growth temperature.

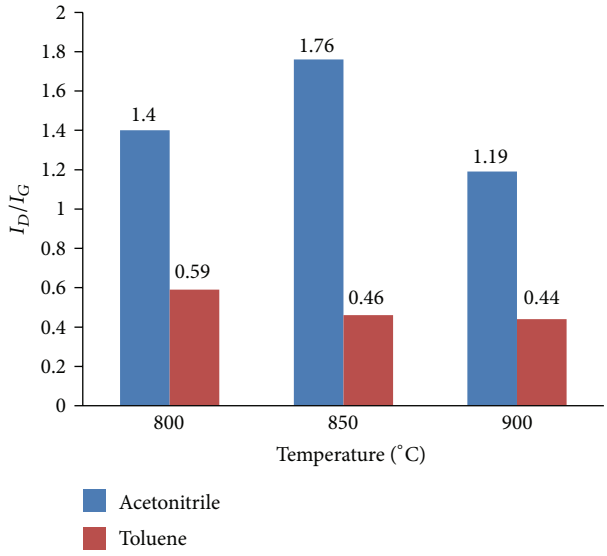

FIGURE 4: Raman chart comparing I_D/I_G ratio at the different growth temperatures.

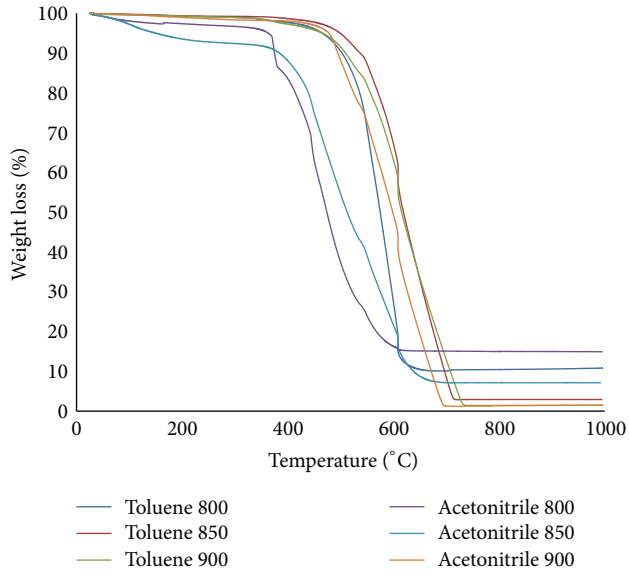

FIGURE 5: Thermogravimetric analysis of SCNMs at different growth temperatures (°C) in a solution of either toluene or acetonitrile.

The OD of the tubes was observed to increase with increase in growth temperature for acetonitrile (Table 1). However, when using a solution of toluene, it was only possible to compare samples at temperatures of 800 and 850°C, and the trend was similar. A possible explanation for the increase in outer diameter with increase in temperature could be due to agglomeration and increase in catalysts particle sizes which favour formation of CNTs with large outer diameters. N-CNTs synthesised with a solution of acetonitrile at 850°C had larger outer diameters (60.79 nm) compared with those grown from a solution of toluene (55.3 nm). In contrast, at 800°C N-CNTs from toluene had bigger outer diameters than those from acetonitrile (60.19 nm compared with 50.64 nm, resp.). As for the internal diameter (I.D.), N-CNTs synthesized from acetonitrile were larger compared with ones grown from toluene. The opposite was observed for the wall thickness of N-CNTs synthesized from toluene that showed thicker walls compared with those grown from acetonitrile as the carbon source.

3.2.3. Graphitic Nature/Crystallinity. Raman spectroscopy was used to study the effect of growth temperature on the graphitic nature of N-CNTs. Two major peaks were observed: the *G*-band (between 1560 and 1599 cm^{-1}) which originates from the Raman E_{2g} mode and the *D*-band (between 1347 and 1363 cm^{-1}) which is the disorder-induced band. The intensities of the *G*-band and *D*-band were observed to differ, and evidence can be seen from the I_D/I_G ratio (Figure 4).

This ratio is an indicator of the graphitic nature of the N-CNTs or degree of disorder, and it was observed to increase from 800 to 850°C for tubes synthesised with acetonitrile. Nitrogen doping in N-CNTs increased as the growth temperature rose from 800 to 850°C which implies a higher level of disorder, and this agrees with the results from elemental analysis and the TEM observations. In contrast, the I_D/I_G ratio of tubes synthesized from toluene decreased between 800 and 850°C, which is an indication of the formation of more graphitic tubes. However, Table 1 shows a reduction of Ac product as the growth temperature increases, and this could also be a possible reason for the increase in the graphitic nature of the product at higher temperature. Generally, the N-CNTs synthesised in a solution of acetonitrile were found to be more disorderly at all growth temperatures, and this is possibly due to the level of nitrogen doping.

Thermogravimetric analysis was used to investigate the thermal stability of SCNMs synthesized at different growth temperatures in a solution of acetonitrile or toluene. Figure 5 shows the thermograms.

SCNMs synthesized from a solution of toluene were thermally more stable compared with those grown from acetonitrile as confirmed by observing the initial decomposition temperature. A possible explanation is that toluene provided more pristine CNTs, which are more structured with fewer defects, while acetonitrile mainly formed N-CNTs, which is inline with our elemental analysis results, TEM observations, and Raman analysis. N-CNTs, synthesized at a temperature of 850°C which had the highest level of nitrogen-doping, showed the least thermal stability. The decomposition temperature increased from 481°C to 600°C for N-CNTs synthesized from acetonitrile at growth temperatures of 850 and 900°C, respectively. This shows that the thermal stability increased as the growth temperature increased from 850 to 900°C which supports the decrease in the level of nitrogen doping.

4. Conclusion

N-CNTs were synthesized by pyrolysis of (4-{[(pyridine-4-yl)methylidene]amino}phenyl)ferrocene in a solution of either toluene or acetonitrile. Acetonitrile formed N-CNTs

with mainly bamboo morphology indicative of nitrogen doping. The N-CNTs were found to be generally less thermally stable and less graphitic. Also the thermal stability decreases as the level of nitrogen doping increases. A solution of toluene formed a mixture of nitrogen-doped and pristine CNTs. In general, the growth temperature was found to affect the yield, type of SCNMs formed, and level of nitrogen doping. Hence, this study has shown that the SCNMs synthesised depend on the conditions of synthesis and the precursors used.

Acknowledgments

The authors wish to thank the University of KwaZulu-Natal, the National Research Foundation (NRF) and the India, Brazil, and South Africa (IBSA) energy project for financial assistance.

References

[1] X. Li, G. Zhu, and Z. Xu, "Nitrogen-doped carbon nanotube arrays grown on graphene substrate," *Thin Solid Films*, vol. 520, no. 6, pp. 1959–1964, 2012.

[2] P. Ayala, R. Arenal, M. Rümmeli, A. Rubio, and T. Pichler, "The doping of carbon nanotubes with nitrogen and their potential applications," *Carbon*, vol. 48, no. 3, pp. 575–586, 2010.

[3] W. H. Shin, H. M. Jeong, B. G. Kim, J. K. Kang, and J. W. Choi, "Nitrogen-doped multi-wall carbon nanotubes for lithium storage with extremely high capacity," *Nano Letters*, vol. 12, pp. 2283–2288, 2012.

[4] G. Zhang, W. Duan, and B. Gu, "Effect of substitutional atoms in the tip on field-emission properties of capped carbon nanotubes," *Applied Physics Letters*, vol. 80, no. 14, pp. 2589–2591, 2002.

[5] S. Boncel, K. H. Müller, J. N. Skepper, K. Z. Walczak, and K. K. K. Koziol, "Tunable chemistry and morphology of multi-wall carbon nanotubes as a route to non-toxic, theranostic systems," *Biomaterials*, vol. 32, no. 30, pp. 7677–7686, 2011.

[6] X. Feng, R. Li, Y. Ma et al., "Nitrogen-doped carbon nanotube/polyaniline composite: synthesis, characterization, and its application to the detection of dopamine," *Science China Chemistry*, vol. 54, no. 10, pp. 1615–1621, 2011.

[7] Y. Shao, J. Sui, G. Yin, and Y. Gao, "Nitrogen-doped carbon nanostructures and their composites as catalytic materials for proton exchange membrane fuel cell," *Applied Catalysis B*, vol. 79, no. 1, pp. 89–99, 2008.

[8] Z. Chen, D. Higgins, and Z. Chen, "Nitrogen doped carbon nanotubes and their impact on the oxygen reduction reaction in fuel cells," *Carbon*, vol. 48, no. 11, pp. 3057–3065, 2010.

[9] Y. Zhao, Y. Tang, Y. Chen, and A. Star, "Corking carbon nanotube cups with gold nanoparticles," *American Chemical Society Nano*, vol. 6, pp. 6912–6921, 2012.

[10] Y. Chen, J. Wang, H. Liu et al., "Nitrogen doping effects on carbon nanotubes and the origin of the enhanced electrocatalytic activity of supported pt for proton-exchange membrane fuel cells," *Journal of Physical Chemistry C*, vol. 115, no. 9, pp. 3769–3776, 2011.

[11] L. G. Bulusheva, O. V. Sedelnikova, and A. V. Okotrub, "Substitutional sites of nitrogen atoms in carbon nanotubes and their influence on field-emission characteristics," *International Journal of Quantum Chemistry*, vol. 111, no. 11, pp. 2696–2704, 2011.

[12] A. Oikonomou, T. Susi, E. I. Kauppinen, and A. Vijayaraghavan, "Growth, dispersion, and electronic devices of nitrogen-doped single-wall carbon nanotubes," *Physica Status Solid B*, vol. 249, pp. 2416–2419, 2012.

[13] O. Stephan, P. M. Ajayan, C. Colliex et al., "Doping graphitic and carbon nanotube structures with boron and nitrogen," *Science*, vol. 266, no. 5191, pp. 1683–1685, 1994.

[14] J. D. Wiggins-Camacho, "Effect of nitrogen-doping on the 4 electronic and catalytic properties of carbon nanotube electrode materials," http://repositories.lib.utexas.edu/bitstream/handle/2152/ETD-UT-2011-05-2669/WIGGINS-CAMACHO-DISSERTATION.pdf?sequence=1.

[15] L. Jiang and L. Gao, "Modified carbon nanotubes: an effective way to selective attachment of gold nanoparticles," *Carbon*, vol. 41, no. 15, pp. 2923–2929, 2003.

[16] T. Schilling and M. Bron, "Oxygen reduction at Fe-N-modified multi-walled carbon nanotubes in acidic electrolyte," *Electrochimica Acta*, vol. 53, no. 16, pp. 5379–5385, 2008.

[17] M. Glerup, J. Steinmetz, D. Samaille et al., "Synthesis of N-doped SWNT using the arc-discharge procedure," *Chemical Physics Letters*, vol. 387, no. 1–3, pp. 193–197, 2004.

[18] D. Golberg, Y. Bando, L. Bourgeois, K. Kurashima, and T. Sato, "Large-scale synthesis and HRTEM analysis of single-walled B- and N-doped carbon nanotube bundles," *Carbon*, vol. 38, no. 14, pp. 2017–2027, 2000.

[19] E. N. Nxumalo, P. J. Letsoalo, L. M. Cele, and N. J. Coville, "The influence of nitrogen sources on nitrogen doped multi-walled carbon nanotubes," *Journal of Organometallic Chemistry*, vol. 695, no. 24, pp. 2596–2602, 2010.

[20] L. Chen, K. Xia, L. Huang, L. Li, L. Pei, and S. Fei, "Facile synthesis and hydrogen storage application of nitrogen-doped carbon nanotubes with bamboo-like structure," *International Journal of Hydrogen Energy*, vol. 38, pp. 3297–3303, 2013.

[21] E. N. Nxumalo, V. P. Chabalala, V. O. Nyamori, M. J. Witcomb, and N. J. Coville, "Influence of methylimidazole isomers on ferrocene-catalysed nitrogen doped carbon nanotube synthesis," *Journal of Organometallic Chemistry*, vol. 695, no. 10-11, pp. 1451–1457, 2010.

[22] G. Dai, J. Zhang, and S. Deng, "Synthesis and characterization of nitrogen-doped monolayer and multilayer graphene on TEM copper grids," *Chemical Physics Letters*, vol. 516, no. 4–6, pp. 212–215, 2011.

[23] S. D. Mhlanga, E. N. Nxumalo, N. J. Coville, and V. V. Srinivasu, "Nitrogen doping of CVD multiwalled carbon nanotubes: observation of a large g-factor shift," *Materials Chemistry and Physics*, vol. 130, no. 3, pp. 1182–1186, 2011.

[24] V. O. Nyamori, S. D. Mhlanga, and N. J. Coville, "The use of organometallic transition metal complexes in the synthesis of shaped carbon nanomaterials," *Journal of Organometallic Chemistry*, vol. 693, no. 13, pp. 2205–2222, 2008.

[25] R. M. Yadav, P. S. Dobal, T. Shripathi, R. S. Katiyar, and O. N. Srivastava, "Effect of growth temperature on bamboo-shaped carbon-nitrogen (C-N) nanotubes synthesized using ferrocene acetonitrile precursor," *Nanoscale Research Letters*, vol. 4, no. 3, pp. 197–203, 2009.

[26] P. Hu, K. Zhao, and H. Xu, "4-nitrophenylferrocene," *Molecules*, vol. 6, no. 12, p. 249, 2001.

[27] A. A. Altaf, N. Khan, A. Badshah et al., "Improved synthesis of ferrocenyl aniline," *Journal of the Chemical Society of Pakistan*, vol. 33, no. 5, pp. 691–693, 2011.

[28] V. O. Nyamori, S. M. Zulu, and B. Omondi, "1-(ferrocen-1-ylmethyl)-3-methyl-imidazol-3-ium hexafluoridophosphate," *Acta Crystallographica E*, vol. 68, no. 4, p. m1535, 2012.

[29] V. O. Nyamori, E. N. Nxumalo, and N. J. Coville, "The effect of arylferrocene ring substituents on the synthesis of multi-walled carbon nanotubes," *Journal of Organometallic Chemistry*, vol. 694, no. 14, pp. 2222–2227, 2009.

[30] E. N. Nxumalo, V. O. Nyamori, and N. J. Coville, "CVD synthesis of nitrogen doped carbon nanotubes using ferrocene/aniline mixtures," *Journal of Organometallic Chemistry*, vol. 693, no. 17, pp. 2942–2948, 2008.

[31] A. A. Koós, F. Dillon, E. A. Obraztsova, A. Crossley, and N. Grobert, "Comparison of structural changes in nitrogen and boron-doped multi-walled carbon nanotubes," *Carbon*, vol. 48, no. 11, pp. 3033–3041, 2010.

[32] S. V. Dommele, *Nitrogen-doped carbon nanotubes synthesis, characterization and catalysis [dissertation]*, Utrecht University, Utrecht, The Netherlands, 2008.

[33] S. Y. Kim, J. Lee, C. W. Na, J. Park, K. Seo, and B. Kim, "N-doped double-walled carbon nanotubes synthesized by chemical vapor deposition," *Chemical Physics Letters*, vol. 413, no. 4–6, pp. 300–305, 2005.

[34] M. I. Ionescu, Y. Zhang, R. Li, H. Abou-Rachid, and X. Sun, "Nitrogen-doping effects on the growth, structure and electrical performance of carbon nanotubes obtained by spray pyrolysis method," *Applied Surface Science*, vol. 258, no. 10, pp. 4563–4568, 2012.

[35] C. Tang, Y. Bando, D. Golberg, and F. Xu, "Structure and nitrogen incorporation of carbon nanotubes synthesized by catalytic pyrolysis of dimethylformamide," *Carbon*, vol. 42, no. 12-13, pp. 2625–2633, 2004.

[36] M. Kumar and Y. Ando, "Chemical vapor deposition of carbon nanotubes: a review on growth mechanism and mass production," *Journal of Nanoscience and Nanotechnology*, vol. 10, no. 6, pp. 3739–3758, 2010.

[37] C. Seah, S. Chai, and A. R. Mohamed, "Synthesis of aligned carbon nanotubes," *Carbon*, vol. 49, no. 14, pp. 4613–4635, 2011.

Hindawi Publishing Corporation
Journal of Nanomaterials
Volume 2013, Article ID 689214, 9 pages
http://dx.doi.org/10.1155/2013/689214

Research Article

Adsorption of Eu(III) on oMWCNTs: Effects of pH, Ionic Strength, Solid-Liquid Ratio and Water-Soluble Fullerene

P. Liu,[1] J. Wang,[1] W. Qi,[1] Zh. Li,[2] JJ. Bi,[1] and WS. Wu[1,3]

[1] *Radiochemistry Laboratory, School of Nuclear Science and Technology, Lanzhou University, Lanzhou, Gansu 730000, China*
[2] *Institute of Modern Physics, Chinese Academy of Sciences, Lanzhou, Gansu 730000, China*
[3] *State Key Laboratory of Applied Organic Chemistry, Lanzhou University, Lanzhou, Gansu 73000, China*

Correspondence should be addressed to Wangsuo WU; wuws@lzu.edu.cn

Received 30 May 2013; Accepted 7 July 2013

Academic Editor: Myoung-Woon Moon

Copyright © 2013 Peng LIU et al. This is an open access article distributed under the Creative Commons Attribution License, which permits unrestricted use, distribution, and reproduction in any medium, provided the original work is properly cited.

The influences of pH, ionic strength, solid-liquid ratio, $C_{60}(C(COOH)_2)_n$, and $C_{60}(OH)_n$ on Eu(III) adsorption onto the oxidation multiwalled carbon nanotubes (oMWCNTs) were studied by using batch technique. The dynamic process showed that the adsorption of Eu(III) onto oMWCNTs could be in equilibrium for about 17 h and matched the quasi-second-order kinetics model. The sorption process was influenced strongly by pH changes and ionic strength. In the pH range of 1.0 to 4.0, the adsorption ratio increased with the increasing of pH values, then the adsorption of Eu(III) was almost saturated in the pH range of 4.0 to 10.0, and the adsorption ratio reached about 90%. The adsorption ratio decreased with the increasing of ionic strength. $C_{60}(C(COOH)_2)_2$ could promote the adsorption process obviously, but $C_{60}(OH)_n$ competed with Eu(III) for the adsorption sites, thus leading to the reducing of Eu(III) adsorption onto oMWCNTs. In the presence of $C_{60}(C(COOH)_2)_n$ or $C_{60}(OH)_n$, the adsorption of Eu(III) onto oMWCNTs could be affected obviously by solid-liquid ratio and the initial concentration of Eu(III).

1. Introduction

The behavior of lanthanides and actinides has received much attention in nuclear waste management [1, 2]. Eu(III) is a trivalent lanthanide ion, and it is also a trivalent actinide chemical element homologue. A large number of Eu(III) exposure in the environment can cause great harm to people's health and life. Thus, the adsorption and migration of Eu(III) on metal oxides and minerals have been studied extensively, and the investigations of their potential pollution towards the natural water and soil environment are of great importance. Xu et al. studied the adsorption of Eu(III) on TiO_2 with the presence of organic matters in different pH values, which indicated its adsorption behavior strongly influenced by the pH changes, and the adsorption mechanism was attributed to the formation of the inner ring complexes [3]. Wang et al. studied the adsorption of Eu(III) on alumina, which was also influenced by the pH changes, and the reaction is a surface complexation reaction [4]. Li et al. studied the adsorption of Eu(III) on iron oxides; the adsorption of Eu(III) was significantly dependent on pH, temperature, and HA [5].

The carbon nanotube is a kind of carbon allotrope with typical layered hollow structure, and it is considered to be a typical one-dimensional material. Multiwalled carbon nanotubes (MWCNTs) are the coaxial tubes formed by several layers to dozens by hexagonal array of carbon atoms, with hybridization of carbon atoms in the tube wall, which can be easily modified; in addition, the carbon atoms exist as SP^2 hybridization in the carbon nanotubes and form the most stable chemical bond C=C covalent bond in nature [6]. Therefore, carbon nanotubes have excellent physiochemical property and versatile applications, especially in mechanics, electromagnetism, optics, electronics, catalysis, and composite materials fields, and have huge potential research value [7]. Due to its special structure, carbon nanotubes have large specific surface area and high chemical stability, and their surfaces can be functionalized easily [8], it is widely used in the adsorption process. Some researchers have done the study about metal ions (Pb(II), Ni(II), and Cd(II)) adsorbed onto oMWCNTs in detail [9–11]. For example, Deng et al. studied the adsorption mechanism of PFCs (perfluorinated compounds) on MWCNTs [12]; their results indicated that

MWCNTs have extremely excellent adsorption properties. And Sheng et al. [13] studied the adsorption of Eu(III) onto titanate nanotubes in microscopic insights.

Compared with experimental environment, the natural environment is more complicated [14]. There are few studies about the behavior of other organic materials on the adsorption of metal ions in the presence of carbon nanomaterials. Therefore, it is of great significance to study the effects of a variety of carbon nanomaterials coexisting on the adsorption of metal ions. In order to simulate the interactions of carbon nanomaterials with metal ions in a real environment, the organic matters are often selected as another study factors in the ternary system to study the adsorption of metal ions [15–19]. In our study, the water-soluble fullerene was selected as the third element of the adsorption system to study its effect on Eu(III) adsorbed onto carbon nanotubes.

The fullerenes are following graphite, diamond, amorphous carbon, and another allotropes of carbon, which has broad applications in the gas storage, the field of optics, the polymer field, enhanced metals, superconducting field, battery materials, catalysts, and biological medical prospects [20]. As a fullerene, C_{60} is the cheapest and easiest to obtain, so C_{60} and its derivatives were used to investigate their properties in the current studies. Due to their large number of π electrons, fullerene is very easy to form π-π stacking with other aromatic materials [21, 22], then to affect its adsorption on metal ion or an organic. And adding the appropriate functional groups to the fullerene skeleton can improve the poor solubility [23]. Therefore, studying the effect of water-soluble fullerene on adsorption of Eu(III) onto carbon nanotubes can provide a new method for the study of trivalent lanthanides and actinides behavior, explore a variety of factors, and provide a theoretical basis for the long-lived radioactive waste disposal security issues.

2. Materials and Methods

2.1. Materials. Multiwall carbon nanotubes (L. MWNTs-1030) materials, purity > 95% (amorphous carbon ≤ 3 wt%, ash content ≤ 0.2 wt%), with a diameter of 10–30 nm, the length of 1–10 μm, specific surface area of 10–100 m^2/g, were purchased from Shenzhen Nanotech Port Company. Oxidation multi-walled carbon nanotubes were made by raw carbon nanotubes and concentrated nitric acid. First, 3 g MWCNTs were added into concentrated nitric acid (400 mL). The mixture was stirred at 80°C for 24 h then quenched with deionized water, and the product was collected. A mixture of concentrated nitric acid and concentrated sulfuric acid (1 : 3, V/V) (400 mL) was added to the above compound and refluxed for 48 h then washed with deionized water (pH ≈ 6) to gain the oxidation multi-walled carbon nanotubes (oxidized MWCNTs, oMWCNTs) [26].

Fullerene (C_{60}), purity > 99.9%, was purchased from Yongxin the fullerene Technology Co. Ltd. of Puyang City, Henan Province. The fullerene hydroxylation process was in accordance with the method of the literature [27]. In a 50 mL round bottom flask containing the benzene solution of C_{60} (1 mg/mL), then added sodium hydroxide solution (2 mL, 0.5 mol/L), 5 drops of 10% tetrabutylammonium hydroxide, and hydrogen peroxide (1 mL, 30%). The solution was stirred at room temperature for 12 h until the color of benzene solution changed from purple to colorless, and the aqueous solution changed from colorless to yellow-brown. The mixture was extracted to obtain a dark brown color of $C_{60}(OH)_x(O)_y$ solution. After added methanol to the solution of $C_{60}(OH)_x(O)_y$, the precipitation was occurred, then the precipitation was filtered, washed with water (pH < 8), and dried under *vacuum*. $C_{60}(OH)_n$ was obtained [28].

Fullerene (C_{60}), purity > 99.9%, was purchased from Yongxin the fullerene Technology Co. Ltd. of Puyang City, Henan Province. The C_{60} and NaH were added into toluene, when the color of the mixture solution changed from purple to deep red, then added diethyl bromomalonate. The residue was dissolved in the toluene, and then added NaH (excess 20-fold than before). The solution was stirred at 80°C for 10 h under the protection of Ar gas and heating. Then, CH_3OH was added to the solution to terminate the reaction immediately, and added 2 mol/L HCl. The precipitate was filtered, collected, and washed by toluene, 2 mol/L HCl, H_2O, and benzene [29].

Unless otherwise noted, materials were obtained from commercial suppliers and were used without further purification.

2.2. Batch Experiments. Determining the equilibrium time and the solid-liquid ratio, in a series of polyethylene centrifuge tube added a certain amount of oMWCNTs, NaCl and a known concentration $EuCl_3$ solution, so that the various components of the system achieved the required concentration. The extremely small amount of HCl or NaOH solution can be added to the system to adjust the pH to a desired value. The samples were centrifuged 30min at 12000 r/min after shaking 72 h in constant temperature. Taking out a certain volume supernatant, the supernatant counts were measured by a liquid scintillation counter. The adsorption of Eu(III) on the oMWCNTs was calculated by before and after the adsorption of Eu(III) in the liquid phase concentration.

2.3. X-Ray Photoelectron Spectroscopy (XPS) Analysis. In order to further analyze the molecular level information of the adsorbent material; the thermoelectric ESCALAB 250 spectrometer was used to identify the property of adsorbent material, the results were shown in Figure 1. The C1s peaks of oMWCNTs samples were at about 285.0, 288.2, and 289.0 eV (Figure 1(a)), which were corresponding the C–C, CO, and COO, respectively [30]. And O1s peaks of oMWCNTs sample at about 532.1, 534.1, and 537.2 eV (Figure 1(b)) were indicated the OH, OH/CO, and COO/H_2O, respectively [31]. C1s peaks of $C_{60}(OH)_n$ at about 285.0 and 286.98 eV (Figure 1(c)) showed the C-C and COO, respectively O1s peak of $C_{60}(OH)_n$ at 532.77 eV (Figure 1(d)) was assigned to bridging OH. C1s peak of $C_{60}(C(COOH)_2)_n$ at about 284.9 and 289.1 eV (Figure 1(e)) was corresponding the C–C and COO, respectively. O1s peak of $C_{60}(C(COOH)_2)_n$ at about 532.4 and 533.5 eV (Figure 1(f)) could be assigned to bridging OH and COO/H_2O, respectively. The related peak areas are shown in Table 1.

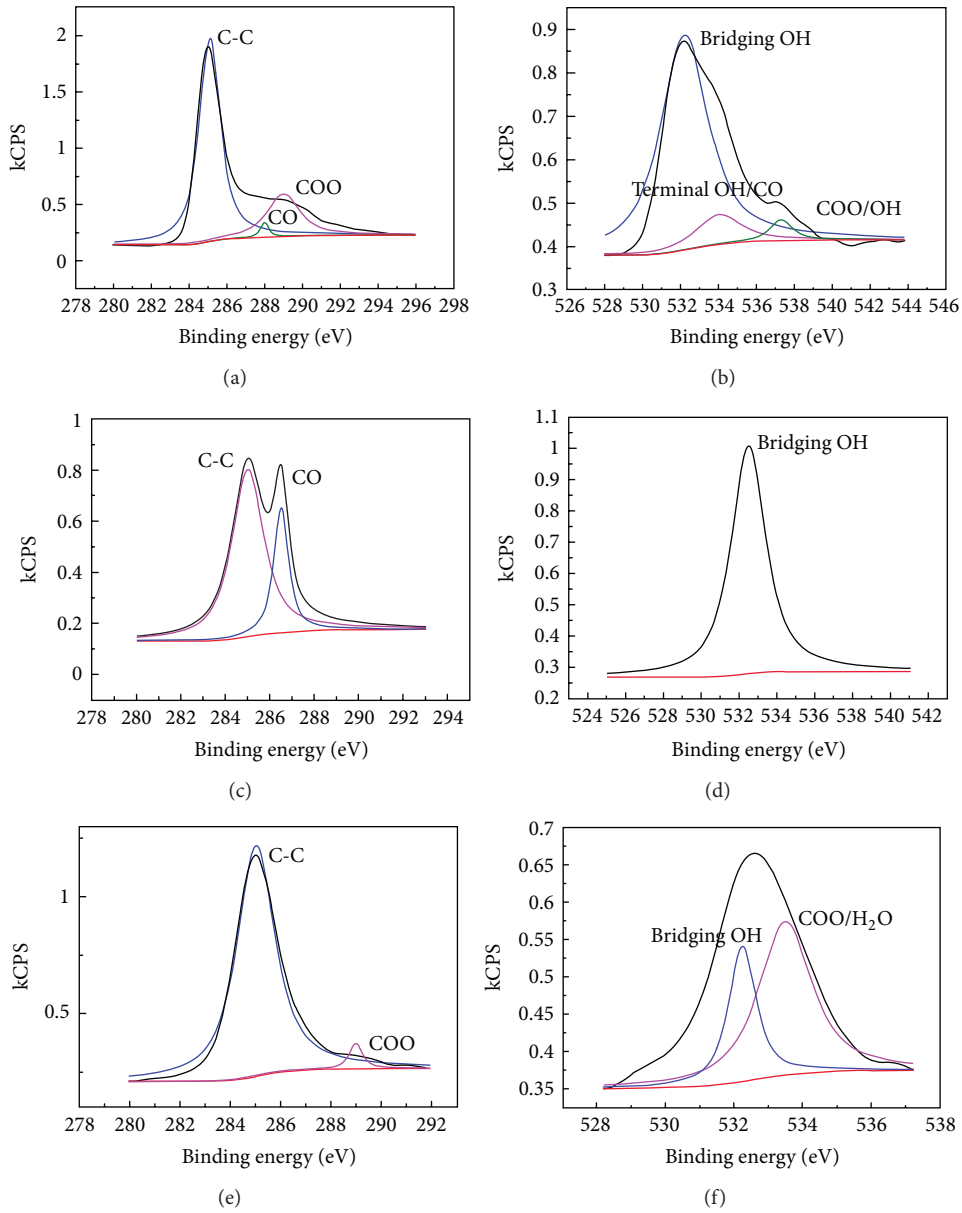

Figure 1: The XPS of nanomaterials. (a) is the oMWCNTs C1s, (b) is oMWCNTs O1s, (c) is $C_{60}(OH)_n$ C1s, (d) is $C_{60}(OH)_n$ O1s, (e) is $C_{60}(C(COOH)_2)_n$ C1s, and (f) is $C_{60}(C(COOH)_2)_n$ O1s.

Table 1: The percentage of various functional groups on different carbon nanomaterials.

Material	oMWCNTs	$C_{60}(OH)_n$	$C_{60}(C(COOH)_2)_n$
C–C (%)	60.143	40.991	83.279
CO (%)	16.098	21.555	—
COO (%)	8.783	—	—
Bridging OH (%)	8.575	17.739	16.721
Terminal OH/CO (%)	6.400	—	—

3. Results and Discussions

3.1. Adsorption Kinetics

3.1.1. Effect of Equilibrium Time on Eu(III) Adsorption onto oMWCNTs. The influence of the shaking time on Eu(III) adsorption onto oMWCNTs is shown in Figure 2. The adsorption ratio was increased with the increase of the shaking time. After 17 h, the adsorption ratio of Eu(III) was close to 100%; after that it was substantially unchanged. These results indicated that the adsorption of Eu(III) onto oMWCNTs was a chemical adsorption process [10]. The 48 h was selected as the equilibrium time in the following experiments.

3.1.2. Pseudo-Second-Order Equation. Quasi-second-order kinetic equation linear expression is

$$\frac{t}{q_t} = \frac{1}{kq_e^2} + \frac{t}{q_e}, \tag{1}$$

where q_t and q_e denote the time t and the equilibrium adsorption amount (mg/g) and k is the second-order rate

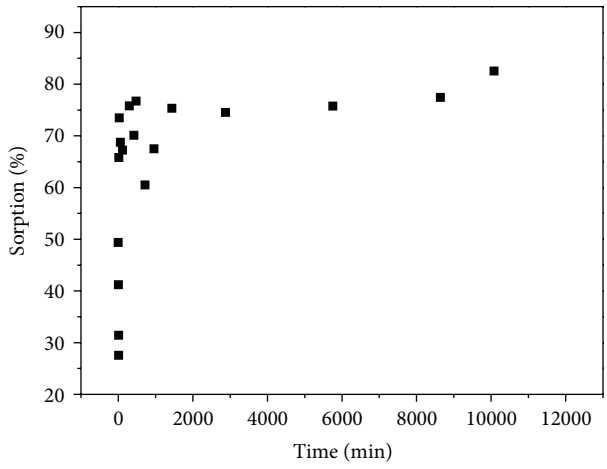

Figure 2: Effect of equilibrium time on Eu(III) adsorption onto oMWCNTs. pH = 3.00 ± 0.05, m/V = 0.0250 g/L, T = (25 ± 1)°C, $C^0_{Eu} = 1.21 \times 10^{-5}$ mol/L.

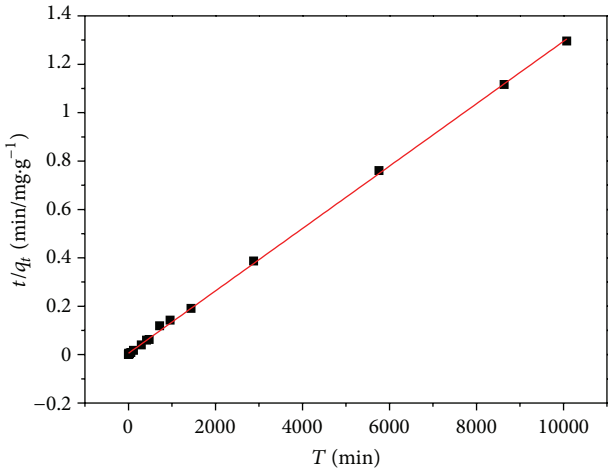

Figure 3: Pseudo-second-order sorption kinetics plot for Eu(III). pH = 3.00 ± 0.05, m/V = 0.0250 g/L, T = (25 ± 1)°C, $C^0_{Eu} = 1.21 \times 10^{-5}$ mol/L.

constant (g · mg^{-1} · min^{-1}). Using this equation to fit the experimental data, the results as shown in Figure 3, quasi-second-order equation is $y = 0.00013x + 0.00552$, calculated by the slope and intercept of $k = 3.3214 \times 10^{-3}$ g/mg · min, the q_e = 0.7757 mg/g and the linear correlation coefficient R^2 = 0.9996 which is almost 1. These results showed that the adsorption of Eu(III) onto oMWCNTs was keeping with the quasi-second-order kinetic model.

3.2. Effect of pH on Eu(III) Adsorption onto oMWCNTs. The influence of different pH on the adsorption was shown in Figure 4. Figure 4 shows that when the solid-liquid is 0.025 g/L and ionic strength is 0.1 mol/L(NaCl), the ratio of Eu(III) adsorption onto oMWCNTs is influenced strongly by the pH. Figure 4 also shows the adsorption ratio of Eu(III) onto oMWCNTs declines with the ionic strength increases, suggesting that the adsorption can be suppressed by ionic

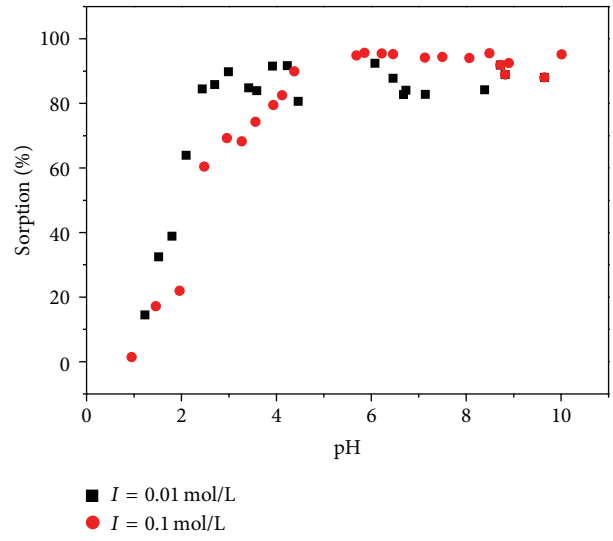

Figure 4: Effect of pH on Eu(III) adsorption onto oMWCNTs. m/V = 0.0250 g/L, T = (25 ± 1)°C, $C^0_{Eu} = 1.21 \times 10^{-5}$ mol/L.

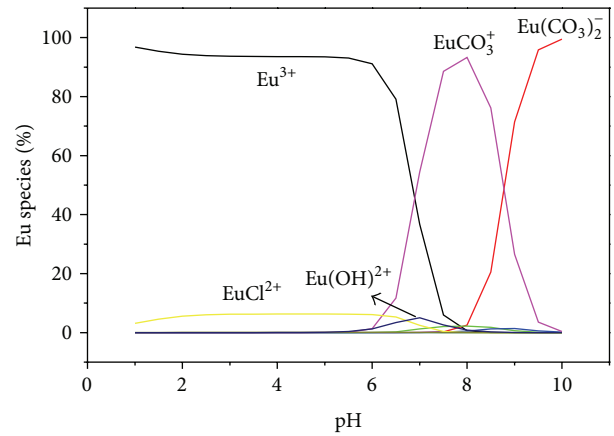

Figure 5: Relative species distribution of Eu(III). T = (25 ± 1)°C, $C^0_{Eu} = 1.21 \times 10^{-5}$ mol/L, $P_{CO_2} = 0.0038$.

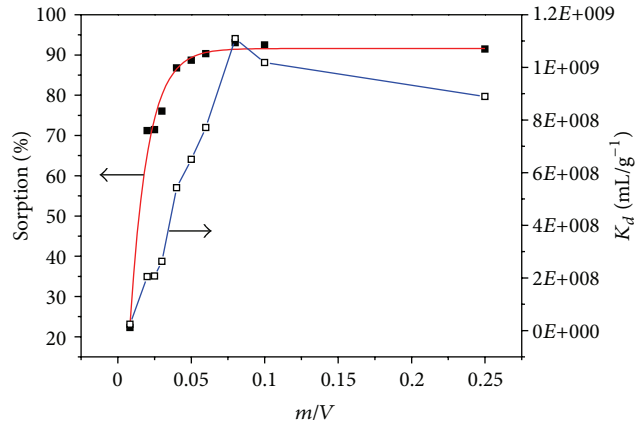

Figure 6: Effect of solid-to-liquid ratio of Eu(III) adsorption onto oMWCNTs. pH = 3.00 ± 0.05, m/V = 0.0250 g/L, T = (25 ± 1)°C, $C^0_{Eu} = 1.21 \times 10^{-5}$ mol/L.

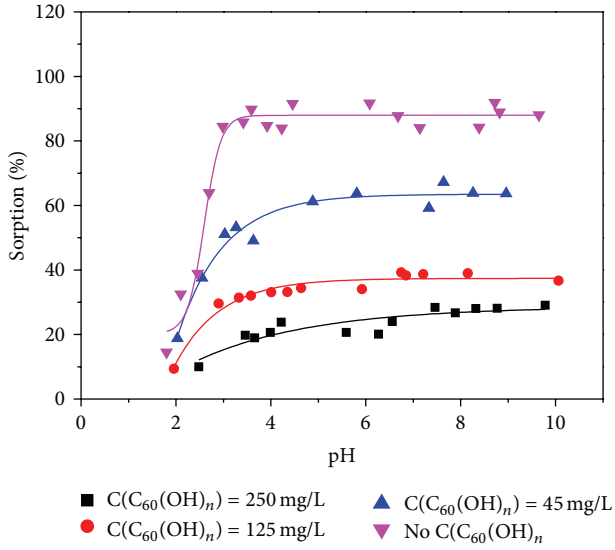

Figure 7: Effect of $C_{60}(OH)_n$ on the adsorption of Eu(III) onto oMWCNTs. pH = 3.00 ± 0.05, m/V = 0.025 g/L, T = (25 ± 1)°C, $C^0_{Eu} = 1.21 \times 10^{-5}$ mol/L.

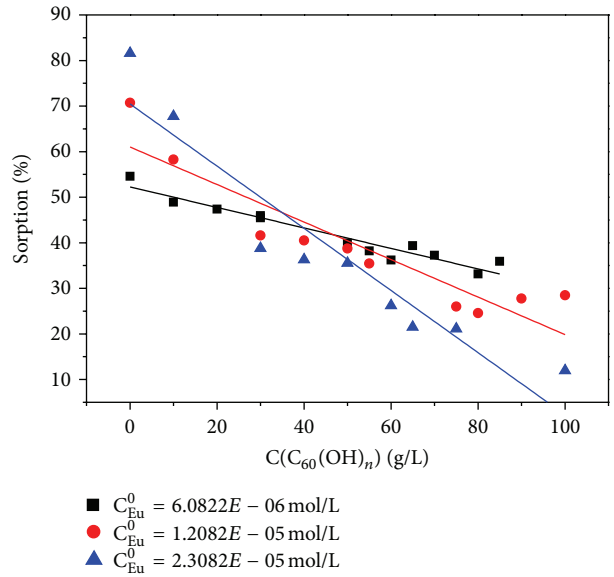

Figure 8: Effect of Eu(III) and $C_{60}(OH)_n$ concentration on the adsorption of Eu(III) onto oMWCNTs. pH = 3.00 ± 0.05, m/V = 0.025 g/L, T = (25 ± 1)°C, $C^0_{Eu} = 1.21 \times 10^{-5}$ mol/L.

strength. Sheng et al. found that the adsorption rate of Th(IV) on raw diatomite increased rapidly to about 100% when the pH value changed from 2 to 4 and was influenced by the ionic strength strongly [13]. Wu et al., Guo et al., and Mingming et al. also found that the adsorption of Eu(III) on sodium bentonite and Na-attapulgite was effected by ionic strength and pH changes strongly [32–34]. The experimental results in this work further confirmed the previous results.

When pH < 1.5, the adsorption ratio was low and almost not changing with the pH increased. In the range pH of 1.5 to 4.0, the adsorption ratio increased rapidly, from 20% to

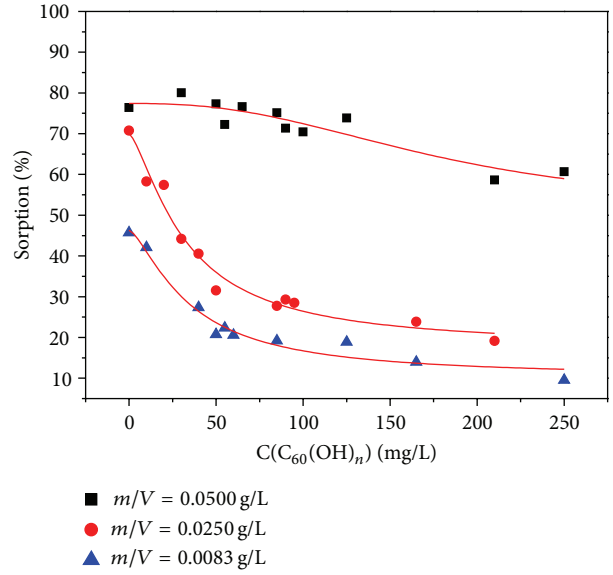

Figure 9: Effect of solid-liquid ratio and $C_{60}(OH)_n$ concentration on the adsorption of Eu(III) onto oMWCNTs. pH = 3.00 ± 0.05, m/V = 0.025 g/L, T = (25 ± 1)°C, $C^0_{Eu} = 1.21 \times 10^{-5}$ mol/L.

about 90%. When pH > 4.0, the adsorption ratio changed not so obviously indicating that the system was in equilibrium. Because the species distribution of Eu(III) can form a water-soluble carbonates at high pH, so the adsorption ratio cannot reach 100%.

The effect of pH on Eu(III) adsorption onto the oMWCNTs could be explained by the surface charge and ionization degree of oMWCNTs. When pH < pH_{pzc}, Eu^{3+} and oMWCNTs surface proton produces electrostatic repulsion, which prevents Eu^{3+} from being adsorbed onto oMWCNTs, resulting in a lower adsorption ratio of Eu(III). When pH > pH_{pzc}, Eu^{3+} interacts with oMWCNTs surface proton by electrostatic attraction making more Eu(III) adsorbed onto oMWCNTs surface, increasing the adsorption ratio of Eu(III). The species changes of Eu(III) with pH in solution is another important influencing factor for the adsorption system. The thermodynamic data used to estimate the Eu(III) species distribution in the solution were listed in Table 2. As shown in Figure 5, when the initial concentration of Eu(III) is 1.21×10^{-5} mol/L with background electrolyte (0.01 mol/L NaCl solution), the main existence forms are Eu^{3+}, $Eu(OH)_2^+$, $EuCl_2^+$, $EuCO_3^+$, $Eu(CO_3)_2^-$. When pH ≤ 6.5, the main species is Eu^{3+}. When pH > 6.5, due to the impact of CO_2, Eu(III) mainly exists as the forms of $EuCO_3^+$ and $Eu(CO_3)_2^-$ in solution, which have relatively low solubility in aqueous solution leading to increase Eu(III) content in the solid phase, so the adsorption ratio of Eu(III) onto oMWCNTs maintains the maximum and no longer changes.

3.3. Effect of Solid-Liquid Ratio on Eu(III) Adsorption onto oMWCNTs. Figure 6 shows that the adsorption ratio transformation of Eu(III) adsorption onto oMWCNTs increases

Table 2: The thermodynamic constants used for species estimates [24, 25].

Reaction	log K
$H_2O \leftrightarrow OH^- + H^+$	−13.8
$Eu^{3+} + H_2O \leftrightarrow [Eu(OH)]^{2+} + H^+$	−7.64
$Eu^{3+} + 2H_2O \leftrightarrow [Eu(OH)_2]^+ + 2H^+$	−15.1
$Eu^{3+} + 3H_2O \leftrightarrow [Eu(OH)_3]^0 + 3H^+$	−23.7
$Eu^{3+} + 4H_2O \leftrightarrow [Eu(OH)_4]^- + 4H^+$	−36.2
$H_2CO_3 \leftrightarrow CO_3^{2-} + 2H^+$	−17.43
$Eu^{3+} + CO_3^{2-} \leftrightarrow [EuCO_3]^+$	8.1
$Eu^{3+} + 2CO_3^{2-} \leftrightarrow [Eu(CO_3)_2]^-$	12.1
$Eu^{3+} + Cl^- \leftrightarrow EuCl^{2+}$	1.10
$Eu^{3+} + 2Cl^- \leftrightarrow EuCl_2^+$	1.50

with the increasing of oMWCNTs concentration. With the increasing of the solid solution ratio in the system, the adsorption ratio of Eu(III) is increasing until Eu(III) is adsorbed completely. While the percentage composition of oMWCNTs increases, the surface adsorption sites also increase, which can promote the adsorption of Eu(III). Figure 6 also shows the influence of different m/V value on the distribution coefficient K_d. K_d values can be estimated by C_s and C_e:

$$K_d = \frac{C_s - C_e}{C_e} \cdot \frac{V}{m}, \quad (2)$$

where V is the volume of the solution (m/L) and m is the weight of solid (g). As shown in Figure 6, with the increasing of the solid-liquid ratio, K_d values also increase gradually, when the solid-liquid ratio exceeds 0.1 mL/g, K_d value declines slightly. Thus, it can be seen from that, K_d value depends on the solid content at low solid concentration, but when the solid content reaches a certain concentration, K_d value is never depend on the solid content. This phenomenon also presents in the adsorption system of the other metal ions and the different adsorbents [35, 36].

3.4. Effect of $C_{60}(OH)_n$ on Eu(III) Adsorption onto oMWCNTs. Figure 7 shows the Eu(III) adsorption border changes in the present of different $C_{60}(OH)_n$ concentration. When the concentration of $C_{60}(OH)_n$ is 250 mg/L, the adsorption capacity of Eu(III) on the oMWCNTs is about 10% at pH 2.5, but it arrives at about 28% at pH 7. While the concentration of $C_{60}(OH)_n$ is 125 mg/L, the adsorption rate increases significantly, which rises from 20% at pH 2.5 to 38% at pH 6.8. Similarly, when the concentration of $C_{60}(OH)_n$ is 45 mg/L, the adsorption of $C_{60}(OH)_n$ reaches the maximum at the same pH value. These results show that the presence of $C_{60}(OH)_n$ can restrain the adsorption of Eu(III) onto oMWCNTs. According to the literatures, in a ternary system, the organic material plays an important role in metal ions adsorbed onto oMWCNTs. It is mainly attributed to the ternary complex which was formed by metal ion, the organics, and the surface functional groups of oMWCNTs through hydrophobic interactions, electrostatic interactions, and hydrogen bonds [37, 38]. But

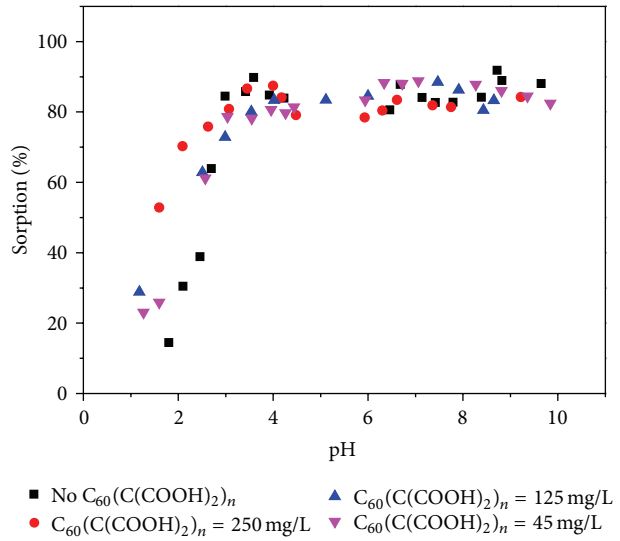

Figure 10: Effect of $C_{60}(OH)_n$ on the adsorption of Eu(III) onto oMWCNTs. pH = 3.00 ± 0.05, m/V = 0.025 g/L, T = (25 ± 1)°C, $C^0_{Eu} = 1.21 \times 10^{-5}$ mol/L.

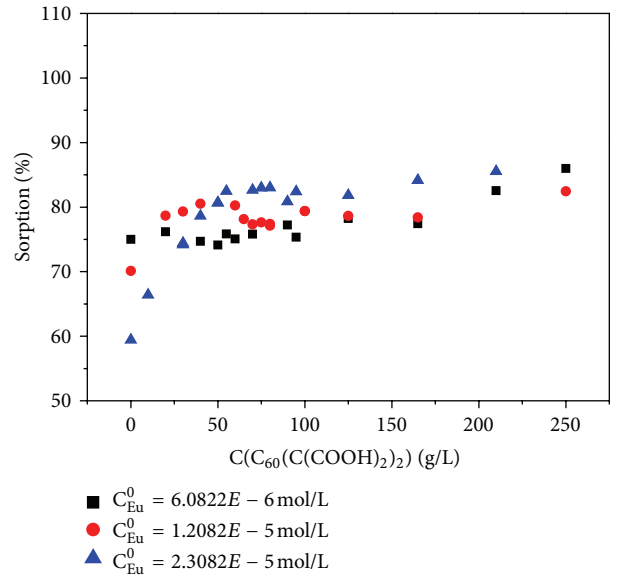

Figure 11: Effect of Eu(III) initial concentrations and $C_{60}(C(COOH)_2)_2$ concentrations on Eu(III) adsorption onto oMWCNTs. pH = 3.00 ± 0.05, m/V = 0.025 g/L, T = (25 ± 1)°C, $C^0_{Eu} = 1.21 \times 10^{-5}$ mol/L.

$C_{60}(OH)_n$ can compete with Eu(III) for the surface adsorption sites of oMWCNTs, which could weaken the adsorption ratio of Eu(III) onto oMWCNTs. With the concentration of $C_{60}(OH)_n$ increasing gradually, more and more $C_{60}(OH)_n$ is connected to oMWCNTs. So $C_{60}(OH)_n$ could affect the surface properties of oMWCNTs as well as the adsorption sites, then the adsorption ratio of Eu(III) onto oMWCNTs is decreased. For further understanding of the effect of $C_{60}(OH)_n$ on the adsorption system, changing the initial concentration of Eu(III) and solid-liquid ratio to observe

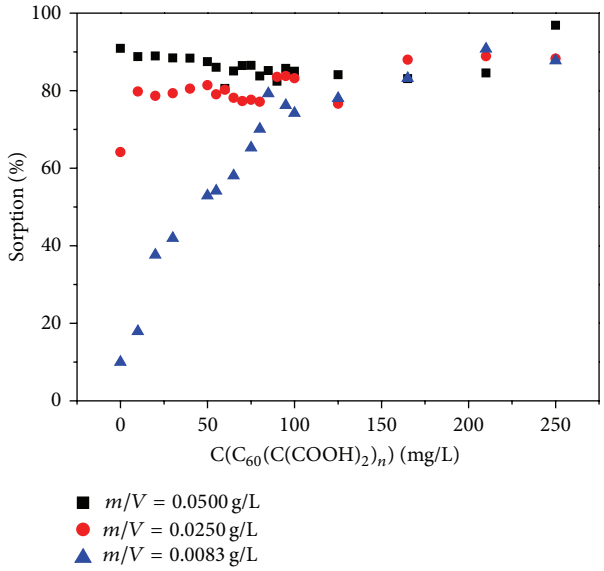

FIGURE 12: Effect of oMWCNTs solid-liquid ratio and $C_{60}(C(COOH)_2)_2$ concentrations on the adsorption of Eu(III) onto oMWCNTs. pH = 3.00 ± 0.05, m/V = 0.025 g/L, T = (25 ± 1)°C, $C^0_{Eu} = 1.21 \times 10^{-5}$ mol/L.

the effects of different $C_{60}(OH)_n$ concentrations on Eu(III) adsorption onto oMWCNTs was investigated (Figures 8 and 9). It indicates that the Eu(III) is only adsorbed on oMWCNTs surface with no interaction with $C_{60}(OH)_n$. As shown in Figure 8, when the initial concentration of Eu(III) is 6.0822×10^{-6} mol/L, the adsorption rate becomes smaller gradually with $C_{60}(OH)_n$ concentration increases. The result shows that Eu(III) is adsorbed by oMWCNTs before the interaction of oMWCNTs with $C_{60}(OH)_n$ due to the low concentration of Eu(III), Conversely, when the initial concentration of the Eu(III) is increased to 2.3082×10^{-5} mol/L, under the same concentration of oMWCNTs and $C_{60}(OH)_n$, the adsorption ratio is increases gradually because the abundant Eu(III) is enough strong to compete with $C_{60}(OH)_n$ for oMWCNTs. Figure 9 shows that when the solid-liquid ratio is 0.0250 g/L or 0.0083 g/L, and the concentration of $C_{60}(OH)_n$ is less than 150 mg/L, the adsorption ratio of Eu(III) declines sharply, and then with the increasing of $C_{60}(OH)_n$, the adsorption rate becomes slow and till to stable. However, when the solid-liquid ratio rises to 0.0500 g/L, the adsorption rate of Eu(III) is slowly decreased, but it is higher than that of the solid-liquid ratio is 0.0250 g/L and 0.0083 g/L. This is because that with the increasing of solid-liquid ratio, the available adsorption sites also increases, so more Eu(III) is adsorbed to oMWCNTs.

3.5. Effect of $C_{60}(C(COOH)_2)_2$ on Eu(III) Adsorption onto oMWCNTs. The effect of $C_{60}(C(COOH)_2)_2$ on the adsorption of Eu(III) is shown in Figure 10. The presence of $C_{60}(C(COOH)_2)_2$ promoted the adsorption of the Eu(III) onto the oMWCNTs in the pH range of 1.5 to 3.5 significantly, and the maximum adsorption ratio is observed at pH > 3.5. Considering the ability of π-π stacking between $C_{60}(C(COOH)_2)_2$ and oMWCNTs is less than that of $C_{60}(OH)_n$, and the space steric effect of $C_{60}(C(COOH)_2)_2$ is stronger than that of $C_{60}(OH)_n$, so the adsorption capacity of $C_{60}(C(COOH)_2)_2$ onto the surface of oMWCNTs is not as large as $C_{60}(OH)_n$, which provides more opportunities for Eu(III) to be adsorbed by oMWCNTs. Under the acidic environment, $C_{60}(C(COOH)_2)_2$ is very easy to combine with H^+ from the solution and oMWCNTs surface, so Eu(III) is adsorbed onto the surface of oMWCNTs more easily. Meanwhile, the presence of hydrolyzate of Eu(III) may also be another reason to increase the adsorption ratio.

Similarly, changing the initial concentration of Eu(III) and the ratio of solid to liquid at pH 3.00 ± 0.05, the effect of $C_{60}(C(COOH)_2)_2$ concentration on the adsorption ratio is shown in Figures 11 and 12. As shown in Figure 11, when the initial concentration of Eu(III) is 6.0822×10^{-6} g/L, there are enough adsorption sites to be occupied by Eu(III), and the adsorption ratio can reach maximum value fast. However, when the initial concentration of Eu(III) is 2.3082×10^{-5} g/L, the adsorption sites of oMWCNTs are occupied completely at absence of $C_{60}(C(COOH)_2)_2$, and the adsorption ratio is low; but once the $C_{60}(C(COOH)_2)_2$ is added, the $C_{60}(C(COOH)_2)_2$ can improve Eu(III) adsorption onto oMWCNTs, thus the adsorption ratio is increased with the increasing of $C_{60}(C(COOH)_2)_2$ concentration until to the maximum, and then maintains this level. As shown in Figure 12, for the low solid-liquid ratio, such as m/V = 0.0083 g/L or 0.025 g/L, the quantity of Eu(III) in the solution are so much more than the adsorption sites of oMWCNTs. After the adsorption process is in the equilibrium at the experimental conditions, the solid-liquid ratio is low, and the sorption ratio also is low. However, when the $C_{60}(C(COOH)_2)_2$ presents at the adsorption system, the adsorption ratio is increased due to $C_{60}(C(COOH)_2)_2$ can promote the adsorption of Eu(III) onto oMWCNTs. And with the increasing of the concentration of $C_{60}(C(COOH)_2)_2$, the adsorption ratio is increased till the Eu(III) adsorbed completely.

4. Conclusion

The effects and behavior of Eu(III) adsorption onto oMWCNTs are studied when the $C_{60}(C(COOH)_2)_2$ or $C_{60}(OH)_n$ is added. The adsorption of Eu(III) onto oMWCNTs is affected strongly by pH and ionic strength. The presence of $C_{60}(C(COOH)_2)_n$ promotes the changes of adsorption ratio obviously. However, $C_{60}(OH)_n$ competes the adsorption sites with Eu(III), leading to reducing the adsorption ratio of Eu(III) adsorbed onto oMWCNTs.

References

[1] X. Tan, Q. Fan, X. Wang, and B. Grambow, "Eu(III) sorption to TiO_2 (anatase and rutile): batch, XPS, and EXAFS studies," *Environmental Science and Technology*, vol. 43, no. 9, pp. 3115–3121, 2009.

[2] G. Montavon, S. Markai, Y. Andrés, and B. Grambow, "Complexation studies of Eu(III) with alumina-bound polymaleic

acid: effect of organic polymer loading and metal ion concentration," *Environmental Science and Technology*, vol. 36, no. 15, pp. 3303–3309, 2002.

[3] J. Z. Xu, Q. Fan, Z. Niu, Y. Li, P. Li, and W. Wu, "Studies of Eu(III) sorption on TiO_2: effects of pH, humic acid and poly(acrylic acid)," *Chemical Engineering Journal*, vol. 179, pp. 186–192, 2012.

[4] X. Wang, D. Xu, L. Chen et al., "Sorption and complexation of Eu(III) on alumina: effects of pH, ionic strength, humic acid and chelating resin on kinetic dissociation study," *Applied Radiation and Isotopes*, vol. 64, no. 4, pp. 414–421, 2006.

[5] P. Li, Q. Fan, D. Pan, S. Liu, and W. Wu, "Effects of pH, ionic strength, temperature, and humic acid on Eu(III) sorption onto iron oxides," *Journal of Radioanalytical and Nuclear Chemistry*, vol. 289, no. 3, pp. 757–764, 2011.

[6] S. Iijima, "Helical microtubules of graphitic carbon," *Nature*, vol. 354, no. 6348, pp. 56–58, 1991.

[7] J. R. Heath, "Nanoscale materials," *Accounts of Chemical Research*, vol. 32, no. 5, p. 388, 1999.

[8] A. Abbaspour and A. Izadyar, "Carbon nanotube composite coated platinum electrode for detection of Cr(III) in real samples," *Talanta*, vol. 71, no. 2, pp. 887–892, 2007.

[9] D. Xu, X. Tan, C. Chen, and X. Wang, "Removal of Pb(II) from aqueous solution by oxidized multiwalled carbon nanotubes," *Journal of Hazardous Materials*, vol. 154, no. 1–3, pp. 407–416, 2008.

[10] S. Yang, J. Li, D. Shao, J. Hu, and X. Wang, "Adsorption of Ni(II) on oxidized multi-walled carbon nanotubes: effect of contact time, pH, foreign ions and PAA," *Journal of Hazardous Materials*, vol. 166, no. 1, pp. 109–116, 2009.

[11] X. Tian, T. Li, K. Yang, Y. Xu, H. Lu, and D. Lin, "Effect of humic acids on physicochemical property and Cd(II) sorption of multiwalled carbon nanotubes," *Chemosphere*, vol. 89, no. 11, pp. 1316–1322, 2012.

[12] S. Deng, Q. Zhang, Y. Nie et al., "Sorption mechanisms of perfluorinated compounds on carbon nanotubes," *Environmental Pollution*, vol. 168, pp. 138–144, 2012.

[13] G. Sheng, J. Hu, and X. Wang, "Sorption properties of Th(IV) on the raw diatomite—effects of contact time, pH, ionic strength and temperature," *Applied Radiation and Isotopes*, vol. 66, no. 10, pp. 1313–1320, 2008.

[14] H. Hyung and J. H. Kim, "Natural organic matter (NOM) adsorption to multi-walled carbon nanotubes: effect of NOM characteristics and water quality parameters," *Environmental Science and Technology*, vol. 42, no. 12, pp. 4416–4421, 2008.

[15] W. Xiangke, D. Wenming, D. Xiongxin, W. Aixia, D. Jinzhou, and T. Zuyi, "Sorption and desorption of Eu and Yb on alumina: mechanisms and effect of fulvic acid," *Applied Radiation and Isotopes*, vol. 52, no. 2, pp. 165–173, 2000.

[16] S. Wang, J. Hu, J. Li, and Y. Dong, "Influence of pH, soil humic/fulvic acid, ionic strength, foreign ions and addition sequences on adsorption of Pb(II) onto GMZ bentonite," *Journal of Hazardous Materials*, vol. 167, no. 1–3, pp. 44–51, 2009.

[17] A. B. M. Giasuddin, S. R. Kanel, and H. Choi, "Adsorption of humic acid onto nanoscale zerovalent iron and its effect on arsenic removal," *Environmental Science and Technology*, vol. 41, no. 6, pp. 2022–2027, 2007.

[18] C. Chen and X. Wang, "Sorption of Th (IV) to silica as a function of pH, humic/fulvic acid, ionic strength, electrolyte type," *Applied Radiation and Isotopes*, vol. 65, no. 2, pp. 155–163, 2007.

[19] T. J. Strathmann and S. C. B. Myneni, "Effect of soil fulvic acid on nickel(II) sorption and bonding at the aqueous-boehmite (γ-AlOOH) interface," *Environmental Science and Technology*, vol. 39, no. 11, pp. 4027–4034, 2005.

[20] R. B. Sardenberg, C. E. Teixeira, M. Pinheiro, and J. M. A. Figueiredo, "Nonlinear conductivity of fullerenol aqueous solutions," *ACS Nano*, vol. 5, no. 4, pp. 2681–2686, 2011.

[21] M. Bühl and A. Hirsch, "Spherical aromaticity of fullerenes," *Chemical Reviews*, vol. 101, no. 5, pp. 1153–1183, 2001.

[22] M. A. Montes-Morán, D. Suárez, J. A. Menéndez, and E. Fuente, "On the nature of basic sites on carbon surfaces: an overview," *Carbon*, vol. 42, no. 7, pp. 1219–1225, 2004.

[23] P. A. Troshin, H. Hoppe, J. Renz et al., "Material solubility-photovoltaic performance relationship in the design of novel fullerene derivatives for bulk heterojunction solar cells," *Advanced Functional Materials*, vol. 19, no. 5, pp. 779–788, 2009.

[24] M. H. Bradbury and B. Baeyens, "Sorption of Eu on Na- and Ca-montmorillonites: experimental investigations and modelling with cation exchange and surface complexation," *Geochimica et Cosmochimica Acta*, vol. 66, no. 13, pp. 2325–2334, 2002.

[25] H. Geckeis, T. Rabung, T. N. Manh, J. I. Kim, and H. P. Beck, "Humic colloid-borne natural polyvalent metal ions: dissociation experiment," *Environmental Science and Technology*, vol. 36, no. 13, pp. 2946–2952, 2002.

[26] F. Avilés, J. V. Cauich-Rodríguez, L. Moo-Tah, A. May-Pat, and R. Vargas-Coronado, "Evaluation of mild acid oxidation treatments for MWCNT functionalization," *Carbon*, vol. 47, no. 13, pp. 2970–2975, 2009.

[27] T. Li, X. Li, K. Huang, H. Jiang, and J. Li, "Synthesis and characterization of hydroxylated fullerene epoxide—an intermediate for forming fullerol," *Journal of Central South University of Technology*, vol. 6, no. 1, pp. 35–36, 1999.

[28] J. Y. Xu, H. Kaiyu, S. Li et al., "Pulmonary responses to polyhydroxylated fullerenols, $C_{60}(OH)_x$," *Journal of Applied Toxicology*, vol. 29, no. 7, pp. 578–584, 2009.

[29] F. Cheng, X. Yang, H. Zhu, J. Sun, and Y. Liu, "Synthesis of oligoadducts of malonic acid C_{60} and their scavenging effects on hydroxyl radical," *Journal of Physics and Chemistry of Solids*, vol. 61, no. 7, pp. 1145–1148, 2000.

[30] H. Wang, A. Zhou, F. Peng, H. Yu, and J. Yang, "Mechanism study on adsorption of acidified multiwalled carbon nanotubes to Pb(II)," *Journal of Colloid and Interface Science*, vol. 316, no. 2, pp. 277–283, 2007.

[31] P. L. Cao, D. E. Ellis, and V. P. Dravid, "First-principles study of initial stage of Ni thin-film growth on a TiO_2 (110) surface," *Journal of Materials Research*, vol. 14, no. 9, pp. 3684–3689, 1999.

[32] W. Wu, Q. Fan, J. Xu, Z. Niu, and S. Lu, "Sorption—desorption of Th(IV) on attapulgite: effects of pH, ionic strength and temperature," *Applied Radiation and Isotopes*, vol. 65, no. 10, pp. 1108–1114, 2007.

[33] Z. Guo, J. Xu, K. Shi, Y. Tang, W. Wu, and Z. Tao, "Eu(III) adsorption/desorption on Na-bentonite: experimental and modeling studies," *Colloids and Surfaces A*, vol. 339, no. 1-3, pp. 126–133, 2009.

[34] W. Mingming, X. Hongqin, T. Liqiang, Q. Jun, T. Xingquan, and W. Cuiping, "Uptake properties of Eu(III) on Na-attapulgite as a function of pH, ionic strength and temperature," *Journal of Radioanalytical and Nuclear Chemistry*, vol. 292, no. 2, pp. 763–770, 2012.

[35] Q. Fan, D. Shao, Y. Lu, W. Wu, and X. Wang, "Effect of pH, ionic strength, temperature and humic substances on the sorption of

Ni(II) to Na-attapulgite," *Chemical Engineering Journal*, vol. 150, no. 1, pp. 188–195, 2009.

[36] G. Zhao, H. Zhang, Q. Fan et al., "Sorption of copper(II) onto super-adsorbent of bentonite-polyacrylamide composites," *Journal of Hazardous Materials*, vol. 173, no. 1–3, pp. 661–668, 2010.

[37] X. Tan, M. Fang, C. Chen, S. Yu, and X. Wang, "Counterion effects of nickel and sodium dodecylbenzene sulfonate adsorption to multiwalled carbon nanotubes in aqueous solution," *Carbon*, vol. 46, no. 13, pp. 1741–1750, 2008.

[38] D. Lin and B. Xing, "Adsorption of phenolic compounds by carbon nanotubes: role of aromaticity and substitution of hydroxyl groups," *Environmental Science and Technology*, vol. 42, no. 19, pp. 7254–7259, 2008.